

AD-A145 864

STUDIES OF GROWN-IN DEFECTS VERSUS GROWTH PARAMETERS IN
III-V COMPOUND SE. (U) FLORIDA UNIV GAINESVILLE DEPT OF
ELECTRICAL ENGINEERING S S LI JUN 84 AFOSR-TR-84-0779

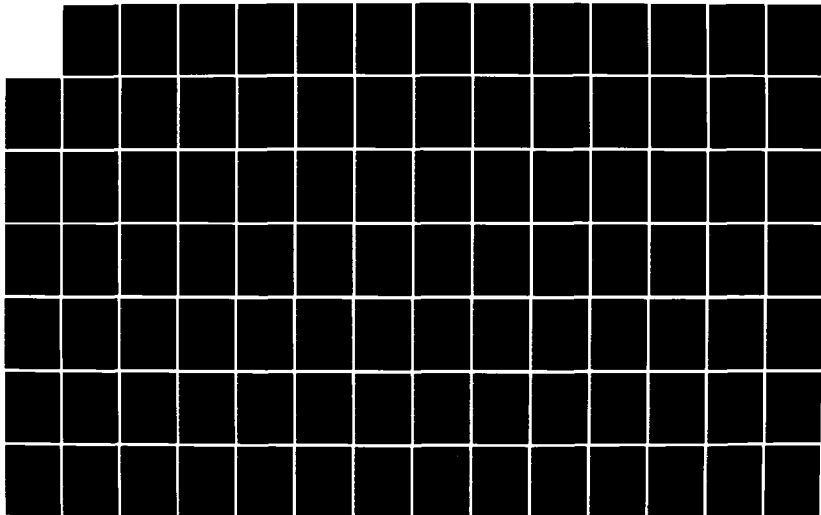
1/2

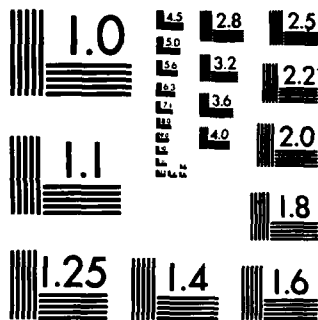
UNCLASSIFIED

AFOSR-81-0187

F/G 20/2

NL





MICROCOPY RESOLUTION TEST CHART
NATIONAL BUREAU OF STANDARDS-1963-A

AFOSR

STUDY OF GROWN-IN DEFECTS AND RADIATION-INDUCED DEFECTS IN III-V COMPOUND SEMICONDUCTORS

17

ANNUAL TECHNICAL REPORT

(For period of June 11, 1983 to June 10, 1984)

STUDIES OF GROWN-IN DEFECTS VS GROWTH PARAMETERS IN III-V COMPOUND SEMICONDUCTORS

by

Sheng S. Li
Department of Electrical Engineering
University of Florida

Gainesville, Florida 32611

JUN 25 1984
A

June 1984

Approved for public release
distribution unlimited

This work was performed for the Air Force Office of Scientific Research (AFOSR), Bolling Air Force Base, under grant No. AFOSR-81-0187

AD-A145 864

DTIC FILE COPY

84 09 17 041

REPORT DOCUMENTATION PAGE		READ INSTRUCTIONS BEFORE COMPLETING FORM
1. REPORT NUMBER AFOSR-TR-82-9	2. GOVT ACCESSION NO. AD-A145864	3. RECIPIENT'S CATALOG NUMBER
4. TITLE (and Subtitle) Study of Grown-in Defects and Radiation Induced Defects in III-V Compound Semiconductors	5. TYPE OF REPORT & PERIOD COVERED Annual Technical Report June 11, 1983 - June 10, 1984	
	6. PERFORMING ORG. REPORT NUMBER	
7. AUTHOR(s) Sheng S. Li	8. CONTRACT OR GRANT NUMBER(s) AFOSR-81-0187A	
9. PERFORMING ORGANIZATION NAME AND ADDRESS University of Florida Gainesville, FL 32611	10. PROGRAM ELEMENT, PROJECT, TASK AREA & WORK UNIT NUMBERS B1	
11. CONTROLLING OFFICE NAME AND ADDRESS Air Force Office of Scientific Research, Bolling Air Force Base, DC 20332	12. REPORT DATE June 20, 1984	
	13. NUMBER OF PAGES 138	
14. MONITORING AGENCY NAME & ADDRESS (if different from Controlling Office)	15. SECURITY CLASS. (of this report) Unclassified	
	15a. DECLASSIFICATION/DOWNGRADING SCHEDULE	
16. DISTRIBUTION STATEMENT (of this Report) Unlimited		
17. DISTRIBUTION STATEMENT (of the abstract entered in Block 20, if different from Report)		
18. SUPPLEMENTARY NOTES		
19. KEY WORDS (Continue on reverse side if necessary and identify by block number) GaAs, InP, AlGaAs, LPE, VPE, MOCVD, LEC, DLTS, grown-in defects, radiation induced defects, defect density, emission rate, capture cross section, EL2, vacancy, arsenic antisite defect, thermal annealing, one-MeV electron irradiation.		
20. ABSTRACT (Continue on reverse side if necessary and identify by block number) Deep-level defects play an important role in influencing the electronic properties and device performance. Study of the physical origins of deep-level defects in III-V compound semiconductors is a subject of great interests in recent years. Although a large number of papers has been devoted to finding the physical origins of deep-level defects in GaAs, unfortunately, none of these published results offering a consistent and unambiguous explanation for the deep-level defects observed in GaAs. For examples, possible physical origins of EL2 electron trap including gallium vacancy (VGa), arsenic-antisite		

(As_{Ga}), arsenic antisite-plus-arsenic vacancy (As_{Ga}V_{As}) complex as well as oxygen complex have been considered by many researchers as the likely candidates for GaAs grown under As-rich or high arsenic pressure condition. However, the subject is still highly controversial, and quantitative modelling of the EL2 electron trap is needed in order to control this native defect in both the bulk and epitaxial grown GaAs.

The objectives of this research are to conduct: (1) A detailed analysis of the grown-in defects and radiation induced defects in GaAs and other III-V materials grown by the LEC, VPE, LPE, and MOCVD techniques under different growth and annealing conditions, (2) Theoretical modelling of the native defects for identifying the physical origins of the deep-level traps in GaAs and other III-V materials, (3) Theoretical and experimental study of the potential well of electron traps from analyzing the electric field enhanced emission rates deduced from the nonexponential DLTS data, and (4) Study of one-MeV electron irradiation induced deep-level defects in GaAs, AlGaAs, and InP materials. The main research accomplishments are summarized as follows:

- (1) Theoretical and experimental studies of native point defects in GaAs grown by the LEC, VPE, LEP, and MOCVD techniques under different growth and annealing conditions have been made in this research. The main findings include: (a) high purity GaAs material can be grown for the low arsenic pressure case under optimum cooling condition, (b) GaAs grown under high arsenic pressure condition will produce more native point defects than under lower arsenic pressure condition, (c) arsenic antisite (As_{Ga}) defect can only be produced in VPE and MOCVD GaAs grown under As-rich or high arsenic pressure condition; this defect can not be produced in LPE GaAs grown under low arsenic pressure condition.
- (2) A new defect model supported by the experimental data has been developed in this work to account for the physical origins of EL2 electron trap in GaAs. It is shown that EL2 electron trap may be attributed to two different types of native defects: One is identified as the EL2a (i.e., E_c-0.83eV) electron trap, and the other is designated as the EL2b (E_c-0.76eV) electron trap. The physical origin for the EL2a level is attributed to the double-charge arsenic antisite (i.e., As_{Ga}⁺⁺) defect, whereas, the physical origin for the EL2b electron trap is due to the arsenic-antisite-plus-arsenic vacancy complex (i.e., As_{Ga}V_{As}). Based on this model, relationship between the density of EL2a and EL2b trap levels and the [As]/[Ga] ratio in the MOCVD and VPE grown GaAs were established. The result shows the density of EL2a trap level is proportional to the mole fraction ratio of (r-1)^{1/2}, while the density of EL2 trap level is proportional to the mole fraction ratio of (r-1)^{1/4}, where r = [As]/[Ga].
- (3) A theoretical model for the nonexponential DLTS response due to field dependent emission rate of trapped charge has been developed. A comparison of the theoretical calculation of the nonexponential DLTS response with the DLTS data for each trap level enable us to determine the potential well of the trap involved. This method has been applied to identify the physical origins of the EL2a electron trap in GaAs.
- (4) Characterization of the low energy proton (50 to 290 keV) and one-MeV electron irradiation induced defects in LPE grown GaAs and LEC grown p-InP materials has been carried out in this work. A comparison of the deep-level defects produced by the one-MeV electron irradiation and the low-energy proton irradiation reveals that there is a significant difference in defect profile as well as types of defects produced in the GaAs LPE layers. The defect profiles are much more complicated for the proton

irradiated GaAs than the one-MeV electron irradiated GaAs. The radiation induced deep-level defects are believed to be due to Frenkel type defects and their complexes. Our study shows that low temperature thermal annealing (i.e., $T \leq 300^\circ \text{C}$) or periodic annealing process is effective in reducing or eliminating these radiation induced defects in both GaAs and InP materials. The shallow traps are much easier to anneal out than the deep-level traps.

SEARCHED FOR
INDEXED
SERIALIZED
FILED

APR 1964

DTIC

Special

AI



TABLE OF CONTENTS

	Page
DOCUMENT PAGE.....	i
LIST OF SYMBOLS	ii
I. INTRODUCTION.....	1
II. REVIEW OF POSSIBLE NATIVE DEFECTS AND DEFECT COMPLEXES	
IN GALLIUM ARSENIDE	6
III. EXPERIMENTAL DETAILS	11
3.1 Current-Voltage (I-V) Measurement.....	11
3.2 A. C. Admittance Measurement.....	13
3.3 Capacitance-Voltage (C-V) Measurement.....	14
3.4 Thermally Stimulated Capacitance (TSCAP) Measurement...	15
3.5 Deep Level Transient Spectroscopy (DLTS) Measurement...	16
3.5.1 Principle of DLTS Measurement.....	16
3.5.2 Defect Concentration.....	17
3.5.3 Activation Energy of Deep-level Defect.....	18
IV. DETERMINATION OF POTENTIAL WELL OF DEEP-LEVEL TRAPS IN GAAS.	21
4.1 Capture and Emission Process at a Deep-Level Trap.....	22
4.2 Overview of the Theory.....	24
4.2.1 Poole-Frenkel effect.....	26
4.2.2 Phonon-assisted tunneling effect.....	28
4.3 Theoretical Calculations of Emission Rate Enhancement for Different Potential Wells.....	31
4.3.1 Coulombic Potential Well.....	31
4.3.2 Dirac Potential Well.....	33
4.3.3 Square Potential Well.....	36
4.3.4 Polarization Potential Well.....	37
4.3.5 Dipole Potential Well.....	39
4.4 Theoretical Calculation of the Nonexponential DLTS Response for Different Potential Wells.....	44
V MODELLING OF NATIVE POINT DEFECTS IN GAAS	54
5.1 Introduction.....	54
5.2 Theoretical Calculations of Vacancy and Interstitial in Undoped GaAs.....	56

5.3	Thermal Kinetics after Crystal Growth.....	60
5.4	The Possible Grown-in Point Defects in GaAs for the As-rich, or High Arsenic Pressure Case.....	64
5.5	The Possible Grown-in Point Defects in GaAs for the Ga-rich, or Low Arsenic Pressure Case.....	65
5.6	Summary and Conclusions.....	65
VI	ON THE PHYSICAL ORIGINS OF EL2 ELECTRON TRAP IN GaAs (THEORETICAL AND EXPERIMENTAL EVIDENCE).....	67
6.1	Review of the EL2 Electron Trap in GaAs.....	68
6.2	Theoretical Modelling of the EL2 Electron Trap in GaAs..	71
6.2.1	Growth Process.....	71
6.2.2	Cooling Process.....	75
6.2.3	Annealing Process.....	77
6.3	Determination of Potential Well for EL2 Electron Trap from Field Enhanced Emission Rate Analysis.....	77
6.4	Summary and Conclusions.....	82
VII.	STUDY OF GROWN-IN DEEP LEVEL DEFECTS VS GROWTH PARAMETERS IN VPE, LEC, LPE AND MOCVD GROWN GaAs	83
7.1	Study of Grown-in Deep Level Defects vs Growth Parameters in the VPE GaAs Layers.....	83
7.1.1	Introduction.....	84
7.1.2	Experimental Details.....	85
7.1.3	Results and Discussions.....	85
7.1.4	Summary and Conclusions	97
7.2	Study of Grown-in Deep Level Defects vs Growth Parameters in LEC Grown GaAs	100
7.2.1	Intrinsic Double Acceptor Level in LEC Grown p-GaAs.....	100
7.2.2	Study of Deep Level Defects vs Annealing Temperature in H ₂ Ambient.....	103
7.3	Grown-in Deep Level Defects vs Growth Parameters in LPE Grown n-GaAs	111
7.4	Grown-in Deep Level Defects vs Growth Parameters in MOCVD Grown n-GaAs	113
7.5	Summary and Conclusions.....	113
VIII.	SUMMARY AND CONCLUSIONS.....	118
IX.	PUBLICATIONS AND CONFERENCE PRESENTATIONS	121
X.	REFERENCES.....	124

LIST OF SYMBOLS

<u>Symbol</u>	<u>Definition</u>
A	Diode area
A_1	$e^2 \alpha_j / 8 \epsilon_0 \epsilon_s^2$ for polarization well.
A_2	$(1/\pi) [Ze^2 / (4 \epsilon_s mc^2)]^2$
B	Proportionality constant for emission rate.
c	Velocity of light.
C_0	Depletion layer capacitance.
$C(t)$	Transient capacitance which is proportional to electrons (holes) emitted to the conduction (valence) band.
ΔC	Capacitance change due to majority (minority) carrier emission from the trap level.
$\Delta C(t)$	$C_0 - C(t)$
D_n (D_p)	Diffusion constant of electrons (holes).
e_n (e_p)	Emission rate of electrons (holes).
e_{n0}	Electron emission rate for zero electric field condition.
e_{n1} (e_{n3})	One- (three-) dimensional emission rate in the presence of applied electric field.
e_{nH}	Total enhanced emission rate.
e_{nt}	Emission rate due to phonon-assisted tunneling effect.
e_{nHC}	Total enhanced emission rate for a Coulombic well.
e_{nHD}	" " " " a dipole well.
e_{nHP}	" " " " a polarization well.
e_{nHR}	" " " " a Dirac well.
e_{nHS}	" " " " a square well.
$e_{nj}(F_j)$	Enhanced emission rate at electric field strength F_j .
E_g	Energy bandgap.

E_H	= 13.6 eV, is the ionization energy of a hydrogen atom.
E_j	Incident particle energy.
E_m	$E_t + \Delta E_b$
E_t	Activation energy of the trap level.
E_{tj}	Ionization energy of the trap level.
E_{th}	Thermal excitation energy or phonon energy.
ΔE_b	Activation energy of capture cross section for the deep-level trap.
ΔE_{tj}	Poole-Frenkel lowering of the potential barrier.
F	Electric field.
F_j	Electric field in the i th segment of the space-charge layer.
F_{max}	Maximum electric field in the p^+-n junction.
g	Degeneracy factor.
h	= $h/2\pi$, Planck constant.
ΔH	Enthalpy change.
L_D	Debye length.
L_n (L_p)	Diffusion length for electrons (holes).
L^*	Effective diffusion length.
m	Electron effective mass.
m_0	Free electron mass.
m_{de} (m_{dh})	Density of state effective mass for electrons (holes).
n	Diode ideality factor.
M_1	Mass of the incident particle.
M_2	" " " " lattice atom.
n_0	Electron concentration.
n_i	Intrinsic carrier density.
N_a (N_d)	Acceptor (donor) density.

N_c	Effective density of conduction band states.
N_t	Trap density.
$N(x)$	Distribution of proton particle.
N	Total number of displacement particles.
P_0	Hole concentration.
P	Probability ratio for electron impinging on a potential barrier.
r	Mole fraction of [As] to [Ga].
r_{max}	Location of maximum Poole-Frenkel barrier lowering.
R	E_{tj}/kT
R_e	The penetration range of electron in mg/cm^2 .
R_0	Distance separating the charge center.
R_p	Shunt resistance.
R_s	Series resistance.
R_p^*	Projected range of proton particle.
ΔR_p	Straggle range of proton particle.
ΔS	Entropy change.
T_m	Maximum energy transferred to the lattice atom.
$\langle v_{th} \rangle$	Average thermal velocity.
V_a	Applied voltage.
V_{bi}	Built-in potential.
V_D	Displacement energy.
w	Depletion layer width.
w_0	Zero bias depletion layer width.
x_1	Proton penetrate depth.
Z	Atomic number of the lattice atom.
$\alpha_H (\alpha_j)$	Polarizability of a hydrogen (neutral impurity) atom.
γ_1	$= 5.405 \times 10^{-4} \text{ eV/k for GaAs.}$

γ_2 = 204 for GaAs.
 θ_F Angle between the electric field and dipole moment.
 θ_m Angle for the maximum barrier lowering occurs for dipole well.
 σ_d Differential scattering cross section.
 σ_n (σ_p) Capture cross section for electrons (holes).
 σ_∞ Capture cross section for $T \rightarrow \infty$.
 ϕ_j Built-in potential.
 ϕ_{Bn} Barrier height of a Schottky diode.
 $\Delta\phi$ Image lowering potential of a Schottky diode.
 ϵ_s Dielectric constant of GaAs.
 τ Carrier emission time constant.
 τ_e Effective carrier lifetime.
 τ_n (τ_p) Lifetime of electrons (holes).

I. INTRODUCTION.

Studies of deep-level defects in III-V compound semiconductors have been reported extensively in the literature^[1-13]. Speculations on the physical origins of defect levels and defect complexes in these materials are still very tentative. It is not even possible to say with any assurance that simple gallium vacancy (V_{Ga}) or arsenic vacancy (V_{As}) can be related to a particular energy level.

In one respect understanding has been improved. Gallium arsenide (GaAs) specimens grown by various techniques such as liquid phase encapsulation (LEC), Bridgmann, vapor phase epitaxy (VPE), metalorganic chemical vapor deposition (MOCVD), liquid phase epitaxy (LPE), and molecular beam epitaxy (MBE), are now recognized as likely to have different properties in terms of energy levels within the bandgap. In each of these techniques, the growth temperature, growth pressure, growth phase, and cooling rate are usually different. For examples, GaAs grown by the LPE technique from a gallium melt is expected to be low in gallium vacancy defects and possibly high in arsenic vacancy. The LPE GaAs usually contains hole traps with energy level of $E_v + 0.71\text{eV}$ (B center), while VPE GaAs grown in the As-rich conditions always contains an electron trap with energy of $E_c - 0.83\text{ eV}$ (EL2 level). The reason for observing these trap levels in the LPE or VPE GaAs is still not clear. Thus, studies of grown-in defects in III-V compound semiconductors are important tasks to undertake in order to obtain a better understanding of the physical properties of deep-level defects in III-V materials.

The main objectives of this research program are to conduct: (1) A detailed analysis of the grown-in defects and radiation-induced defects in

GaAs and other III-V compounds grown by the LEC, VPE, LPE, and MOCVD techniques under different growth and annealing conditions, (2) theoretical modelling to identify the physical origins of the deep-level traps, in particular the EL2 electron trap in GaAs, (3) theoretical and experimental studies to determine the potential well of electron traps from analyzing the field enhanced emission rates deduced from the nonexponential DLTS response data, and (4) experimental studies of the grown-in defects and one-MeV electron irradiation-induced defects in GaAs and InP under different radiation fluences and annealing conditions.

A detailed theoretical and experimental study of the grown-in defects and radiation induced defects in GaAs and InP has been carried out in this work and the results are summarized as follows:

- (1) Theoretical modelling of native defects in GaAs has been developed. GaAs specimen grown by the LEC, VPE, LPE, and MOCVD techniques under different growth and annealing conditions have been studied in this work in order to verify this model. GaAs specimen used in this study include: (i) VPE GaAs epilayers grown on $\langle 100 \rangle$, $\langle 211A \rangle$, and $\langle 211B \rangle$ oriented semi-insulating (S.I.) Cr-doped GaAs substrates with [Ga]/[As] ratios varying from 2/1 to 6/1, (ii) LEC grown n-GaAs samples which were used for study of the effect of hydrogen heat treatment on deep-level defects, (iii) LPE GaAs samples grown under two different temperatures (ie., 700 and 800°C) and two cooling rates (0.4 and 1°C/min.), and (iv) MOCVD GaAs epilayers grown on S.I. GaAs substrate and S.I. Ge substrates. Theoretical modelling of native point defects is described in chapter V. Experimental results for some of the native point defects observed in the samples cited above are described in chapter VII.

- (2) Deep-donor trap, commonly known as EL2 center, with activation energy ranging from $E_C - 0.76$ to $E_C - 0.83$ eV, has been observed in GaAs grown by LEC, VPE, and MOCVD techniques. The EL2 level acts as a recombination center for lifetime reduction. The physical origin of this electron trap is a subject of greater interest in recent years. Although a large number of papers has been devoted to finding the physical origins of the EL2 electron trap, unfortunately, none of these published results offered a convincing and unambiguous explanation for the observed EL2 trap in GaAs. Our theoretical modelling and experimental evidence lead us to believe that the EL2 center in GaAs may be attributed to two different types of native defects: one is identified as the EL2-a electron trap which has an activation energy of $E_C - 0.83$ eV and is due to the As_{Ga} antisite defect; the other is designated as the EL2-b electron trap which has an activation energy of $E_C - 0.76$ eV and is attributed to the $As_{Ga} - V_{As}$ defect complex. A detailed theoretical and experimental study of the EL2 electron trap has been carried out in this work, and the results are discussed in chapter VI.
- (3) DLTS signals are often analyzed assuming that the capacitance transient is exponential.^[7,14] However, most of the DLTS signals are nonexponential transient.^[15,16] In this work, we present the theoretical analysis of nonexponential capacitance transients due to electric field dependent emission rate of trapped charge. Emission rate of trapped charge carriers is enhanced by the Poole-Frenkel and phonon-assisted tunneling effects in the presence of an applied electric field. Since the electric field varies with position within

the depletion region of a reverse biased p-n junction, the emission rate is not constant within the same region. The DLTS response due to nonuniformed emission rates can in general be expressed as $S(\omega) = \sum \exp(-e_{nj} t_1) - \sum \exp(-e_{nj} t_2)$. Based on the nonexponential capacitance transient, theoretical calculations of DLTS response for deep-level traps in GaAs were made using five different potential wells; namely, the Coulombic well which has a positive charge state for the empty state; the Dirac well, square well, polarization well, and dipole well which all have neutral charge state from different physical origins. A comparison of the theoretical calculation of the nonexponential DLTS response with the DLTS data for each trap would allow us to determine the potential well of the trap involved. This model was applied to the calculations of potential well for the EL2a electron trap and other electrontraps. The results will be discussed in chapter IV.

- (4) Characterization of low energy proton and one-MeV electron irradiation induced defects in the LPE grown GaAs has been carried out, and the results were described in details in the 1983 AFOSR Annual Technical Report.

Experimental tools employed in this study include the current-voltage (I-V), capacitance-voltage (C-V), thermally stimulated capacitance (TSCAP) and the deep-level transient spectroscopy (DLTS) measurements. From these measurements, one can determine the energy levels, density of defects, defect profile, and the capture cross section for each trap level.

Chapter II reviews the possible native defects and impurity complexes in GaAs. Chapter III presents the experimental details. Determination of

potential well of deep level traps using field enhanced emission rate analysis of nonexponential DLTS in GaAs will be described in chapter IV. Chapter V depicts the modelling of the grown-in native point defects in GaAs. The physical origin of the EL2 electron trap in GaAs is explained in chapter VI. Chapter VII described the study of grown-in defects vs growth parameters in VPE, LEC, VPE, and MOCVD grown GaAs. Summary and conclusions are given in chapter VIII.

II. REVIEW OF NATIVE DEFECTS AND DEFECT COMPLEXES IN GALLIUM ARSENIDE.

The number of possible native defects in GaAs is large as may be seen in table 2.1. None of these native defects has been identified with any confidence. This is due to the fact that experiments for studying such defects tend to be too uncontrollable. In addition to the defects shown in table 2.1, other types of defects such as impurity, complexes of impurity may also be expected in GaAs as well as other III-V materials. In this chapter, we will focus our attention on a few native defects listed in table 2.1, which are believed to be related to the electron or hole traps observed in this study.

Defects can be represented by their chemical symbols. For examples, vacancy is represented by V and interstitial by i. Subscript indicates the lattice site. Thus, V_{Ga} denotes the gallium vacancy, Ga_i represents the gallium interstitial site defect. In addition to these simple point defects, defect complexes (for example: $V_{Ga}^- As_{Ga}^{++} V_{Ga}^-$) might be expected to form as the crystal cooling down from high growth temperature to room temperature. Another type of defect, namely, the antisite defect must also be considered. The antisite defects such as As_{Ga}^{++} , Ga_{As}^{--} , and $As_{Ga}^{++} Ga_{As}^{--}$, are believed to be important native defects in GaAs.

A survey of the literature on the subject of defects in GaAs grown by the Liquid Encapsulation Czochraski (LEC), Horizontal Bridgman-Stockbargen (HB), Vapor Phase Epitaxy (VPE), Liquid Phase Epitaxy (LPE), Molecular Beam Epitaxy (MBE), and Organometallic Chemical Vapor Deposition (MOCVD) techniques showed that only a few electron and hole traps are common point defects observed in both the bulk and epitaxial grown GaAs material. It should be noted that defects observed in one GaAs specimen may not be

observed in other GaAs specimen if the growth processes were different. A list of the electron and hole traps observed in this study compared with others^[23-33] are given respectively in table 2.2 and 2.3.

The EL2 electron trap (same as EF10, ET1, EB2, ES1 cited in the literature) is the dominant electron trap in the VPE, MOCVD, and bulk grown GaAs, and is absent in the LPE and MBE grown GaAs epitaxial layers. Trap densities of EL3, EL5, and EL12 levels are varied by different growth conditions , and density of these traps can be easily reduced by annealing. This suggests that they are due to native point defects. On the other hand, EL11 is not affected by heat treatment, and therefore could be due to an impurity complex. Crystals grown by different growth techniques are expected to produce different electron traps, and only a few of them are common and independent of methods of crystal growth. For example, both EL6 (bulk) and EL7 (MBE) levels could be the same defect observed in the bulk and MBE grown GaAs, yet it was not observed in VPE grown GaAs. EL10 (MBE) and EL11 (VPE) could be the same level, yet it was not observed in bulk GaAs material. Most of these deep level defects are believed to be either due to the vacancy related defects, antisite defects or vacancy-impurity complex defects. For the hole trap levels in GaAs, HL2, HL5, HL7, HL9, and HL11 may be related to native defects, while the other trap levels are related to the impurity defects.

Table 2.1 Possible Native Defects in GaAs.

1. One Component Defects:

- a. Vacancy: V_{Ga}, V_{As}
- b. Interstitial: Ga_j, As_j

2. Two Component Defects:

- a. Divacancy: $V_{Ga}V_{Ga}, V_{Ga}V_{As}, V_{As}V_{As}$
- b. Antisite: Ga_{As}, As_{Ga}
- c. Di-interstitial: Ga_jAs_j
- d. Vacancy-interstitial: $V_{Ga}Ga_j, V_{Ga}As_j, V_{As}Ga_j, V_{As}As_j$

3. Three Component Defects:

- a. Antisite-vacancy complexes: $As_{Ga}V_{Ga}, As_{Ga}V_{As}, Ga_{As}V_{Ga}, Ga_{As}V_{As}$
- b. Trivacancy: $V_{Ga}V_{As}V_{Ga}, V_{As}V_{Ga}V_{As}$

4. Four Component Defects:

- a. Antisite-divacancy complexes: $V_{Ga}As_{Ga}V_{Ga}, V_{As}Ga_{As}V_{As}$
- b. Di-antisite: $Ga_{As}As_{Ga}$

Table 2.2. Electron traps in n-GaAs.

Level	Activation energy (eV)	Capture Cross Section (cm^2)	Growth method	Ref.
ET1	$E_c - 0.85$	6.5×10^{-13}	Bulk	23
ET2	0.30	2.5×10^{-15}	"	"
ES1	0.83	1.0×10^{-13}	Bulk	24
EI1	0.43	7.3×10^{-16}	VPE	25
EI2	0.19	1.1×10^{-14}	VPE	"
EI3	0.18	2.2×10^{-14}	VPE	"
EB1	0.86	3.5×10^{-14}	Cr-doped LPE	26
EB2	0.83	2.2×10^{-13}	as-grown VPE	"
EB3	0.90	3.0×10^{-11}	Electr. irradi.	27
EB4	0.71	8.3×10^{-13}	" "	"
EB5	0.48	2.6×10^{-13}	MBE	28
EB6	0.41	2.6×10^{-13}	Electr. irradi.	27
EB7	0.30	1.7×10^{-14}	MBE	28
EB8	0.19	1.5×10^{-14}	MBE	28
EB9	0.18	-	Electr. irradi.	27
EB10	0.12	-	" "	"
EL1	0.78	1.0×10^{-14}	Cr-doped bulk	29
EL2 (A)	0.83	1.2×10^{-13}	VPE	30
EL3 (B)	0.58	"	"	"
EL4	0.51	1.0×10^{-12}	MBE	
EL5 (C)	0.42	1.2×10^{-13}	VPE	30
EL6	0.35	1.5×10^{-13}	Bulk	29
EL7	0.30	7.2×10^{-15}	MBE	
EL8 (D)	0.28	7.7×10^{-15}	VPE	30
EL9	0.23	6.8×10^{-15}	"	"
EL10	0.17	1.8×10^{-15}	MBE	
EL11 (F)	0.17	3.0×10^{-16}	VPE	30
EL12 (A)	0.78	4.9×10^{-12}	"	"
EL14	0.22	5.2×10^{-16}	Bulk	29
EL15	0.15	5.7×10^{-13}	Electr. irradi.	
EL16	0.37	4.0×10^{-18}	VPE	30
EF1	0.11		Proton irradi.	18
EF2	0.14		" "	"
EF3	0.20		" "	"
EF4	0.31		Electr. irradi.	21
EF5	0.35		n-LEC	
EF6	0.52		Proton irradi.	18
EF7	0.60		n-LEC	
EF8	0.71		Electr. irradi.	21
EF9	0.76		LEC	
EF10	0.83		LEC, VPE, MOCVD	31
EF11	0.90		Electr. irradi.	21

Table 2.3 Hole traps in p-GaAs.

Level	Activation energy (eV)	Capture Cross Section (cm ²)	Growth method	Ref.
HT1	$E_v+0.44$	1.2×10^{-14}	VPE	23
HS1	0.58	2.0×10^{-19}	LPE	24
HS2	0.64	4.1×10^{-16}	"	"
HS3	0.44	4.8×10^{-18}	"	"
HB1	0.78	5.2×10^{-16}	Cr-doped LPE	26
HB2 (B)	0.71	1.2×10^{-14}	as-grown LPE	"
HB3	0.52	3.4×10^{-16}	Fe-doped LPE	"
HB4	0.44	3.4×10^{-14}	Cu-doped LPE	"
HB5 (A)	0.40	2.2×10^{-13}	as-grown LPE	"
HB6	0.29	2.0×10^{-14}	Electr. irradi.	27
HL1	0.94	3.7×10^{-14}	Cr-doped VPE	
HL2	0.73	1.9×10^{-14}	as-grown LPE	32
HL3	0.59	3.0×10^{-15}	Fe-doped VPE	33
HL4	0.42	3.0×10^{-15}	Cu-doped VPE	"
HL5	0.41	9.0×10^{-14}	as-grown LPE	32
HL6	0.32	5.6×10^{-14}	VPE	33
HL7	0.35	6.4×10^{-15}	MBE	"
HL8	0.52	3.5×10^{-16}	MBE	"
HL9	0.69	1.1×10^{-13}	VPE	"
HL10	0.83	1.7×10^{-13}	VPE	"
HF0	0.082		LEC (p)	17
HF1	0.13		Electr. irradi.	21
HF2	0.17		Proton irradi.	18
HF3	0.20		" "	"
HF4	0.29		Electr. irradi.	21
HF5	0.35		" "	"
HF6	0.40		" "	"
HF7	0.44		Proton irradi.	18
HF8	0.52			"
HF9	0.57			"
HF10	0.71		Electr. irradi.	21

III. EXPERIMENTAL DETAILS

Experimental tools employed in this study include current-voltage (I-V) measurement, a.c. admittance measurement, capacitance-voltage (C-V) measurement, thermally stimulated capacitance (TSCAP) measurement, and deep level transient spectroscopy (DLTS) measurement. From these measurements, one can determine the diode characteristics and the defect parameters such as defect energy levels, defect densities, and capture cross sections. Each of these measurement technique is described as follows:

3.1. Current-Voltage (I-V) Measurement:

Measurement of the current-voltage (I-V) characteristics under forward bias condition can yield useful information concerning the conduction mechanisms, recombination processes in the space charge region of a p-n junction diode or a Schottky barrier diode. For a good p-n diode with no surface leakage, the total current is composed of the diffusion current in the quasi-neutral region (QNR) and the recombination current in the space charge region (SCR). When bulk diffusion current component dominates, the current expression is given by:^[34]

$$I_f = I_d [\exp(V_a/V_T) - 1] \quad (3.1)$$

where V_a is the applied voltage; $V_T = kT/q$, and I_d is the magnitude of the saturation diffusion current.

$$I_d = qn_i^2 A [(D_n/L_n N_a) + (D_p/L_p N_d)] \quad (3.2)$$

where n_i is the intrinsic carrier density; A is the diode area; D_n (D_p) is the diffusion constant for electrons (holes); L_n (L_p) is the diffusion length for electrons (holes), and N_a (N_d) is the acceptor (donor) density.

If bulk generation-recombination current dominates, then the current expression is given by:^[34]

$$I_r = I_{rg} \exp(V_a/2V_T) \quad (3.3)$$

where I_{rg} is the magnitude of the generation-recombination current.

$$I_{rg} = qn_j W/2\tau_e \quad (3.4)$$

In Eq.(3.4), W denotes the depletion layer width; $\tau_e = (\tau_n \tau_p)^{1/2}$ is the effective carrier lifetime in the space charge region;^[35] τ_n (τ_p) is the lifetime of electrons (holes), defined by:

$$\tau_n = 1 / (N_t \sigma_n \langle v_{th} \rangle) \quad (3.5)$$

where N_t is the trap density; σ_n (σ_p) is the capture cross section for electrons (holes); $\langle v_{th} \rangle$ is the average thermal velocity.

The total current can be expressed by:

$$I_t = I_f + I_r = I_0 \exp(V_a/nV_T) \quad (3.6)$$

where I_0 is the saturation current; n is the ideality factor of a p-n diode which is usually used to identify the dominant current component in a p-n diode. Inspection of Eqs.(3.1) and (3.3) shows that the bulk diffusion current depends more strongly on temperature than the recombination current in the junction space charge region (SCR). Since the recombination current in the junction SCR is inversely proportional to the effective carrier lifetimes (and hence directly related to the defect density in the transition region), measurements of I-V characteristics under forward bias conditions would allow us to determine the effective lifetimes in GaAs.

3.2. A. C. Admittance Measurement.

A useful experimental tool for evaluating shunt (R_p) and series resistance (R_s) across a p-n junction diode is by using a.c. admittance measurement technique.^[36] A p-n junction diode can be represented by a three element device with shunt resistance, junction capacitance, and series resistance. Measurements of the admittance as a function of frequencies (e.g. from 110 kHz to 700 MHz) will enable us to determine values of R_s , R_p , and C in a p-n diode. The impedance of the p-n junction diode is given by:

$$\begin{aligned} Z(\omega) &= R_s + \{R_p(1/j\omega C)/[R_p + (i/j\omega C)]\} \\ &= R_D(\omega) + jX_D(\omega) \end{aligned} \quad (3.7)$$

where

$$R_D(\omega) = R_s + R_p/(1+\omega^2 C^2 R_p^2) \quad (3.8)$$

$$X_D(\omega) = R_p \omega C/(1+\omega^2 C^2 R_p^2) \quad (3.9)$$

The admittance is the inverse of the impedance in a p-n junction diode, which is given by:

$$\begin{aligned} Y(\omega) = 1/Z(\omega) &= \{R_D(\omega)/[R_D^2(\omega) + X_D^2(\omega)]\} \\ &\quad - j\{X_D(\omega)/[R_D^2(\omega) + X_D^2(\omega)]\} \end{aligned} \quad (3.10)$$

In the low frequency and high frequency limits:

$$\omega \rightarrow 0, \text{ Re } Y(\omega) = 1 / [R_p + R_s] \quad (3.11)$$

$$\omega \rightarrow \infty, \text{ Re } Y(\omega) = 1 / R_s \quad (3.12)$$

Thus, from a plot of the $\text{Im } Y(\omega)$ vs. $\text{Re } Y(\omega)$, the series resistance and shunt resistance of the diode can be determined. The a.c. admittance

technique can be very useful in evaluating the shunt leakage problems in a p-n diode and allows accurate determination of the R_s , R_p , and C over a wide range of frequencies.

3.3. Capacitance-Voltage (C-V) Measurement:

The capacitance-voltage (C-V) measurement can be used to determine the background doping concentration in the n- or p-GaAs epitaxial layers using a Schottky barrier structure or a one-sided abrupt p⁺-n (or n⁺-p) junction. The depletion capacitance across the Schottky barrier diode is given by:

$$C(V_r) = \epsilon_s A/W = A \{q\epsilon_s N_D / [2(\phi_j + V_r - kT/q)]\}^{1/2} \quad (3.13)$$

where ϵ_s is the dielectric constant of GaAs; ϕ_j is the built-in potential; and V_r is the applied reverse voltage. Eq.(3.13) shows that the depletion capacitance of a Schottky diode is proportional to the square root of dopant concentration and inversely proportional to the square root of the applied voltage. If the inverse of the capacitance square (C^{-2}) is plotted as a function of the reverse bias voltage V_r , then, the background concentration, can be calculated from the slope of C^{-2} vs V_r using the following expression:

$$C^{-2}(V_r) = [2 / (q \epsilon_s A^2 N_D)] (\phi_j + V_r) \quad (3.14)$$

The intercept of C^{-2} vs. V_r plot in the voltage axis yields values of ϕ_j which is related to the barrier height of a Schottky diode by:

$$\phi_{Bn} = \phi_j + V_n + kT/q - \Delta\phi \quad (3.15)$$

where

$$V_n = E_c - (kT/q) \ln(N_D/N_C) \quad (3.16)$$

and $\Delta\phi$ is the image lowering potential of a Schottky diode; N_C is the effective density of states in the conduction band.

3.4. Thermally Stimulated Capacitance (TSCAP) Measurement:

Another interesting experiment, which is known as the thermally stimulated capacitance (TSCAP) measurement technique [37,38] will be described in this section. The TSCAP experiment is carried out by first reverse biasing a p-n diode or a Schottky diode, and then the diode is cooled down to liquid nitrogen temperature (77°K). After temperature reaches 77°K, the diode is momentarily zero biased to fill the majority carrier traps and returned to reverse bias condition, and the temperature is then raised from 77 to 400 °K. The thermal scan of capacitance vs temperature plot is then taken by using an X-Y recorder. A capacitance step is observed from the C vs T plot if majority or minority carrier emission is taking place in a trap level within a certain temperature range. The amplitude of this capacitance step is directly proportional to the trap density. The trap density for an n-GaAs can be calculated from the following expression:

$$N_t = N_d(2 \Delta C / C_0) \quad (3.17)$$

where C_0 is the depletion layer capacitance and ΔC is the capacitance change due to the majority or minority carrier emission. Thus, knowing N_d (or N_a) and C_0 at the temperature where the capacitance step was observed, the trap density can be calculated from Eq.(3.17). Note that Eq.(3.17) is valid only for the case when N_t is less than 0.1 N_d . For the case of large trap density with $N_t > 0.1 N_d$, a more exact expression should be used instead.

3.5. DLTS Measurement:

The Deep-Level-Transient-Spectroscopy (DLTS) experiment is a high frequency (20 MHz) transient capacitance technique, which was introduced first by Lang in 1974 [7,14]. The DLTS scan displays the spectrum of deep level traps in the forbidden gap of a semiconductor as positive or negative peaks on a flat baseline as a function of temperature. Although this kind of measurement is time consuming, it offers several advantages such as sensitive, easy to analyze and capable of measuring the traps over a wide range of depth in the forbidden gap. By properly changing the experimental conditions, one can measure the following parameters:

- Minority and majority carrier traps.
- Activation energy of each defect level.
- Defect concentration which is directly proportional to the peak height.
- Defect concentration profile.
- Electron and hole capture cross sections.

3.5.1. Principles of the DLTS Technique.

The capacitance transient is associated with the return to thermal equilibrium of the carrier occupancy in a trap level following an initial nonequilibrium condition. The polarity of the DLTS peak depends on the capacitance change after trapping the minority or majority carriers. Because an increase in trapped minority carriers in the SCR would result in an increase in the junction capacitance, the minority carriers trapping will produce a positive polarity peak, and vice versa. For example, in a p^+n junction diode, the SCR extends mainly into the n-region, and the local charges are due to positively charged ionized donors. If a forward bias is

applied, the minority carriers (holes) will be injected into this region. Once the holes are trapped in a defect level the net positive charges in such region will increase. This results in a narrower SCR width which implies a positive capacitance change. Thus, the DLTS signal will have a positive peak. Similarly, if the majority carriers are injected into this region and captured by the majority carrier traps, which reduces the local charges, the SCR width will be wider, implying a decrease of the junction capacitance. Therefore, the majority carrier trapping will result in a negative DLTS peak. The same argument can be applied to the n^+p junction diodes. All of the samples used in the DLTS measurements are p^+n diodes so that a positive peak represents the hole trap and a negative peak represents the electron trap.

3.5.2. Defect Concentration

The defect concentration is directly proportional to the peak height as described before, and the peak height is proportional to the capacitance change $C(\theta)$. Therefore, the defect concentration N_t is proportional to $C(\theta)$ which can be derived as follows: Let $C(t)$ be the capacitance transient^[39,40] which is proportional to electrons (hole) emitted to the conduction (valence) band, then,

$$\begin{aligned} C(t) &= A\{q \epsilon_s [N_d - N_t \exp(-t/\tau)] / [2(\phi_j + V_r + kT/q)]\}^{1/2} \\ &= C_0 \{1 - [N_t \exp(-t/\tau) / N_d]\}^{1/2} \end{aligned} \quad (3.18)$$

where t is time; τ is the carrier emission time constant; $C_0 = C(V_r)$, as shown in Eq.(3.13), is the junction capacitance at the quiescent reverse bias condition. Using binomial expansion and the condition that $N_t/N_d \ll 1$, Eq. (3.18) reduces to a simple form as:

$$C(t) = C_0 [1 - N_t \exp(-t/\tau) / 2N_d] \quad (3.19)$$

Eq.(3.19) can be rewritten as:

$$N_t \exp(-t/\tau) = (2 \Delta C(t) / C_0) N_d \quad (3.20)$$

where $\Delta C(t) = C_0 - C(t)$. From DLTS measurement, $C(0)$ can be determined. The junction capacitance C_0 and the background concentration can be obtained from C-V measurements. Thus, the defect concentration N_t can be calculated easily by using Eq.(3.20) at $t=0$.

3.5.3. Activation Energy of the Defect Level

The decay time constant in the capacitance transient during the DLTS experiment is associated with a specific time constant which is equal to the reciprocal of the emission rate. For an electron trap, the emission rate " e_n " is functions of temperature, capture coefficient and activation energy, and can be expressed by^[41,42]

$$e_n = (\sigma_n \langle v_{th} \rangle N_c / g) \exp[(E_c - E_t)/kT] \quad (3.21)$$

where E_t is the activation energy of the trap; g is the degeneracy factor; σ_n is the electron capture cross section which is temperature dependent^[43], and is given by

$$\sigma_n = \sigma_{\infty} \exp(-\Delta E_p/kT) \quad (3.22)$$

where σ_{∞} is the capture cross section at very high temperature; ΔE_p is the activation energy of the capture cross section for the trap. e_n can be written as:

$$\begin{aligned} e_n &= BT^2 \exp\{[E_c - (E_t + \Delta E_p)] / kT\} \\ &= BT^2 \exp [(E_c - E_m) / kT] \end{aligned} \quad (3.23)$$

where B is the proportionality constant, and is independent of temperature. From this relation, e_n increases with increasing temperature. The capacitance transient is rearranged from Eq.(3.19) as:

$$\begin{aligned} C(t) &= C_0 (N_t / 2N_d) \exp(-t/\tau) \\ &= \Delta C(\theta) \exp(-t/\tau) \end{aligned} \quad (3.24)$$

where $\tau = e_n^{-1}$, is the reciprocal emission time constant.

The procedures for determining the activation energy of a defect level in a semiconductor is described as follows. We first set t_1 and t_2 in a dual-gated integrator boxcar, then we can write:

$$C(t_1) = C(\theta) \exp(-t_1/\tau) \quad (3.25)$$

$$C(t_2) = C(\theta) \exp(-t_2/\tau) \quad (3.26)$$

The DLTS scan along the temperature axis is obtained by taking the difference of Eq.(3.25) and (3.26), which yields:

$$S(\tau) = C(\theta) [\exp(-t_1/\tau) - \exp(-t_2/\tau)] \quad (3.27)$$

The maximum emission rate, τ_{\max}^{-1} , is obtained by differentiating $S(\tau)$ with respect to τ , and sets $dS(\tau)/d\tau = 0$, which yields:

$$\tau_{\max} = (t_1 - t_2) / \ln(t_1/t_2) \quad (3.28)$$

Under this condition, $S(\tau)$ reaches its maximum value at a specific temperature. The emission rate is given by $e_n = 1/\tau_{\max}$ for each t_1 and t_2 setting. By changing t_1 and t_2 several times, a set of temperatures correspond to this set of τ_{\max} (or emission rate e_n) can be obtained as shown in Fig.3.1. The activation energy of the trap can be calculated from the slope of the Arrhenius plot.

D L T S

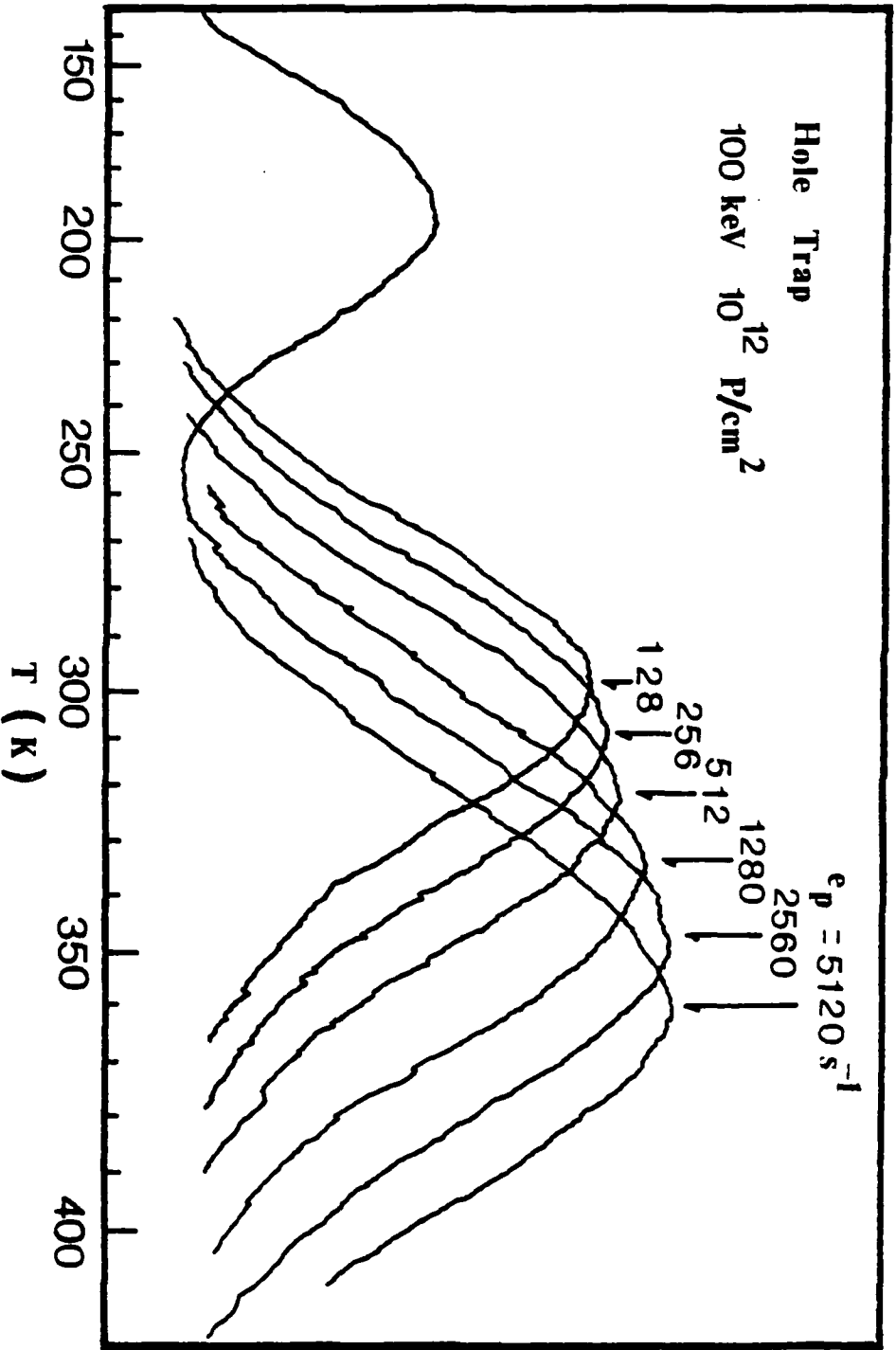


Fig.3.1 DLTS scans of hole traps in proton irradiated GaAs for different window rates.

IV. DETERMINATION OF POTENTIAL WELL OF DEEP-LEVEL TRAPS IN GaAs

Deep-Level Transient Spectroscopy (DLTS) signals are often analyzed assuming that the capacitance transient is exponential. However, most of the DLTS signals are nonexponential transient^[15,16]. Nonexponential capacitance transients may occur from: (1) electric field dependent emission rate of the trapped charge^[44,45], (2) multiexponential decay due to several trap levels with similar emission rates, and (3) trap density of the same magnitude as that of the shallow dopant density^[46,47]. This chapter will deal with cases (1) and (2).

To determine the nonexponential capacitance transient due to electric field dependent emission rate of the trapped charge, Makran-Ehid^[48,49] and Wang et al^[50,51] have measured the field enhancement emission rate. In this chapter, we present the theoretical analysis of nonexponential capacitance transients due to the electric field dependence emission rate of trapped charge and multiexponential decay. Emission rate of trapped charge carriers is enhanced by the Poole-Frenkel effect and phonon-assisted tunneling effect in the presence of an applied electric field. Since the electric field varies with position within the depletion region of a reverse biased p-n junction, the emission rate is not constant within the same region. The DLTS response due to the nonuniformed emission rates can in general be expressed by $S(t) = \sum \exp(-e_{nj}t_1) - \sum \exp(-e_{nj}t_2)$. Based on the nonexponential capacitance transient, theoretical calculations of DLTS response for the deep-level traps in GaAs are made using five different potential wells; namely, the Coulombic potential well which has a positive charge state for the empty state, the Dirac well, square well, polarization well as well as dipole well which all have a neutral charge state from different physical origins. A comparison of the theoretical

calculations of nonexponential DLTS response with the DLTS data for each trap level would allow us to determine the potential well for the trap involved. This model was applied to the calculations of potential well for the EL2 level and other electron traps in GaAs. We found that the EL2 electron trap was due to Coulombic potential well with a double charge state (i.e., As_{Ga}^{++}). Details of the results will be discussed in this chapter 6..

4.1 Capture and Emission process at a Deep-Level Trap.

In the study of electric field dependence of emission rate, it is important to know the charge state of a trap so that the type of potential well for such a trap can be determined. The charge state of a deep-level trap may be either positively charged, neutral, or negatively charged^[10] (i.e., N_t^+ , N_t^0 or N_t^-). For example, if an electron is captured by a positive donor trap, then the kinetic equation for the capture process requires that:

$$N_t^+ + e = N_t^0. \quad (4.1)$$

In this case, the capture process is Coulombic attractive. Similarly, the emission process for the same trap can be written as

$$N_t^0 = N_t^+ + e, \quad (4.2)$$

which again is an attractive process. This attractive capture-emission process is the feature of a Coulombic potential well. In GaAs, for example, the deep-level defects such as arsenic vacancy^[52] (V_{As}^+) and arsenic antisite^[13] (As_{Ga}^{++}) defects have a Coulombic potential well.

For an empty neutral trap with N_t^0 , the capture process is given by

$$N_t^0 + e = N_t^-, \quad (4.3)$$

, and the emission process for the same trap is given by

$$N_t^- = N_t^0 + e. \quad (4.4)$$

The potential wells for a deep-level neutral trap in a semiconductor may include Dirac delta potential well^[53], square potential well, polarization potential well and dipole potential well^[54]. The Dirac delta potential well does not show Poole-Frenkel effect. Neutral arsenic vacancy (V_{As}^0) defect in a GaAs crystal behaves as a Dirac delta potential well in the capture-emission process. For the square potential well, its potential well has a depth of V_0 for $r < r_0$ and zero for $r > r_0$. Deep-level defect such as neutral arsenic interstitial (As_i^0) has this characteristics. The potential of a polarization potential well has the form $V(r) = -A_1 / r^4$, where $A_1 = e^2 \alpha_j / 8 \epsilon_0 \epsilon_s^2$; α_j is the polarizability of a neutral impurity atom, and ϵ_s is the relative dielectric constant of the host crystal. Lax^[55] used a polarization potential well to model capture of electrons and holes by neutral impurities. Tasch and Sah^[44] used this potential well to model the observed field dependence of Au in silicon. Neutral impurity trap such as Al_{Ga}^0 has the properties of a polarization potential well. A complex of two oppositely charged centers, each with charge magnitude of Zq , will form a dipole potential well. The potential is represented by a dipole potential, $V(r) = q\vec{r} \cdot \vec{P} / 4 \epsilon_0 \epsilon_r s^2$, with a dipole moment given by $P = Z q R_0$, where R_0 is the distance separating the two charge centers. The antisite pair defect ($As_{Ga}^{++} Ga_{As}^{--}$) behaves as a dipole potential well in the capture-emission process.

For the process $N_t^- + e = N_t^{--}$, the trapping process is repulsive and the trap in N_t^- state has a Coulombic energy barrier that the electron must surmount thermally or tunnel through. Thus one may expect its capture cross section to be very small ($\sim 10^{-21}$ cm² or less) and with a strong temperature dependent property.

In DLTS technique^[7,14], electrons captured by a trap level are occurred in the quasi-neutral region (QNR) of a p-n diode which has zero electric field. On the other hand, electrons emission from a trap level usually take place in the space-charge region (SCR) of a p-n diode in which high electric field prevails in this region. Fig.4.1 shows that the capture process in QNR and emission process in SCR. The effect of electric field on the emission process is to enhance the emission rate by either Poole-Frenkel effect or phonon-assisted tunneling effect to be discussed in next section. The emission rate enhanced by the electric field will result in a nonexponential DLTS response.

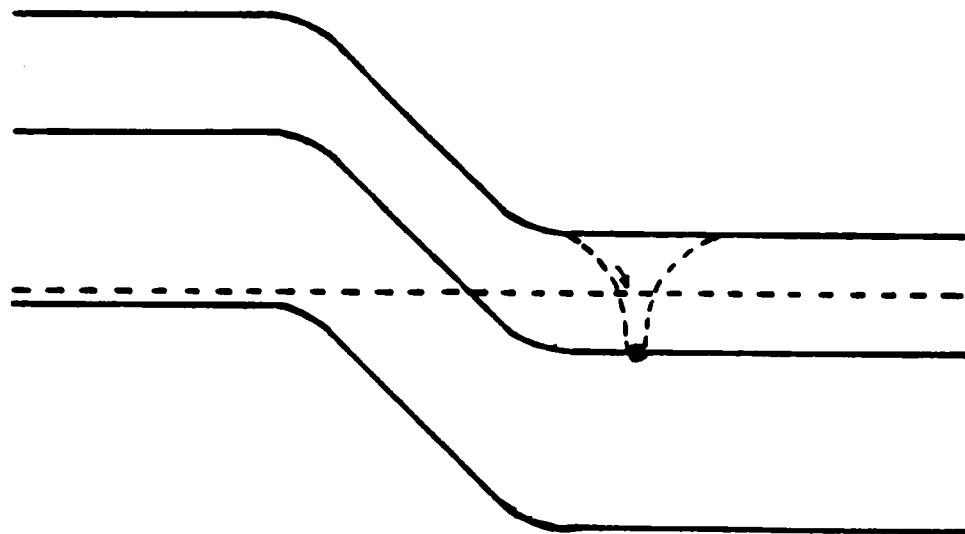
4.2 Overview of the Theory.

The emission rate is based on the detailed balance expression^[41,42], and under zero electric field condition, Eq.(3.23) is rearranged as:

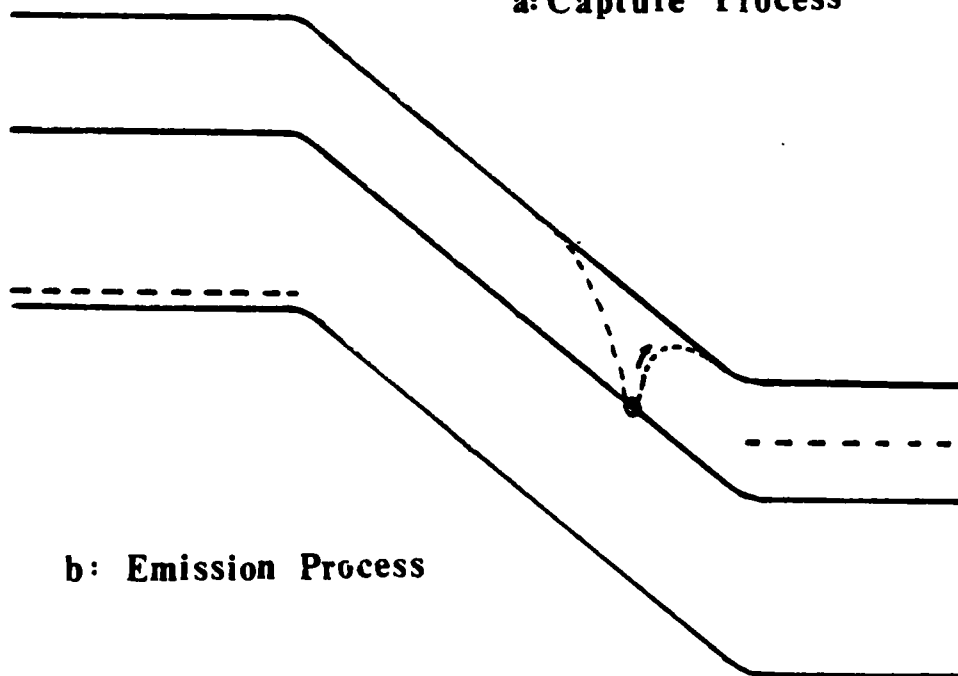
$$e_{no} = e_n \exp(- E_{tj}/kT) \quad (4.5)$$

where E_{tj} is the ionization energy of the trap level, and e_n contains the matrix elements of the transition. Fig.4.2 shows a trap level under high electric field. There are three basic mechanisms^[54] which affect the emission rate enhancement under high electric field conditions.

- (1) Poole-Frenkel effect, in which electrons climb over a barrier lowered by the presence of applied electric field.
- (2) Phonon-assisted tunneling effect, in which electrons absorb



a: Capture Process



b: Emission Process

Figure.4.1 (a) Electron captured by a trap center in the quasi-neutral region (QNR) of the p-n junction.
 (b) Electron emission from a neutral trap center in the space-charge region of the p-n junction.

thermal energy from the lattice, and then tunnel through the barrier at a higher energy.

- (3) Pure quantum mechanical tunneling effect. Since pure tunneling becomes important only at very high electric fields^[56] (i.e. $F > 10^7$ V/cm), we will not consider this effect in our DLTS analysis.

4.2.1 Poole-Frenkel effect.

The Poole-Frenkel effect is associated with the lowering of potential barrier of a deep-level trap in a bulk semiconductor. Both the donor and acceptor traps will show the Poole-Frenkel effect. The enhancement of emission rate from a Coulombic potential well due to Poole-Frenkel effect was first done in a one-dimensional model by Frenkel^[57], and later extended to three-dimensional case independently by Hartke^[58] and Jonscher^[59]. A similar calculation for the polarization well and dipole well was done by Martin et al^[54].

In this section we will consider the general case for calculating the emission rate enhancement due to Poole-Frenkel effect. The potential for a deep-level trap in an electric field, F , can be expressed by:

$$V_T(r) = V(r) - q F r \cos(\theta) \quad (4.6)$$

where $V(r)$ is the potential of a deep-level trap. For $0 < \theta < \pi/2$, the minimum potential was found by setting $dV_T(r)/dr = 0$ at $r = r_{\max}$. The lowering of potential barrier due to the presence of an applied electric field is found by evaluating $V_T(r)$ at $r = r_{\max}$. Thus,

$$\Delta E_{ti}(\theta) = V_T(r_{\max}) \quad (4.7)$$

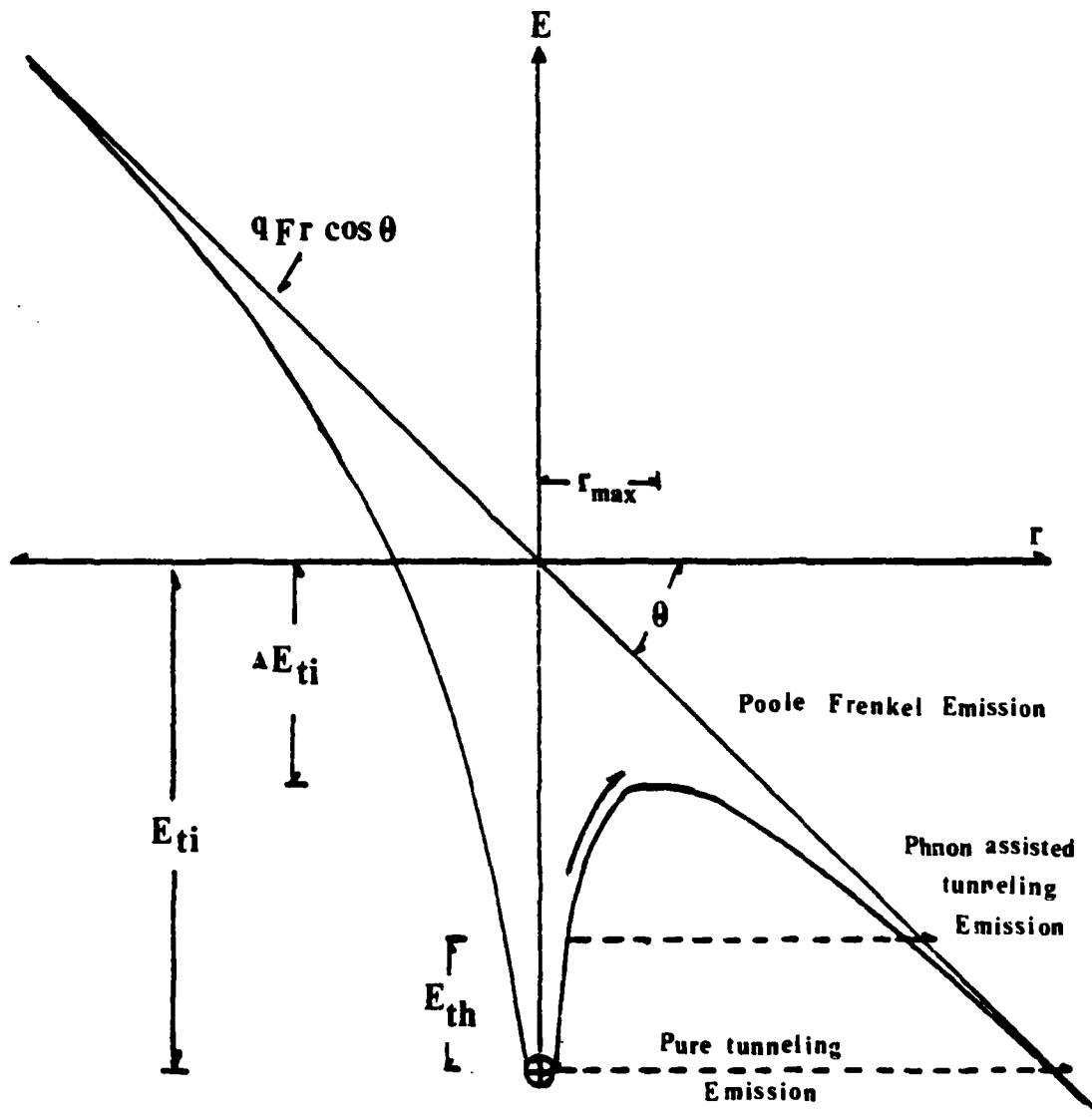


Fig.4.2 Enhancement of electron emission rate by: (1) Poole-Frenkel effect, (2) phonon-assisted tunneling effect, (3) pure quantum mechanical tunneling effect.

One dimensional result is given by setting $\theta = 0$. The Poole-Frenkel effect leads to a decrease in ionization energy, and the one dimensional thermal emission rate, e_{n1} , in the presence of an electric field can be written as

$$\begin{aligned} e_{n1} &= e_{n0} \exp[-(E_{tj} - \Delta E_{tj}) / kT] \\ &= e_{n0} \exp(E_{tj}/kT) \end{aligned} \quad (4.8)$$

where e_{n0} is the thermal emission rate at zero electric field given by Eq.(4.5). The three-dimensional calculation requires an integration over θ due to the spatial variation of $E_{tj}(\theta)$. For $0 < \theta < \pi/2$, the emission rate is proportional to θ , and for $\pi/2 < \theta < \pi$, it is assumed that the emission rate does not change with electric field. Thus,

$$e_{n3}/e_{n0} = (1/4\pi) \left[\int_0^{2\pi} d\phi \int_0^{\pi/2} \sin(\theta) \exp(\Delta E_j/kT) d\theta + \int_0^{2\pi} d\phi \int_{\pi/2}^{\pi} \sin(\theta) d\theta \right] \quad (4.9)$$

where e_{n3} is the three dimensional thermal emission rate.

4.2.2 Phonon-assisted tunneling effect.

There are several different types of potential wells which may exist in a deep-level trap, depending on the charge state of a particular trap. The potential well may be affected by an external electric field. Fig.4.3 shows a potential well for a trap level with energy of E_{tj} as a function of the radial coordinate. A trapped electron can absorb a phonon and tunnel through the barrier. The tunneling process can be treated by using the WKB^[60] (Wentzel-Kramers-Brillouin) approximation for the potential barrier. The probability ratio^[61], (or the barrier penetration factor, P) for an electron impinging on the barrier is given by

$$P = \exp\left[-2 \int_{x_1}^{x_2} k(x) dx\right]$$

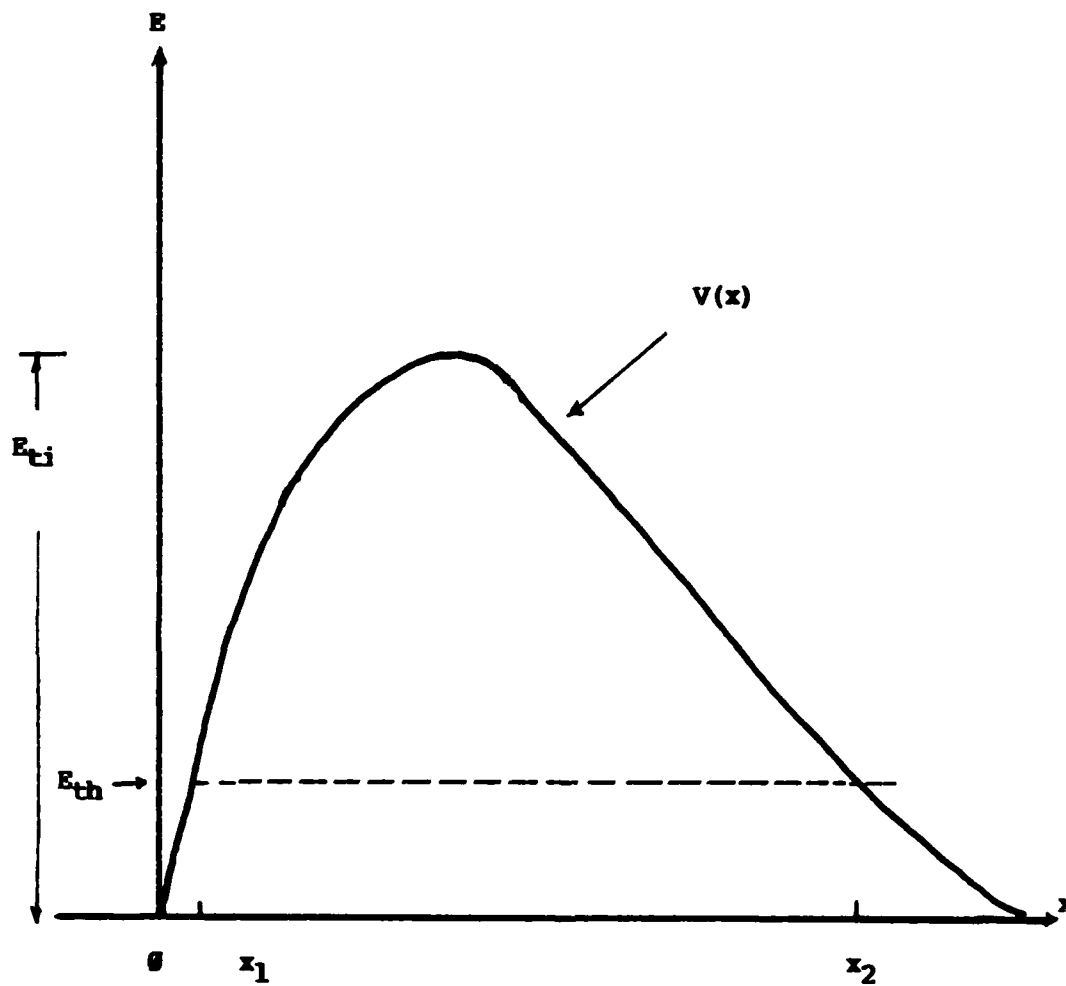


Fig. 4.3 Phonon-assisted tunneling of an electron through a potential barrier of a trap center.

$$= \exp\{-[(8m^*)^{1/2}/\hbar] \int_{x_1}^{x_2} [V(x)-E]^{1/2} dx\} \quad (4.10)$$

where $k(x) = [(2m^*)^{1/2}/\hbar] \times [V(x)-E]^{1/2}$ is positive when $V(x) > E$. $V(x)$ is the potential well for the trap level. E is the electron energy. x_1 and x_2 are the two turning points for which electron energy is equal to the barrier energy of the trap potential well.

A trapped electron can absorb a phonon with energy of $\exp(-E_{th}/kT)$ and tunnel through the barrier at a higher energy. The probability of this composite event is

$$P_C = \exp(-E_{th}/kT) P \quad (4.11)$$

where E_{th} is the thermal excitation energy or phonon energy; and P is given by Eq.(4.10). The emission rate due to phonon-assisted tunneling effect is given by integrating Eq.(4.11) over the phonon energy, E_{th} .

$$e_{nt} = \int_0^{E_j/kT} P_C dE_{th}/kT \quad (4.12)$$

where $1/kT$ is a normalization factor. The normalized emission rate enhancement is obtained by dividing Eq.(4.12) by the zero electric field emission rate e_{no} , which yields

$$\begin{aligned} e_{nt}/e_{no} &= \exp(E_j/kT) \int_0^{E_j/kT} P_C dE_{th}/kT \\ &= \exp[(E_{tj}-E_{th})/kT] \int_0^{E_j/kT} \exp\{-[(8m^*)^{1/2}/\hbar] \\ &\quad \times [V(x)-E] dx\} dE_{th}/kT \end{aligned} \quad (4.13)$$

Eq.(4.13) is a general expression for the emission rate enhancement due to phonon-assisted tunneling effect.

The total emission rate enhancement is obtained from the sum of Poole-Frenkel effect and phonon-assisted tunneling effect. From Eq.(4.9) and (4.13), one obtains:

$$e_{nH} = e_{no}(e_{n3} + e_{nt}) \quad (4.14)$$

Vincent et al [53] and Martin et al [54] showed that for a Coulombic well and other types of potential wells, both the Poole-Frenkel effect and phonon-assisted tunneling effect are important over the field range of interest ($10^6 - 10^8$ V/m at 300 K). Our results are in good agreement with this observation, as will be shown next.

4.3 Theoretical calculations of the emission rate enhancement for different potential wells.

4.3.1 Coulombic potential well.

A donor type electron trap, which has a Coulombic potential well, is positively charged (e.g., N_t^+) when it is empty. The capture and emission process for a such trap is given by Eq.(4.1) and (4.2), respectively. Assuming an electron is at a distance , r , from the trap, the attractive force between a positive trap and the electron is given by

$$F(r) = -q^2 / 4\pi \epsilon_0 \epsilon_r s^2 \quad (4.15)$$

The potential for the trap is obtained by integrating Eq.(4.15) from infinity to r . Thus,

$$V(r) = \int_{\infty}^r F(r) dr = -q^2 / 4\pi \epsilon_0 \epsilon_r r \quad (4.16)$$

When an external field, F , is applied, the total potential energy as a function of distance is given by

$$V_T(r) = -q^2 / 4\pi \epsilon_0 \epsilon_r r - qFr \cos(\theta) \quad (4.17)$$

Electron traps such as As vacancy (V_{As}^+) and As antisite (As_{Ga}^{++}) defects have coulombic potential well for electrons. Eq. (4.17) can also be applied to an acceptor type hole trap, which also has a Coulombic potential well. In this case, the Coulombic potential well is negatively charged when it is empty. The capture process for such a hole trap is

$$N_t^- + h^+ = N_t^0 \quad (4.18)$$

and the emission process is

$$N_t^0 = N_t^- + h^+ \quad (4.19)$$

Hole traps such as Ga vacancy (V_{Ga}^-) and Ga antisite (Ga_{As}^{--}) defects have Coulombic potential well for holes. Compare to other types of potential wells, Coulombic potential well shows a very large Poole-Frenkel effect.

4.3.1.1 Poole-Frenkel effect:

The Poole-Frenkel lowering potential E_{tj} and the location of lowering r_{max} are given by the condition $dV_T(r)/dr = 0$, or

$$r_{max} = \{q/[4\pi \epsilon_0 \epsilon_s F \cos(\theta)]\}^{1/2}$$

$$E_{tj} = q [q F \cos(\theta)/\pi \epsilon_0 \epsilon_r]^{1/2} \quad (4.20)$$

The Poole-Frenkel effect leads to a decrease of ionization energy E_{tj} , and the one-dimensional thermal emission rate is given by Eq. (4.8).

For three-dimensional case, the emission rate of a trapped electron may be obtained by assuming that emission rate is field dependent for $0 < \theta < \pi/2$, and is independent of electric field for $\pi/2 < \theta < \pi$. Integrating Eq.(4.9) yields:

$$e_{n3}/e_{no} = (1/R^2) [e^{R(r-1)} + 1] + 1/2 \quad (4.21)$$

where

$$R = q (qF/\pi \epsilon_0 \epsilon_s)^{1/2} / kT = \Delta E_{tj} / kT \quad (4.22)$$

4.3.1.2 Phonon-assisted tunneling effect:

The phonon-assisted tunneling effect may be evaluated by substituting Eq.(4.17) to Eq.(4.13). Vincent et al [53] has obtained a closed form for the phonon-assisted tunneling effect for a Coulombic potential well, which reads:

$$e_{nt}/e_{no} = \int_0^{(E_{tj} - \Delta E_{tj})/kT} \exp\{z - z^{3/2} [4(2m^*)^{1/2} (kT)^{3/2} / 3qhF]\} \times [1 - (\Delta E_{tj} / zkT)^{5/3}] dz \quad (4.23)$$

The total emission rate consists of Poole-Frenkel and phonon-assisted tunneling effects, which is expressed by:

$$e_{nhc} = e_{no} (e_{n3} + e_{nt}) \quad (4.24)$$

Fig. 4.4 shows the normalized enhanced emission rate vs electric field for the Coulombic potential well for the $E_c - 0.35$ eV electron trap observed in GaAs. It is noted that Poole-Frenkel effect dominates when electric field is lower than 2×10^4 V/cm, while phonon-assisted tunneling effect becomes important for electric field higher than 2×10^4 V/cm.

4.3.2 Dirac Delta Potential well

The potential for a Dirac delta well is given by:

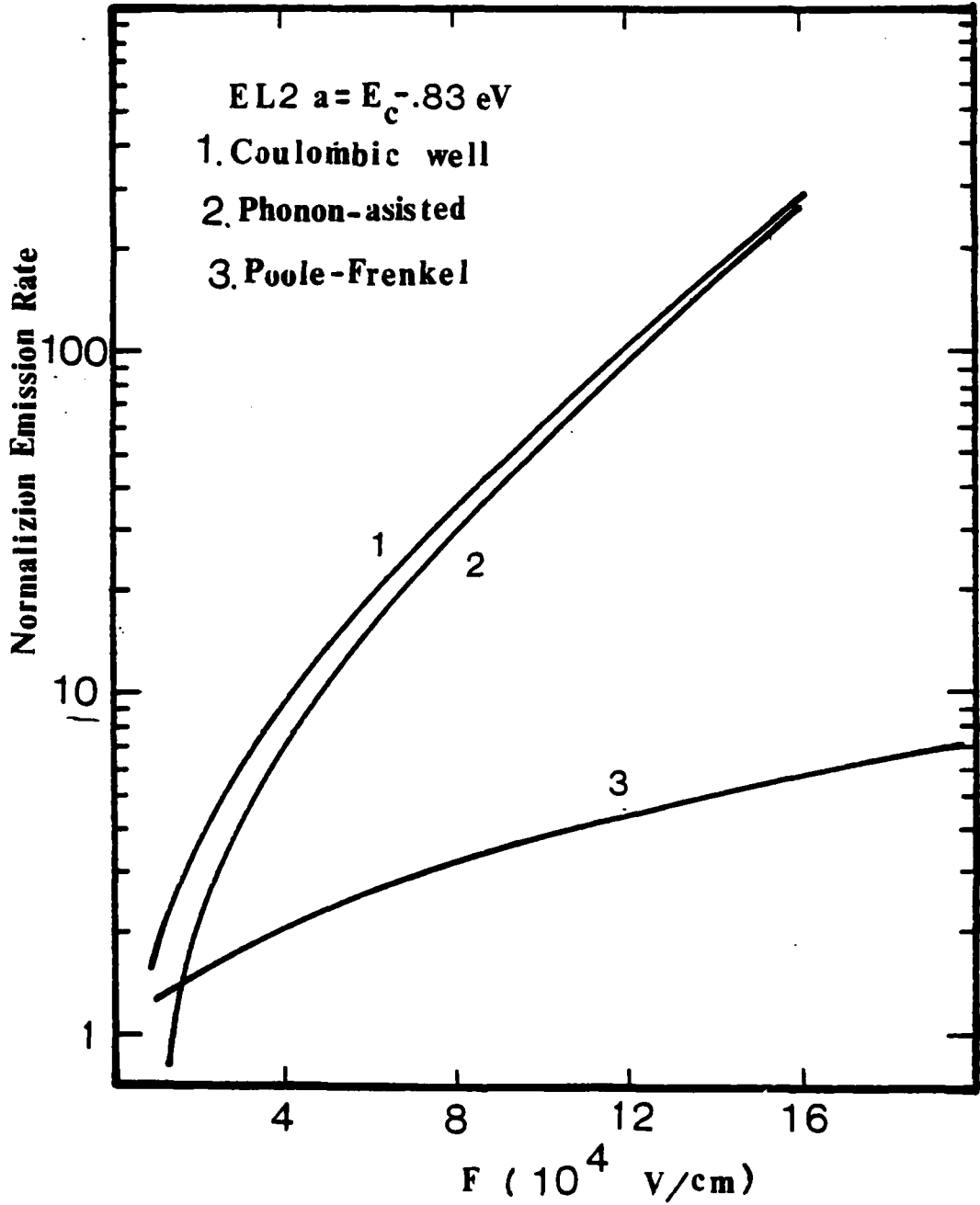


Fig.4.4 Normalized field enhanced emission rate vs electric field for the EL2a electron trap in GaAs calculated at 300 K for (1) Coulombic potential well, (2) phonon-assisted tunneling effect, and (3) Poole-Frenkel effect.

$$\begin{aligned}
 V(r) &= -V_0 & \text{for } r = 0 \\
 &= 0 & \text{for } |r| > 0
 \end{aligned}
 \tag{4.25}$$

In the presence of an applied electric field, the potential is given by

$$\begin{aligned}
 V(r) &= -V_0 - qFr \cos(\theta) & \text{for } r = 0 \\
 &= -qFr \cos(\theta) & \text{for } |r| > 0
 \end{aligned}
 \tag{4.26}$$

Neutral vacancy trap such as neutral arsenic vacancy (V_{As}^0), may possess a Dirac potential well. For this potential well, the Poole-Frenkel lowering potential is equal to zero, and only the phonon-assisted tunneling effect is considered. For the case of a one-dimensional calculation, $\cos(\theta)$ is equal to 1, and the emission rate enhancement is obtained by substituting Eq. (4.26) into Eq. (4.13), which yields:

$$\begin{aligned}
 e_{nt}/e_{no} &= \{ \exp[(E_{ti} - E_{th})/kT] \} \int_0^{E_{ti}/kT} \{ \exp[-(8m^*)^{1/2}/\hbar] \\
 & \quad [\int_{x_2}^{x_1} (-qFx + E_{ti} - E_{th})^{1/2} dx] dE_{th}/kT \} \tag{4.27}
 \end{aligned}$$

Eq.(4.27) gives an analytical form for the transparency of triangular barrier of a Dirac well. For the triangular well, $x_1 = 0$. and $x_2 = (E_{ti} - E_{th})/qF$. Integrating Eq.(4.27) over E_{th} and let $z = (E_{ti} - E_{th})/kT$, we obtain the enhanced emission rate for the phonon-assisted tunneling effect

$$e_{nt}/e_{no} = \int_0^{E_{ti}/kT} \exp\{z - z^{3/2} [4(2m^*)^{1/2} (kT)^{3/2} / 3qF]\} dz \tag{4.28}$$

The total emission rate due to Dirac well can be expressed by:

$$e_{nhr} = e_{no} (1 + e_{nt}) \tag{4.29}$$

4.3.3 Square Potential Well

The same treatment can be applied to the square well. The potential of a square well in the presence of an applied electric field is

$$\begin{aligned} V(r) &= V_0 - qFr \cos(\theta) && \text{for } r < r_0 \\ &= -qFr \cos(\theta) && \text{for } r > r_0 \end{aligned} \quad (4.30)$$

where r_0 is the radius of the trap potential well. Neutral interstitial trap such as neutral arsenic interstitial (As_i^0), may have such a potential well. The barrier lowering due to Poole-Frenkel effect is equal to qFr_0 . The enhanced emission rate for a one-dimensional and a three-dimensional Poole-Frenkel effect is given respectively by:

$$e_{n1}/e_{no} = \exp(R) \quad (4.31)$$

$$e_{n3}/e_{no} = (1/2R)[\exp(R) - 1] + 1/2$$

where $R = qFr_0/kT$.

For the enhanced emission rate due to phonon-assisted tunneling effect, Eq.(4.27) is still valid. In a square well, $x_1 = r_0$ and $x_2 = (E_{tj} - E_{th})/kT$. The range of phonon energy, E_{th} is from 0 to $(E_{tj} - E_{tj})/kT$. Thus, we obtain an expression for the normalized enhanced emission rate due to phonon-assisted tunneling effect:

$$\begin{aligned} e_{nt}/e_{no} &= \int_0^{(E_{tj} - E_{tj})/kT} \exp\{z - z^{3/2} [4(2m^*)^{1/2}(kT)^{3/2}/3q\mathcal{F}]\} \\ &\times [1 - (qFr_0/zkT)^{3/2}] dz \end{aligned} \quad (4.32)$$

The total emission rate for the square well is equal to the sum of Eq.(4.31) and Eq.(4.32), which is given by:

$$\epsilon_{nhs} = \epsilon_{no} (\epsilon_{n3} + \epsilon_{nt}) \quad (4.35)$$

4.3.4 Polarization potential well

An electron with charge, e , at a distance r from a trap center with polarizability, α_j , will induce a dipole moment, $p = \alpha_j e / \epsilon_s r^2$. This dipole will produce an attractive force on the charge of $pe / 2\epsilon_0 \epsilon_s r^3 = \alpha_j e^2 / (2\epsilon_0 \epsilon_s^2 r^5)$. Thus, the attractive potential is given by:

$$V(r) = -A_1 / r^4 \quad (4.34)$$

where $A_1 = \alpha_j e^2 / (8\pi \epsilon_0 \epsilon_s^2)$

The polarizability of the atom can be expressed by

$$\alpha_j / \alpha_H = (m_0 / m) (E_H / E_{tj})^2 \quad (4.36)$$

where E_{tj} is the ionization energy of the trap; $E_H = 13.6$ eV is the ionization energy of a hydrogen atom; $\alpha_H = 0.666 \times 10^{-24}$ cm³ is the polarizability of a hydrogen atom; α_j is the polarizability of the trap; m_0 is the free electron mass; and m is the effective electron mass. Lax^[55] used the polarization potential well to model capture of electrons and holes by neutral impurities. Tasch and Sah^[44] used this potential well to model the observed field dependence emission rate of Au in silicon. Neutral impurity trap such as Al_{Ga}^0 has the properties of a polarization potential well. In the presence of an electric field, the total potential of polarization well is given by

$$V_T(r) = -A_1 / r^4 - qFr \cos(\theta) \quad (4.36)$$

4.3.4.1 Poole-Frenkel effect

The minimum potential is obtained by setting $dV_T(r)/dr = 0$ at $r = r_{max}$, and the result is given by:

$$r_{max} = [4A_1/qF\cos(\theta)]^{1/5} \quad (4.37)$$

$$E_{tj} = -1.649 A_1^{1/5} [qF\cos(\theta)]^{4/5}$$

Note that the emission rate is field dependent for $0 < \theta < \pi/2$, and is independent of electric field for $\pi/2 < \theta < \pi$. Thus, the normalized field enhanced emission rate due to Poole-Frenkel effect can be written as:

$$e_{n1}/e_{no} = \exp(R) \quad (4.38)$$

for the one dimensional case, and

$$e_{n3}/e_{no} = (1/2) [1 + (5/4) \int_0^1 R t^{1/4} \exp(R) dt] \quad (4.39)$$

for the three dimensional case. Here $R = 1.649 A_1^{1/5} (qF)^{4/5} / kT$.

4.3.4.2 Phonon-assisted tunneling effect

Substituting Eq.(4.36) into Eq.(4.13) and letting $z = (E_{tj} - E_{th})/kT$ yields the normalized enhanced emission rate due to the phonon-assisted tunneling effect:

$$e_{nt}/e_{no} = \int_0^{(E_{tj} - \Delta E_{tj})/kT} \exp\{z - [(8m^*)^{1/2}/M] (-A_1/r^4 - qFx + zkT)^{1/2} dx\} dz \quad (4.40)$$

Numerical integration can be carried out by assuming $x_1 = (A_1 / z k T)^{1/4}$ and $x_2 = z k T / q F$. The total enhanced emission rate is

$$e_{nhp} = e_{no} (e_{n3} + e_{nt}) \quad (4.41)$$

Note that integrals given in Eq.(4.39) and (4.40) can not be solved analytically. The numerical calculations of the enhanced emission rates as a function of the electric field are shown in Fig.4.5 for $E_c = 0.35$ eV trap in GaAs at 300 K. The Poole-Frenkel effect is dominant when electric field is lower than 4×10^4 V/cm, while phonon-assisted tunneling effect becomes important for electric field greater than 4×10^4 V/cm.

4.3.5 Dipole potential well

The dipole potential can be represented by a trap center with two oppositely charged ions, each with charge Zq .

$$V(r) = r \cdot p / 4\pi\epsilon_0\epsilon_s r^2 \quad (4.42)$$

where p is the dipole moment. $p = ZqR_0$; R_0 is the distance between two oppositely charges. Antisite pair defect ($As_{Ga}^{++} Ga_{As}^{--}$) behaves as the dipole potential well in the capture-emission process. As is shown in Fig.4.6, if the applied electric field F , forms an angle θ_F with z axis, and is polarized along the z direction, then the total potential becomes:

$$\begin{aligned} V_T(r) = & -qP \cos \theta / 4\pi\epsilon_0\epsilon_s r^2 - qFr \sin(\theta_F) \sin \theta \cos \phi \\ & - qrF \cos(\theta_F) \cos(\theta) \end{aligned} \quad (4.43)$$

4.3.5.1 Poole-Frenkel Effect

The minimum potential is obtained by setting $dV_T(r)/dr = 0$, which yields:

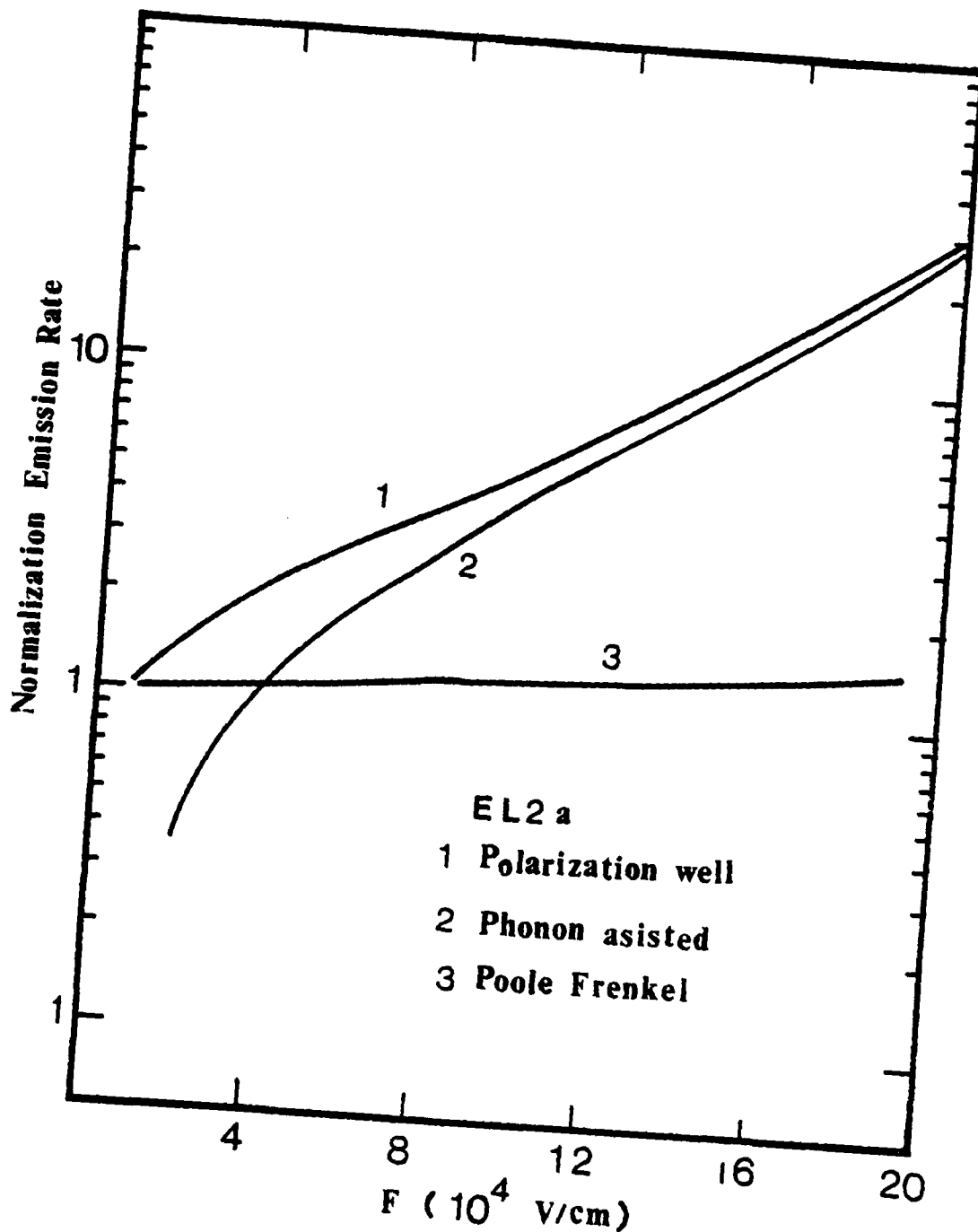


Fig.4.5 Normalized enhanced electron emission rate vs electric field for the EL2-a electron trap in GaAs, assuming (1) polarization potential well, and taking into account (2) phonon-assisted tunneling effect, and (3) Poole-Frenkel effect.

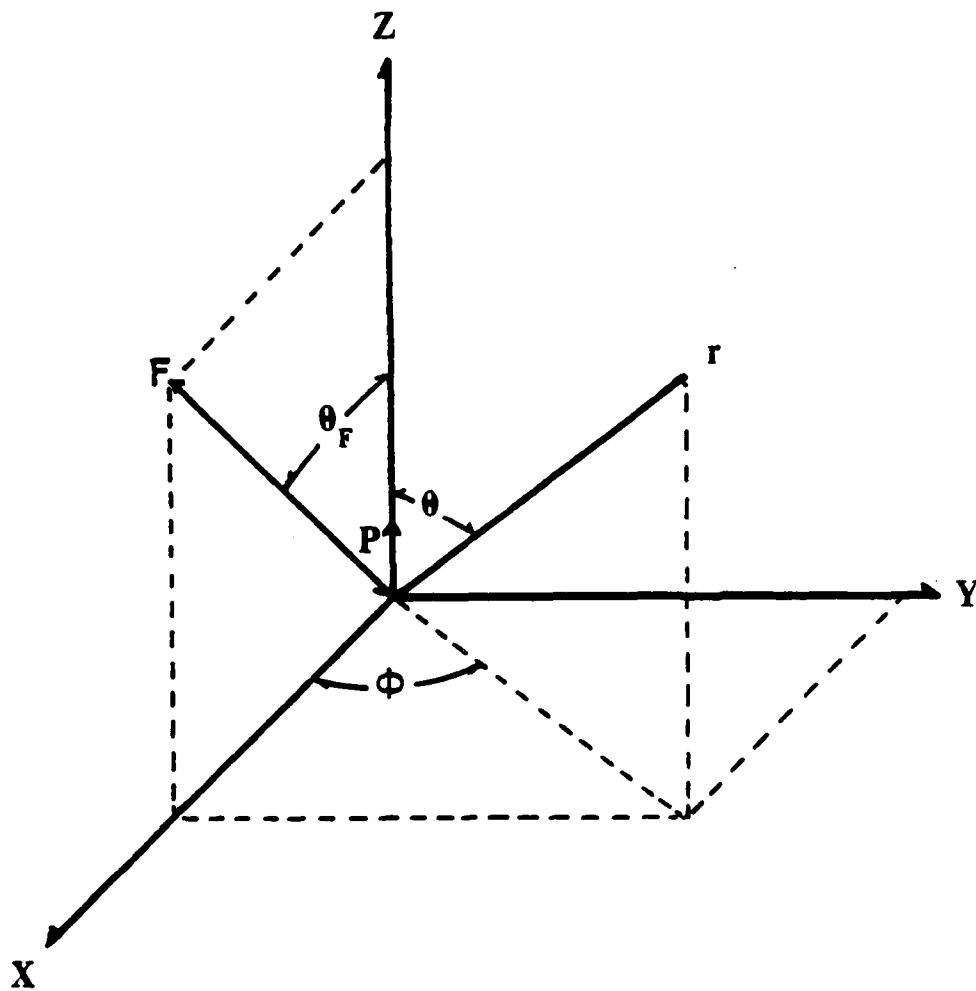


Fig.4.6 Coordinates for the external electric field (F) and dipole moment (P) for a polarization potential well.

$$r_{\max} = \{ P \cos(\theta) / 2\pi \epsilon_0 \epsilon_r [F \sin(\theta_F) \sin(\theta) \cos(\phi) + F \cos(\theta_F) \cos(\theta)] \}^{1/3} \quad (4.44)$$

, and the change in barrier height is given by

$$E_{tj}(\theta, \phi) = -(3 \times 2^{-2/3}) [P \cos(\theta) / 4\pi \epsilon_0 \epsilon_r]^{1/3} \times [F \sin(\theta_F) \sin(\theta) \cos(\phi) + F \cos(\theta_F) \cos(\theta)]^{2/3} \quad (4.45)$$

Unlike other types of potential wells, the dipole potential experiences a barrier lowering which is field dependent. The integral falls into two cases according to the incident angle, θ_F .

1. Case 1: $\theta < \theta_F < \pi/2$

The barrier is lowered for $-\pi/2 < \phi < \pi/2$, and for $\pi/2 < \phi < 3\pi/2$, $\theta < \theta < \tan^{-1}[-\cot(\theta_F)/\cos(\phi)]$.

The normalized field enhanced emission rate is thus given by:

$$e_{n3}/e_{no} = (1/2\pi) \int_{-\pi/2}^{\pi/2} d\phi \int_0^{\pi/2} \sin(\theta) \exp[-\beta \Delta E_{tj}(\theta, \phi)] d\theta + (1/2\pi) \int_{\pi/2}^{3\pi/2} d\phi \int_0^{\tan^{-1}(-\cot\theta_F/\cos(\phi))} \sin(\theta) \exp[-\beta \Delta E_{tj}(\theta, \phi)] d\theta + (1/2\pi) \int_{\pi/2}^{3\pi/2} \{1 + [\cot(\theta_F)/\cos(\phi)]^2\}^{-1/2} d\phi \quad (4.46)$$

2. Case 2: $\pi/2 \leq \theta_F < \pi$

The barrier is increased for $\pi/2 < \phi < 3\pi/2$, and for $-\pi/2 < \phi < \pi/2$, $\theta < \theta < \tan^{-1}[-\cot(\theta_F)/\cos(\theta)]$. The barrier is lowered for $-\pi/2 < \phi < \pi/2$, and for $\tan^{-1}[-\cot(\theta_F)/\cos(\phi)] < \theta < \pi/2$.

The normalized field enhanced emission rate for this case is given by:

$$e_{n3}/e_{no} = 1 - (1/2\pi) \int_{-\pi/2}^{\pi/2} \{1 + [\cot(\theta_F)/\cos(\phi)]^2\}^{-1/2} d\phi \\ + (1/2) \int_{-\pi/2}^{\pi/2} d\phi \int_{\tan^{-1}(-\cot(\theta_F)/\cos(\phi))}^{\pi/2} \sin(\theta) \exp[-\beta \Delta E_{ti}(\theta, \phi)] d\theta \quad (4.47)$$

For $\theta_F = \theta$, the θ dependence disappears, and the problem can be solved analytically. The barrier lowering simplifies to

$$E_{ti} = -1.9 (p/4\pi\epsilon_0\epsilon_r)^{1/3} F^{2/3} \cos(\theta) \quad (4.48)$$

, and the normalized Poole-Frenkel effect emission rate enhancement is given by

$$e_{n3}/e_{no} = (1/R) [\exp(R) - 1] \quad (4.49)$$

where $R = 1.9 (p/4\pi\epsilon_0\epsilon_r)^{1/3} F^{2/3} / kT$.

4.3.5.2 Phonon-assisted Tunneling Effect

For the potential wells studied here, the one-dimensional analysis was done for $\theta = \theta$, where the Poole-Frenkel barrier lowering is dominant. For the dipole well, the maximum barrier lowering occurs at $\theta = \theta_m$, where $\theta < \theta_m < \theta_F$ and $\phi = \theta$. Now, differentiating Eq.(4.46) for ΔE_{ti} with respect to θ at $\phi = \theta$, and setting the result equal to zero, we obtain a solution for θ_m

$$\theta_m = \tan^{-1} \{ (8 + \cos^2(\theta_F))^{1/2} - 3 \cos(\theta_F) \} / 2 \sin(\theta_F) \quad (4.50)$$

Substituting Eq.(4.50) into Eq.(4.44) and Eq.(4.44) into Eq.(4.13), and

letting $z = (E_{tj} - E_{th}) / kT$, the field enhanced emission rate due to phonon-assisted tunneling effect can be expressed as

$$e_{nt}/e_{no} = \int_0^{(E_{tj} - \Delta E_{tj})/kT} \exp\{z - [(8m^*)^{1/2}/h] \int_{r_1}^{r_2} [-qP\cos(\theta_m)/4\pi\epsilon_0\epsilon_s r^2 - qrF \sin(\theta_F)\sin(\theta_m) - qrF \cos(\theta_F)\cos(\theta_m) + zkT]^{1/2} dr\} dz \quad (4.51)$$

Here $r_1 = (qP\cos\theta_m/4\pi\epsilon_0\epsilon_s zkT)^{1/2}$ and $r_2 = zkT/qF[\sin(\theta_F)\sin(\theta_m) + \cos(\theta_F)\cos(\theta_m)]$. The normalized field enhanced emission rate due to phonon-assisted tunneling effect and Poole-Frenkel effect can be calculated by numerical method. The results are shown in Fig.4.7. Thus, the total field enhanced emission rate is

$$e_{nHD} = e_{no} (e_{n3} + e_{nt}) \quad (4.52)$$

Table 4.1 shows the plots for the Coulombic potential well, Dirac well, square well, polarization well and the dipole well. Table 4.2 summarizes the one-dimensional and three-dimensional emission rate due Poole-Frenkel effect for five different potential wells. Fig.4.8 shows the emission rate vs electric field for the Dirac well, square well, polarization well and the Coulombic well as compared with the zero electric field values. The enhanced emission rates are nearly identical for the neutral trap with Dirac well, square well or polarization well. However, the enhanced emission rate for the Coulombic well depends very strongly on the electric field.

4.4 Theoretical Calculations of the Nonexponential DLTS Response for Different Potential Wells.

From the analysis of field enhanced emission rate, the electric field dependent DLTS response can be calculated. This is discussed as follows:

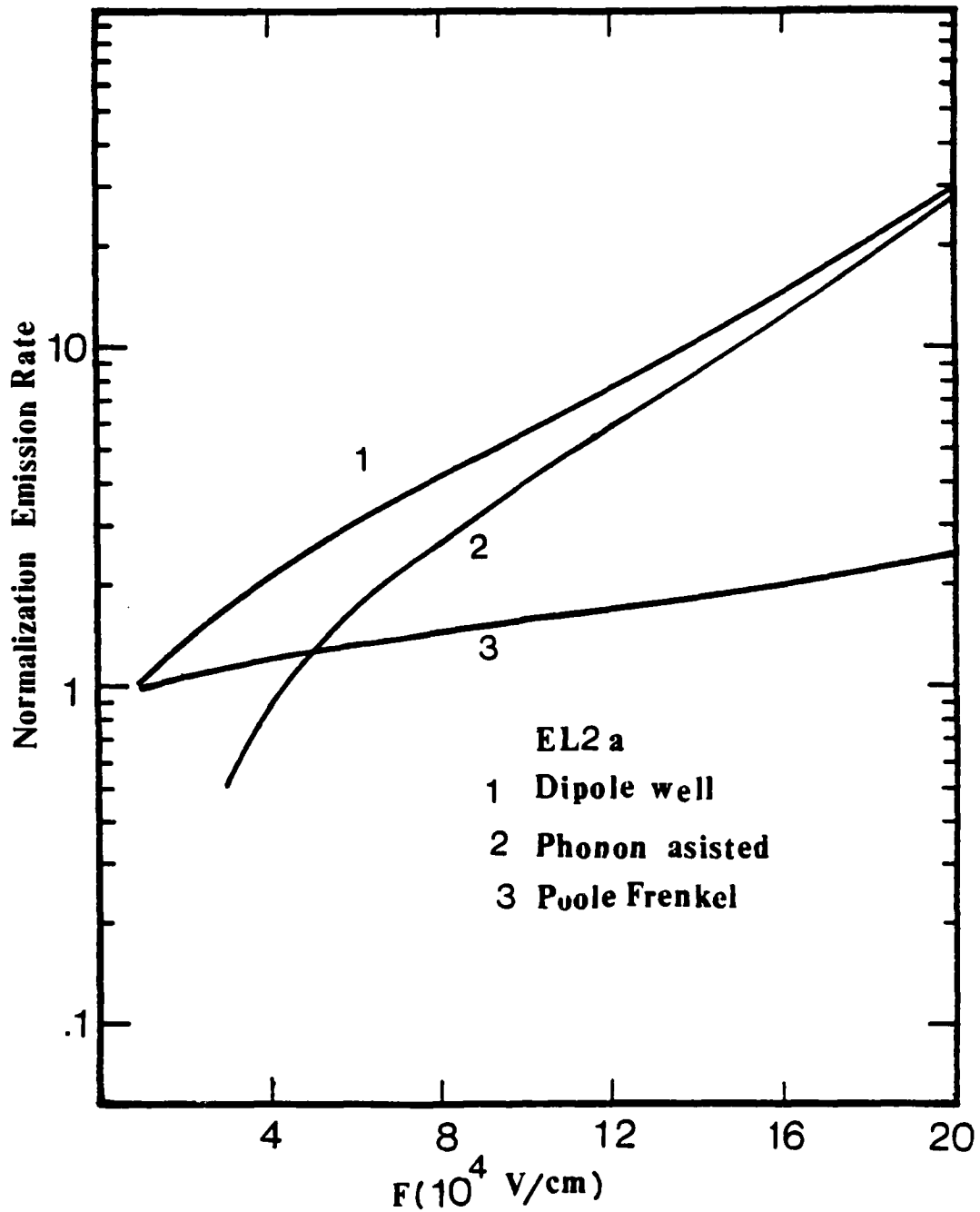


Fig.4.7 Normalized enhanced electron emission rate vs electric field for the EL2-a electron trap in GaAs, assuming (1) dipole potential well and taking into account (2) phonon-assisted tunneling effect and (3) Poole-Frenkel effect, calculated at 300 K.

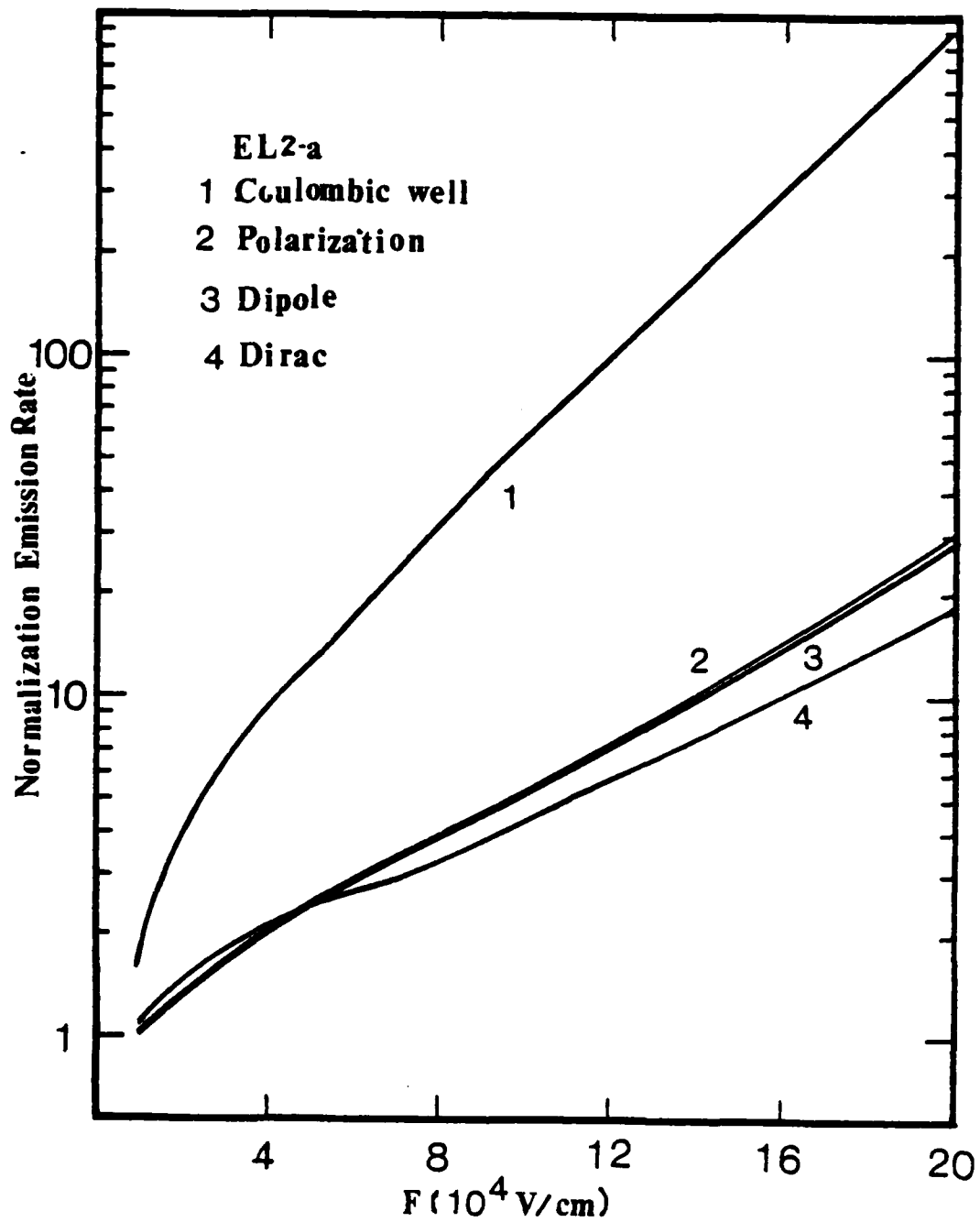


Fig.4.8 Normalized enhanced electron emission rate vs electric field for the EL2-a electron trap in GaAs, assuming (1) Coulombic well, (2) polarization well, (3) dipole well and (4) Dirac well, calculated at 300 K.

Consider a p⁺/n abrupt junction diode, the electric field is in general spatial dependent within the depletion region and can be expressed by:

$$F = F_{\max}(1 - x/W) \quad (4.53)$$

where x is the distance from the junction; F_{max} is the maximum electric field occurred at the metallurgical junction of the diode, and is given by

$$F_{\max} = qN_D w / \epsilon_o \epsilon_r \quad (4.54)$$

w is the depletion width under reverse bias condition.

$$\begin{aligned} w &= [2\epsilon_o \epsilon_r (V_{bi} + V_r) / qN_D]^{1/2} \\ &= L_D [2(V_{bi} + V_r) / kT - 2]^{1/2} \end{aligned} \quad (4.55)$$

L_D is the extrinsic Debye length which is given by

$$L_D = [\epsilon_o \epsilon_r kT / (q^2 N_D)]^{1/2} \quad (4.56)$$

V_{bi} is the built-in potential which reads:

$$V_{bi} = (kT/q) \ln(N_D/n_i) \quad (4.57)$$

n_i is the intrinsic carrier density,

$$\begin{aligned} n_i &= (N_C N_V)^{1/2} \exp(-E_g/2kT) \\ &= 4.9 \times 10^{15} (m_{de} m_{dh} / m_o^2)^{3/4} T^{3/2} \exp(-E_g/2kT) \end{aligned} \quad (4.58)$$

and E_g is the energy bandgap, which is a function of temperature^[41].

$$E_g(T) = E_g(\theta) - \gamma_1 T_2 / (T + \gamma_2) \quad (4.59)$$

E_g(θ) = 1.519eV, γ₁ = 5.405 × 10⁻⁴ eV/K, and γ₂ = 204 for GaAs. Electrons

which are located in the region between W_0 (i.e., zero bias depletion layer width) and W (reverse bias depletion layer width) will be emitted into the conduction band when an applied bias is increased from 0 to $-V_r$, as is shown in Fig.4.9. The depletion width in the junction space charge region is first divided into equally spaced small segments. In each small segment, both the electron trap density and electric field are assumed constant. For each electric field (F_j) strength, there is a corresponding enhanced emission rate, $e_{nj}(F_j)$. If one assumes that the electron emission is exponential transient within each segment, namely, $\exp(e_{nj}t)$, then the total emission transients in the depletion layer region is equal to the sum of the individual components, which can be expressed by:

$$\sum_{j=1}^n \exp[-e_{nj}(F_j)t] \quad (4.60)$$

Thus, the DLTS signal for the nonexponential transient can be expressed by

$$S(\tau) = \sum \exp[-e_{nj}(F_j)t_1] - \sum \exp[-e_{nj}(F_j)t_2] \quad (4.61)$$

where e_{nj} is the electron emission rate within each small segment of the depletion region, as is shown in Eq.(4.14). Values of e_{nj} can be calculated for different potential wells using the equations derived above. From Eq.(4.61), it is noted that the DLTS spectral response is nonexponential. Fig.4.10 illustrates the DLTS response for the EL2 electron trap in GaAs calculated from Eq.(4.61) for different potential wells and for zero electric field. Theoretical calculations showed that the location of DLTS signal peak for the attractive or neutral trap is different along the temperature axis. For Coulombic potential well, the DLTS signal peak occurs at the lowest temperature, while for the neutral trap with Dirac well, square well, or polarization well the peak of the

DLTS signal occurs nearly at the same temperature. Fig.4.11 shows the DLTS spectral response for the EL2 electron trap for the cases of Coulombic well with single- and double-charge state as well as the experimental results. Fig.4.12 illustrates the DLTS signal for the EL2 electron trap in GaAs for a Coulombic well with a double charge states for different window rates. By comparison of the theoretical and experimental DLTS spectral response vs temperature will enable us to determine the potential well for the EL2 electron trap. Our results showed that the most probable potential well for the EL2 trap is the Coulombic well with a double charge states (e.g., $As_{Ga^{++}}$ arsenic antisite defect).

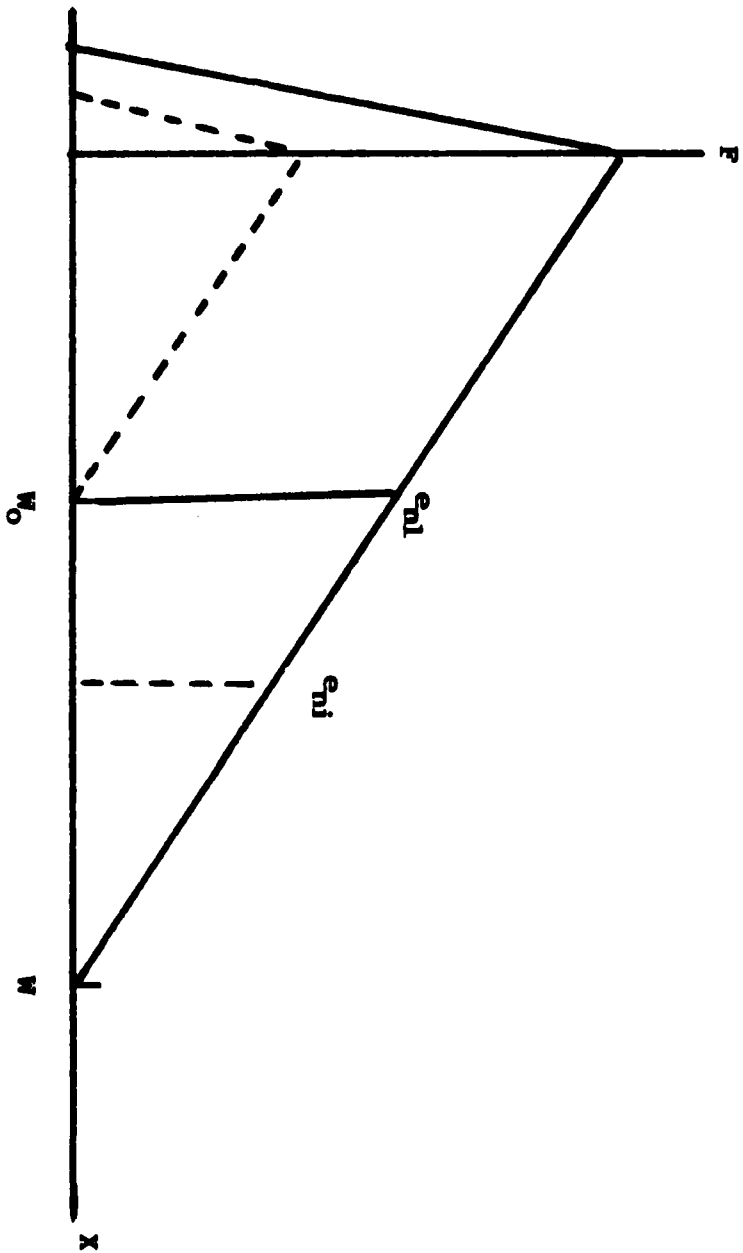


Fig.4.9 Spatial dependence of electric field (F) and electron emission rates (e_{nj}) in the space-charge region of a p^+/n junction diode.

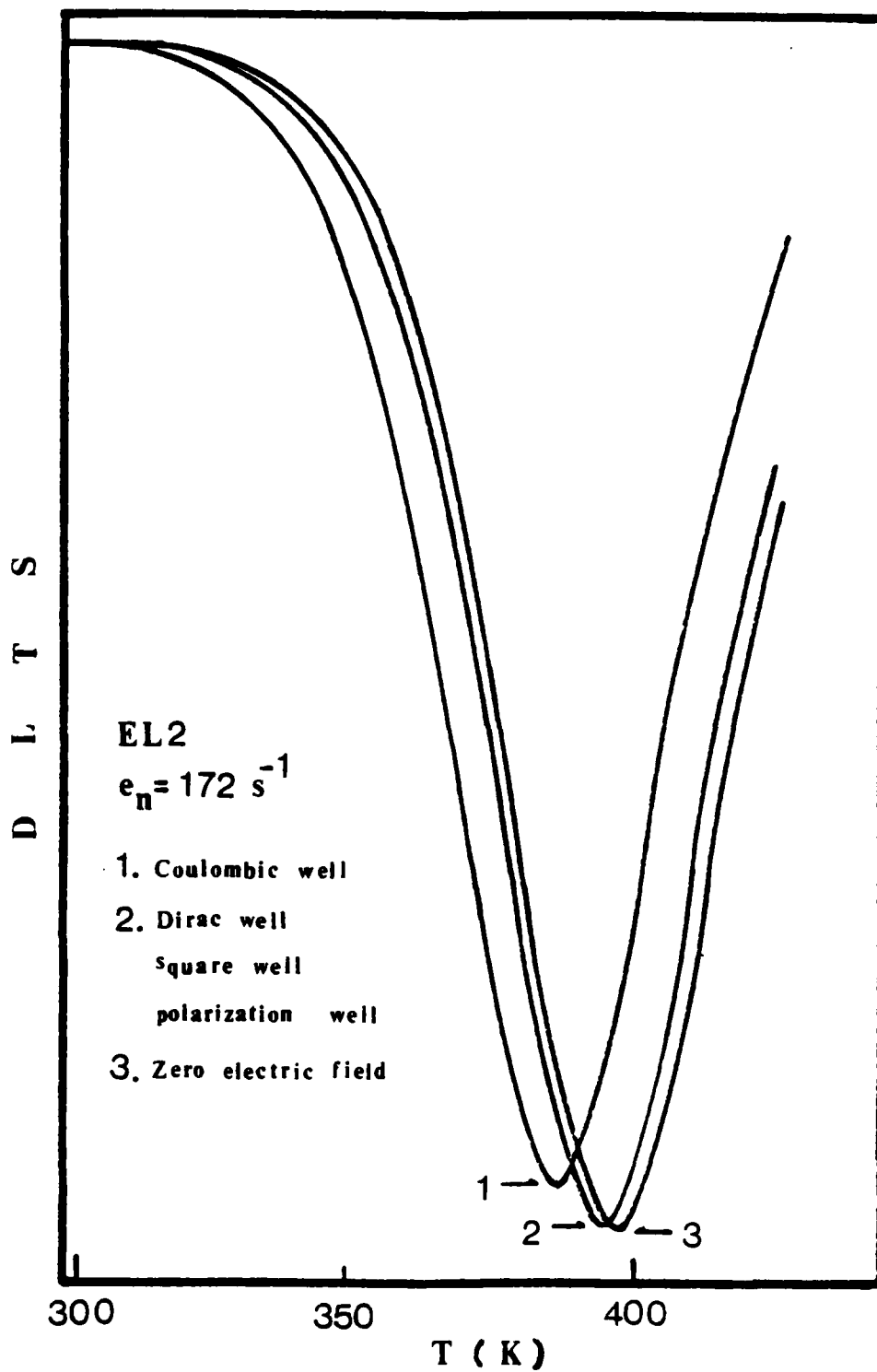


Fig.4.10 Calculated DLTS response for the EL2-a trap in GaAs, assuming (1) Coulombic well, (2) Dirac well, and (3) zero electric field.

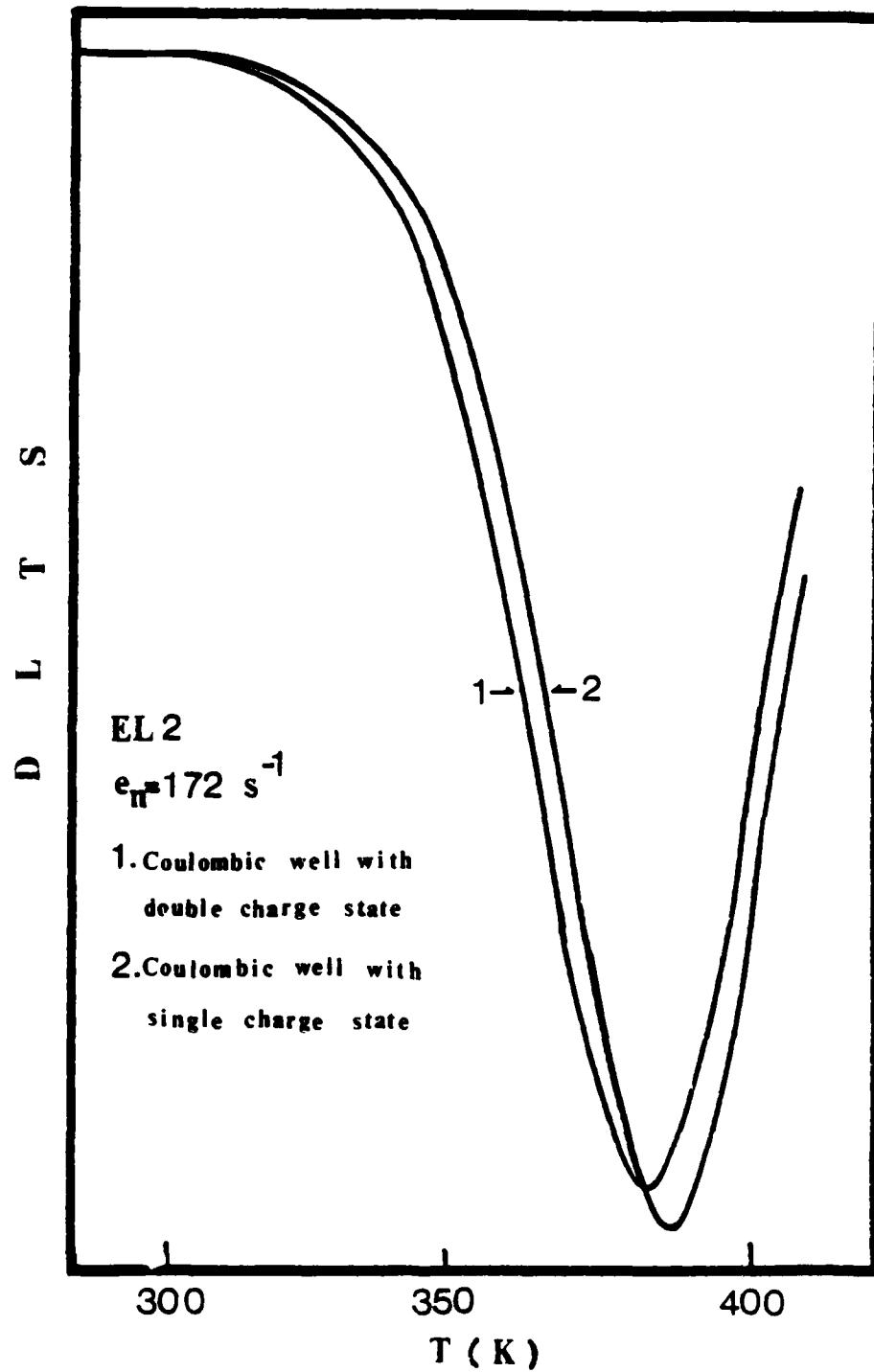


Fig.4.11 Calculated DLTS response for the EL2-a trap in GaAs, assuming Coulombic well with (1) double charge state and (2) single-charge state.

D
L
T
S

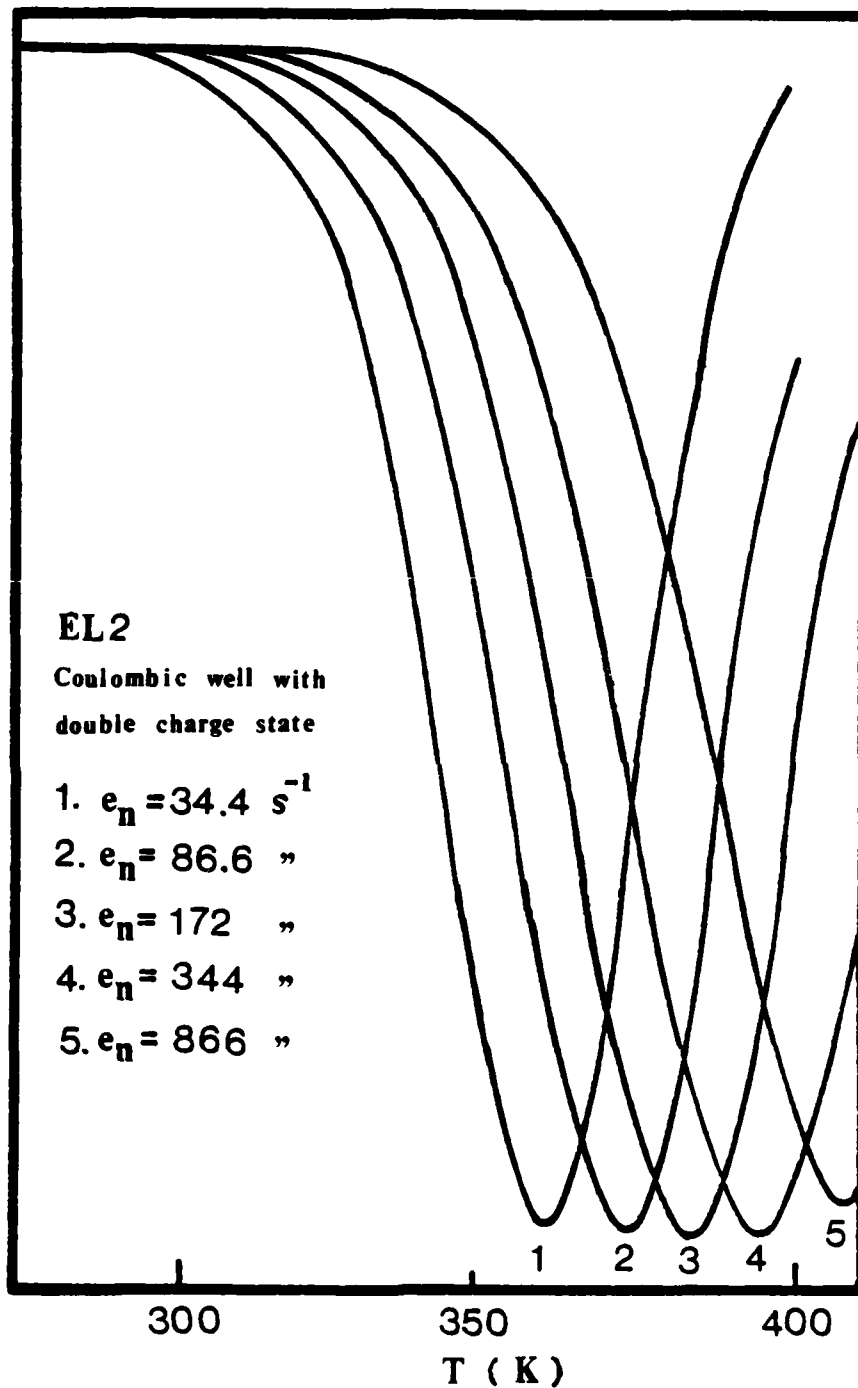
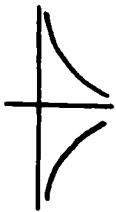
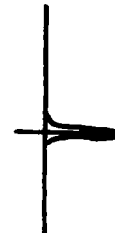
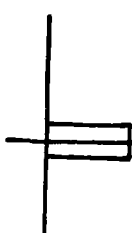
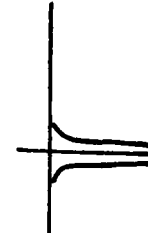


Fig.4.12 Calculated DLTS response for the EL2-a trap in GaAs, assuming Coulombic well with double charge state for five different electron emission rates.

Table 4.1 Summary of the potential, Poole-Frenkel barrier, and r_{\max} for five different potential wells.

Potential well	$V_T(r)$	E_{tj}	r_{\max}
Coulombic well	$-q^2/(4\pi\epsilon_0\epsilon_s r) - qF\cos(\theta)$	$-q(qF/[\pi\epsilon_0\epsilon_s])^{1/2}$	$[q/(4\pi\epsilon_0\epsilon_s F)]^{1/2}$
Dirac well	$V_0 - qF\cos(\theta)$ for $r=\theta$ $-qF\cos(\theta)$ for $r>\theta$	θ	θ
Square well	$V_0 - qF\cos(\theta)$ for $r < r_0$ $-qF\cos(\theta)$ for $r > r_0$	$-qFr_0$	r_0
Polarization well	$-A_1/r^4 - qF\cos(\theta)$	$-1.649A_1^{1/5} (qF)^{4/5}$	$[4A_1/qF]^{1/5}$
Dipole well	$-qP\cos(\theta)/(4\pi\epsilon_0\epsilon_s r^2)$ $-qFr[\sin(\theta_F)\sin(\theta)\cos(\phi) + \cos(\theta_F)\cos(\theta)]$	$-(3x2^{-2/3}) [P\cos(\theta)/(4\pi\epsilon_0\epsilon_s)]^{1/3}$ $x [F\sin(\theta_F)\sin(\theta)\cos(\phi) + F\cos(\theta_F)\cos(\theta)]^{2/3}$	$\{P/[2\pi\epsilon_0\epsilon_s \cos(\theta)]$ $x F[\sin(\theta_F)\sin(\theta)\cos(\phi) + F\cos(\theta_F)\cos(\theta)]\}^{1/3}$

Table 4.2 Summary of enhanced emission rate of one-dimensional and three-dimensional Poole-Frenkel effect for four different potential wells.

Potential well	γ	e_{n1}/e_{n0}	e_{n3}/e_{n0}	Sketch of potential well
Coulombic	$\Delta E_{tj}/kT$	$\exp(\gamma)$	$[\exp(\gamma) (\gamma-1) + 1]/\gamma^2 + 1/2$	
Dirac	0	0	0	
Square	$\Delta E_{tj}/kT$	$\exp(\gamma)$	$[\exp(\gamma) - 1]/(2\gamma) + 1/2$	
Polarization	$\Delta E_{tj}/kT$	$\exp(\gamma)$	$(5/4) \int_0^1 \gamma t^{1/4} \coth(\gamma t) dt$	

V. MODELLING OF NATIVE POINT DEFECTS IN GaAs

Theoretical modelling of native point defects in GaAs is presented in this chapter. Based on chemical reaction and principles of thermodynamics, expressions for the equilibrium defect concentration as functions of temperature and arsenic pressure during crystal growth are derived. Thermal kinetic equations are then employed to predict the possible native defects in GaAs after crystal cooling. For GaAs grown under As-rich or high arsenic pressure condition, it is shown that several native defects such as gallium vacancy (V_{Ga}), arsenic interstitial (As_i), arsenic antisite (As_{Ga}), arsenic antisite-plus-arsenic vacancy ($V_{As}As_{Ga}$) and their complexes may be observed in GaAs material.

5.1 Introduction

GaAs specimens grown by various techniques such as Liquid Encapsulation Czochraski (LEC), Vapor Phase Epitaxy (VPE), Liquid Phase Epitaxy (LPE), Organometallic Chemical Vapor Deposition (MOCVD), and Molecular Beam Epitaxy (MBE) are known likely to produce different defect properties in terms of energy levels within the bandgap of a semiconductor due to differences in the native defects and trace impurities or impurity complexes. In each of these techniques, the growth temperature, growth pressure, growth phase, and cooling rate are usually different. For example, GaAs grown by LPE technique from a gallium melt is expected to be low in gallium vacancy defects and high in arsenic vacancy. The LPE GaAs usually contains hole traps with energy level of $E_v + 0.71$ eV (B-center), while the VPE GaAs grown in high arsenic pressure condition always contains an electron trap with energy of $E_c - 0.83$ eV (EL2 level).

In this chapter, the chemical-thermodynamic principles and thermal kinetic equations are introduced to model the grown-in defects in GaAs. Using chemical-thermodynamic principles to analyze point defects in GaAs was first proposed by Logan and Hurle [52]. They considered the shallow vacancy as well as shallow interstitial levels. Bublik [62] modified their model, and applied it to the deep vacancy level. More recently, Hurle [63] used Frenkel defect instead of Schottky defect for the arsenic vacancy and arsenic interstitial defects. During crystal growth, both V_{Ga} and V_{As} Schottky vacancy pairs are important defects for the undoped GaAs. In the present work, we use V_{Ga} and V_{As} Schottky vacancy pairs with As-Frenkel defect to calculate the vacancy and interstitial concentrations during crystal growth. During crystal cooling from high temperature to room temperature, thermal kinetics is expected to be the dominant mechanism. Since the formation energy for antisite defect is very low in the after-growth condition ($V_{Ga} + As_j = As_{Ga}$, $H = 0.35$ eV), the antisite defect is likely to be the dominant defect after crystal growth, as was proposed by Van Vechten [64].

From the theoretical analysis of GaAs material grown under As-rich or high arsenic pressure condition (e.g., LEC, VPE, and MOCVD techniques), defects such as arsenic interstitial (As_j), gallium vacancy (V_{Ga}), arsenic antisite (As_{Ga}), arsenic antisite-plus-arsenic vacancy ($V_{As}As_{Ga}$), and their complexes are the possible defects in undoped GaAs, while, gallium vacancy (V_{Ga}), arsenic vacancy (V_{As}) and their complexes are the possible grown-in defects in both the MBE and LPE GaAs under low arsenic pressure condition.

Section 5.2 deals with the theoretical calculations of vacancy and interstitial defects in GaAs during crystal growth. Thermal kinetic equations are described in section 5.3. Section 5.4 discusses the possible

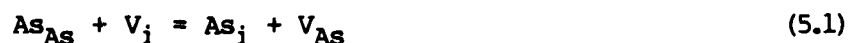
grown-in point defects in GaAs for the As-rich or high arsenic pressure case. The possible grown-in point defects in GaAs for the Ga-rich or low arsenic pressure cases are depicted in section 5.5.

5.2 Theoretical Calculations of Vacancy and Interstitial in Undoped GaAs

In this section, the chemical-thermodynamic principles [62-69] are employed to derive expressions for thermal equilibrium defect concentration as functions of temperature and arsenic pressure in GaAs. Hurle [63] calculated the point defects by considering only As-vacancy and As-interstitial defects in undoped GaAs. However, it is known that Ga-vacancy related defects may play an important role in antisite formation.

In this chapter, we consider several types of point defects such as arsenic monovacancy, V_{As} , positively charged arsenic monovacancy, V_{As}^+ , arsenic interstitial, As_i , positively charged arsenic interstitial, As_i^+ , gallium monovacancy, V_{Ga} , and negatively charged gallium monovacancy V_{Ga}^- .

To deal with the problem of native point defects in GaAs, one can write down the kinetic reaction equations for formation of each type of defects as well as formation of electrons and holes in the crystal. There is an additional reaction equation which represents the transfer of atoms between gas and solid phases. For each of these reactions, there is a mass action which applies in equilibrium. The mass action can be written in terms of concentration. To these mass action equations one adds the condition of charge-neutrality, and the resulting set of equations can then be solved as a function of arsenic partial pressure. Considering the defects cited above, one has the following reaction equations.





Eqs.(5.1) through (5.4) represent the reactions for forming the ionized arsenic Frenkel defects. Eq.(5.5) denotes the transfer of arsenic atoms between solid and gas phases. Eq.(5.6) shows the formation of Schottky pairs. Eq.(5.7) represents the ionization of a Ga-vacancy. The mass action relationships corresponding to the above reactions are given as follows:[62,63]

$$\begin{aligned} K_{fa} &= [\text{As}_j] [V_{\text{As}}] \\ &= 2.92 \times 10^6 \exp(-4.845/kT) \end{aligned} \quad (5.8)$$

$$\begin{aligned} K_{av} &= n [V_{\text{As}}^+] / [V_{\text{As}}] \\ &= 442 \exp(-0.27/kT) \end{aligned} \quad (5.9)$$

$$\begin{aligned} K_{aj} &= n [V_j^+] / [\text{As}_j] \\ &= 4.9 \times 10^9 \times T^{3/2} \exp(-0.4/kT) \end{aligned} \quad (5.10)$$

$$\begin{aligned} K_{cv} &= np \\ &= 1 \times 10^{-12} T^3 \exp(-1.62/kT) \end{aligned} \quad (5.11)$$

$$\begin{aligned} K_{\text{As}2j} &= [\text{As}_j] P_{\text{As}2}^{-1/2} \\ &= 16.4 \exp(-1.125/kT) \end{aligned} \quad (5.12)$$

$$\begin{aligned}
K_S &= [V_{Ga}] [V_{As}] \\
&= 3.286 \times 10^4 \exp(-3.6/kT)
\end{aligned}
\tag{5.13}$$

$$\begin{aligned}
K_{qv} &= p [V_{Ga}^-] / [V_{Ga}] \\
&= 3.7 \times 10^{-8} T^{3/2} \exp(-0.66/kT)
\end{aligned}
\tag{5.14}$$

Square brackets in the above equations denote the concentration. The As_{As} represents arsenic atom at the arsenic site, and is taken as unity. The partial pressure of As_2 in the gas phase is denoted by P_{As_2} . The equilibrium constants appearing on the right handside of Eqs.(5.8) through (5.14) have the general form:

$$K = \exp(S/k) \exp(-H/kT) = K_0 \exp(-H/kT) \tag{5.15}$$

where S and H are the entropy and enthalpy changes for each reaction, respectively. The charge neutrality condition is obtained from Poisson equation:

$$n + [V_{Ga}^-] = p + [V_{As}^+] + [As_j^+] \tag{5.16}$$

Solving Eqs.(5.8) through (5.16) one obtains an expression for n^2 as:

$$\begin{aligned}
n^2 &= \{K_{cv} + (K_{av}K_{fa}/K_{As_2i}) P_{As_2}^{-1/2} + K_{aj}K_{As_2i} P_{As_2}^{1/2}\} \\
&\quad / (1 + K_{qv}K_s K_{As_2i} P_{As_2}^{1/2} / K_{fa}K_{cv})
\end{aligned}
\tag{5.17}$$

Thus, the electron concentration, n , can be calculated from Eq.(5.17), and other defect density can also be deduced from n via Eqs.(5.8) to (5.16). Fig.5.1 shows the defect concentration vs P_{As_2} for $T = 1000$ K. Note that Ga vacancy is the dominant point defect in the entire As_2 pressure range shown. The LPE GaAs is usually grown in the lower As_2 pressure range with

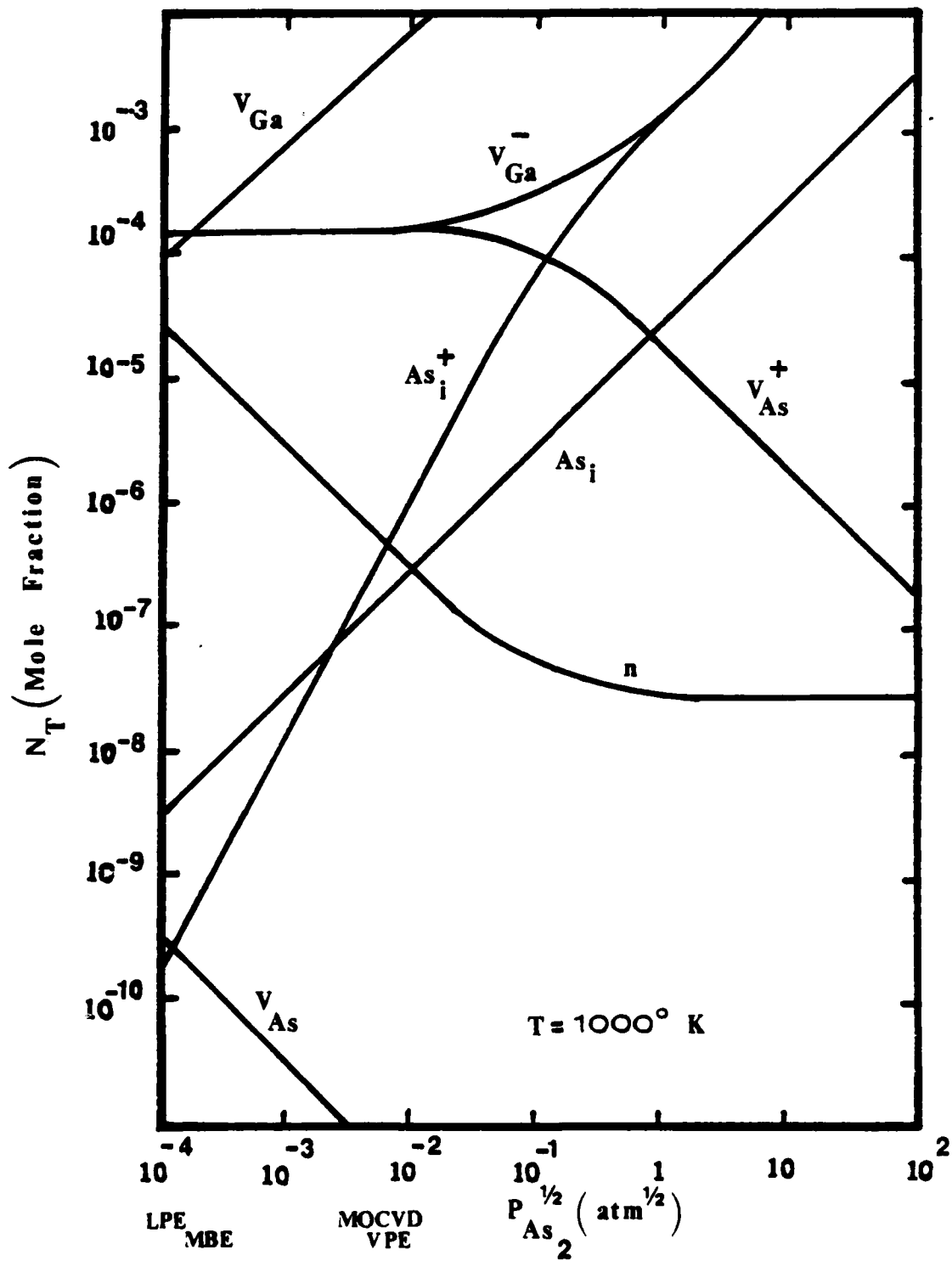


Fig.5.1 Density of native point defects vs As partial pressure for GaAs grown at 1000 K.

$P_{As_2} = 10^{-8}$ atm, and defects such as V_{Ga} , V_{Ga}^- , and V_{As}^+ are the dominant defects. For VPE GaAs with a corresponding partial pressure of 10^{-4} atm, defects such as V_{Ga} , V_{Ga}^- , V_{As}^+ , As_j^+ , and As_j are the dominant defects. In the pressure range between LPE and VPE growth, the concentration of V_{Ga}^- is equal to the concentration of V_{As}^+ . Figure 5.1 also shows that the grown-in defects for the VPE and MOCVD techniques are much more than LPE and MBE growth techniques. Fig.5.2 shows defect density as a function of growth temperature for $P_{As_2} = 5 \times 10^{-3}$ atm. The concentration of V_{Ga}^- monovacancy and V_{As}^+ monovacancy increases with increasing growth temperature, but the density of As_j^+ mono-interstitial decreases with increasing growth temperature.

5.3 Thermal Kinetics after Crystal Growth:

In general, defects will migrate as the crystal cools down from the growth temperature. Thus, one would expect defect concentrations to reach a new equilibrium condition at lower temperature [64,71]. The enthalpy of a single vacancy migration in GaAs is 1.6 eV [64,72]. For examples, if the jump attempt frequency is equal to Debye frequency, then the jump rate will be $4 \times 10^7 \text{ s}^{-1}$ at 1400 K and $5 \times 10^4 \text{ s}^{-1}$ at 1000 K. For example, for a typical crystal to cool down from 1050 K to 950 K in 10 min., simple vacancy would pass through more than 10^8 lattice sites in that period. The migration of vacancy will produce antisite defects, antisite pairs or impurity complexes. In LPE grown GaAs samples, we have observed that samples with faster cooling rate (1° C/min.) would produce more defects than slower cooling rate (0.4° C/min.). Most of the simple vacancies are ionized, and may encounter with other defects to form bound complexes. At room temperature, almost all the vacancies present are likely to interact with other defects to form complexes. To consider the ultimate fate of a

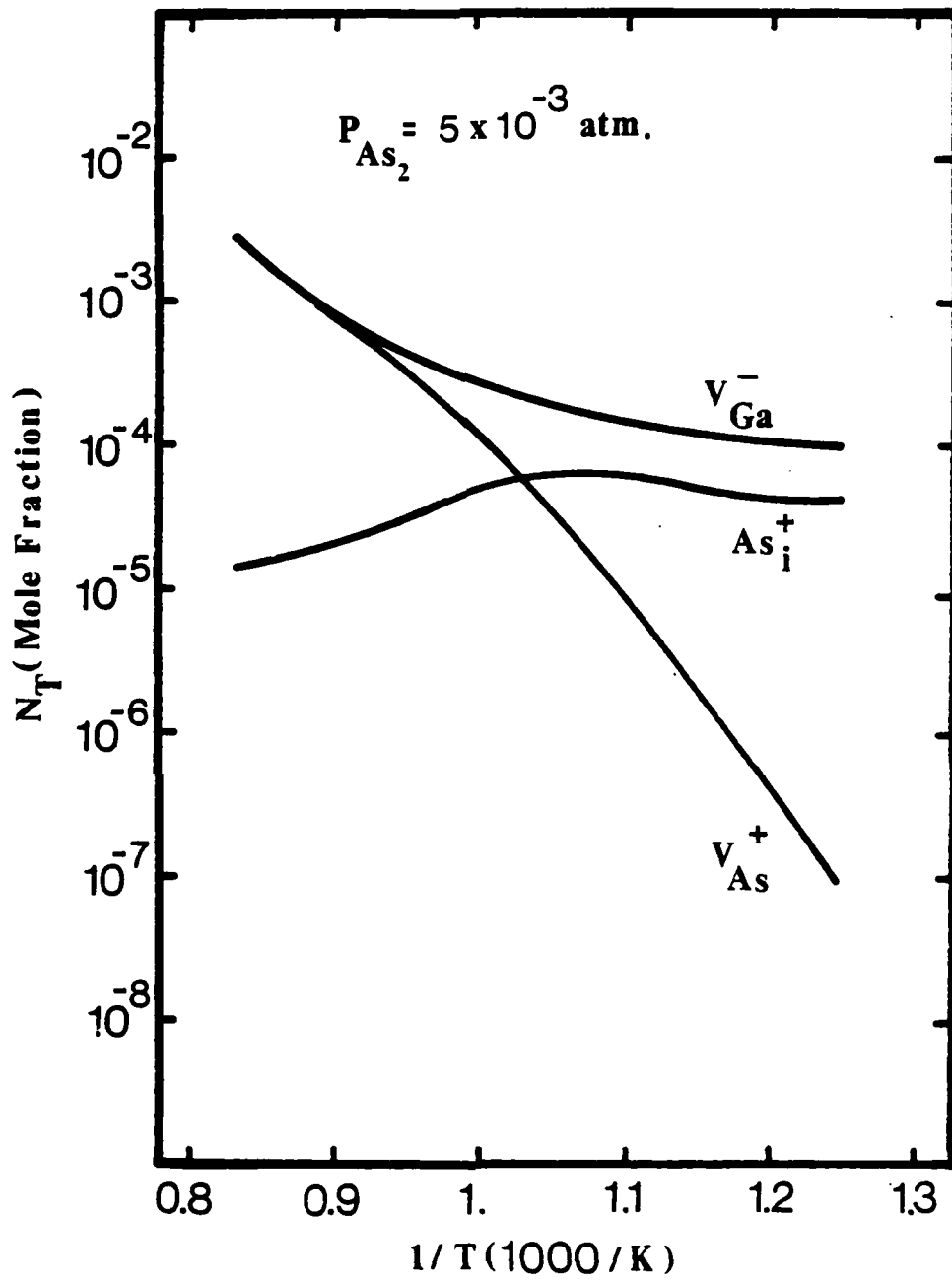
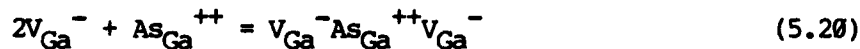


Fig.5.2 Density of native point defects vs temperature for GaAs grown at an arsenic pressure of 5×10^{-3} atm.

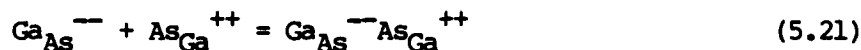
simple point defect introduced during crystal growth, several types of defects and defect complexes should be considered. It seems likely that the most common defect complexes will be those which have no net charge because these would have the greater binding energy. For example, a negatively charged gallium vacancy and a positively charged arsenic vacancy may produce a neutral gallium-arsenic divacancy. This can be expressed by:



In addition, the antisite-divacancy complexes may be formed by the reaction equations shown below:



The antisite pair defect complexes can be written as:



The interaction of V_{As}^{+} (V_{Ga}^{-}) with a single acceptor (or donor) impurity, A^{-} (D^{+}), can be written as:



which should have about the same binding energy as the gallium-arsenic divacancy complex given by Eq.(5.18). From Fig.5.1, it is noted that the concentration of V_{Ga} is very high, and the following reactions are prevailed:

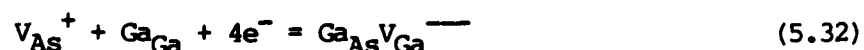
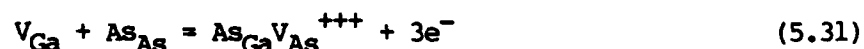
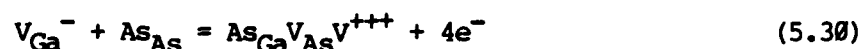


In general, the concentration of positively charged and negatively charged simple point defects introduced during crystal growth are not equal. Therefore, the concentration of one type of simple defects may be exhausted as shown by the reaction equations (5.18) to (5.25). This can be illustrated by the following kinetic equations:

(1) Arsenic antisite can be formed by As_j^+ , As_j , V_{Ga}^- , and V_{Ga} .



(2) Antisite-vacancy complexes can be expressed by:



which will occur everytime a vacancy migrates to a nearest neighbor site.

(3) Impurity-vacancy complexes can be written as:



and



Eq.(5.33) and (5.34) are the interaction of V_{Ga}^- with a acceptor (donor) substitutional site. For examples, $Te_{As}V_{Ga}^-$ defect complex may be formed in Te-doped GaAs, while, $Sn_{Ga}V_{Ga}^-$ and $Ge_{Ga}V_{Ga}^-$ defect complexes may be formed in Sn-doped and Ge-doped GaAs, respectively.

The V_{As}^+ may migrate to a donor substitutional site, and the reaction equation is given by:



Obviously, such reactions act as to compensate the dopant and to prevent the Fermi-level from approaching either band edge during crystal cooling.

5.4 The Possible Growth-in Defects in GaAs Under As-rich or High Arsenic Pressure Condition

Applying defect model to the high arsenic pressure conditions, the V_{Ga} , V_{Ga}^- , V_{As}^+ , As_j^+ , and As_j are found to be the dominant defects when the arsine partial pressure, P_{As_2} , is greater than 10^{-5} atm (e.g., GaAs grown by LEC, VPE, and MOCVD techniques); this is shown in Fig.5.1. The migration of V_{Ga} , V_{Ga}^- , and V_{As}^+ defects may result in forming complexes given by Eqs.(5.18) to (5.20) and Eqs.(5.22) to (5.35) after crystal growth. If we neglect the neutral defect complexes, then native defects such as $As_{Ga}V_{As}^{+++}$, As_{Ga}^{++} , V_{Ga}^- , $Ga_{As}V_{Ga}^{---}$, V_{As}^+ , As_j^+ , V_{Ga} , As_j , and impurity complexes D_{Ga}^+ , $A_{As}V_{Ga}^-$, $D_{Ga}V_{Ga}^-$, $D_{Ga}V_{As}^+$ are the possible defects which may be performed in high arsenic pressure conditions. In As-rich condition, the concentration of V_{As}^+ may be decreased, As_j^+ may be increased, and $As_{Ga}V_{As}^{+++}$, As_{Ga}^{++} , V_{Ga}^- , As_j^+ , V_{Ga} , As_j , and impurity complexes are the possible defects.

5.5 The Possible Grown-in Point Defects in GaAs for the Ga-rich or Low Arsenic Pressure Case.

Apply defect model to the low arsenic pressure condition, V_{Ga} , V_{Ga}^- , and V_{As}^+ are found to be the dominant point defects when P_{As_2} is less than 10^{-7} atm; this is the case for the LPE and MBE grown GaAs. The vacancy migration after crystal growth will result in the formation of complexes given by Eqs.(5.18) to (5.20), Eqs.(5.22) to (5.24), and Eqs.(5.30) to (5.35). If we neglect the neutral defect complexes, then native defects such as V_{Ga}^- , V_{As}^+ , $Ga_{As}V_{Ga}^{---}$, $As_{Ga}V_{As}^{+++}$, V_{Ga} and impurity complexes such as D_{Ga}^+ , $A_{As}V_{Ga}^-$, $D_{Ga}V_{Ga}^-$, $D_{Ga}V_{As}^+$ are the possible defects in low arsenic pressure conditions. The concentration of V_{Ga}^- is almost equal to that of V_{As}^+ , as is shown in Fig.5.1, and the binding energy for the gallium-arsenic divacancy is very high, as given in Eq.(5.18). Thus, high purity GaAs can be grown in this case under optimum cooling condition. In Ga-rich and low arsenic pressure conditions, the concentration of V_{Ga}^- and V_{Ga} may be decreased, gallium interstitial may be reacted with V_{As}^+ to form Ga_{As}^{--} . Thus the possible defects are V_{As}^+ , Ga_{As}^{--} , and $Ga_{As}V_{Ga}^{---}$ in undoped GaAs grown under Ga-rich condition.

5.6 Summary and Conclusions

In this chapter, we presented a new defect model for predicting native point defects in GaAs. During crystal growth, the chemical-thermodynamic principles are used to derive the density of vacancy and interstitial defects under thermal equilibrium condition. After crystal growth, thermal kinetic equations are employed to predict the antisite defects and impurity complexes. Conclusions are listed as follows:

- (1) High purity GaAs material can be grown for the low arsenic pressure case under optimum cooling condition.

- (2) GaAs grown under high arsenic pressure condition will produce more native point defects than under low arsenic pressure condition.
- (3) Native defects such as As_{Ga} , $As_{Ga}V_{As}$, V_{Ga} , and As_i and impurity complexes such as D_{Ga}^+ , $A_{As}V_{Ga}^-$, $D_{Ga}V_{Ga}^-$ are the possible defects for GaAs layers grown under the As-rich or high arsenic pressure condition.
- (4) Native defects such as V_{Ga} , V_{As} , $Ga_{As}V_{Ga}$, $As_{Ga}V_{As}$ and impurity complexes such as D_{Ga} , $A_{As}V_{Ga}$, $D_{Ga}V_{Ga}$, $D_{Ga}V_{As}$ are the possible defects for GaAs grown under low arsenic pressure condition.
- (5) Native defects such as V_{As} , Ga_{As} , $Ga_{As}V_{Ga}$ and impurity complexes such as $D_{Ga}V_{As}^+$ are the possible defects for GaAs grown under Ga-rich and low arsenic pressure conditions.
- (6) Arsenic antisite (As_{Ga}) defect can only be observed in GaAs grown under As-rich or high arsenic pressure conditions; this defect can not be produced under low arsenic pressure and Ga-rich conditions.

**VI. THE PHYSICAL ORIGINS OF EL2 ELECTRON TRAP IN GaAs.
(THEORETICAL AND EXPERIMENTAL EVIDENCE)**

The activation energy for the EL2 electron trap in GaAs reported in the literature ranges from $E_c - 0.76\text{eV}$ to $E_c - 0.83\text{eV}$. The physical origin of this trap is a subject of great interests in recent years. A large number of papers has been devoted to this subject. Based on our theoretical model and experimental results, we found that EL2 level is formed by two electron traps. One is identified as the EL2a ($E_c - 0.83\text{eV}$) electron trap, the other is denoted as the EL2b ($E_c - 0.76\text{eV}$) trap. The physical origin of EL2a level is attributed to the arsenic antisite (As_{Ga}) defect, whereas, the physical origin of the EL2b level is due to arsenic antisite-plus-arsenic vacancy ($\text{As}_{\text{Ga}}\text{V}_{\text{As}}$) defect complex.

Based on the native defect model presented in chapter 5, modelling of the EL2 electron trap is derived in GaAs material grown under As-rich or high arsenic pressure condition. Furthermore, from calculations of the trap density for the MOCVD and VPE grown GaAs with As to Ga mole fraction ratio greater than one, it is found that the density of EL2a trap is proportional to the mole fraction ratio of $(r-1)^{1/2}$; whereas, the density of EL2b trap is proportional to $(r-1)^{1/4}$, where $r = [\text{As}]/[\text{Ga}]$.

Theoretical calculations of the nonexponential DLTS signal for the EL2a trap revealed that the best fitted potential well for this charged center was due to a Coulombic potential well with double charge state (ie., $\text{As}_{\text{Ga}}^{++}$). This was verified by taking into account the Poole-Frenkel effect and phonon-assisted tunneling effect of the electric field enhanced electron emission rates data for this trap.

To provide the experimental evidence for the proposed physical origins of the EL2 electron traps discussed above, DLTS measurements were performed on VPE GaAs layers grown on different orientations (e.g., (100), (211A), (211B)) and LEC GaAs layers annealed in hydrogen gas at different temperatures (e.g., 200, 300, 500°C). From the results of our annealing study of the LEC grown GaAs, it was found that EL2b trap would disappear, and EL2a trap would emerge in the DLTS scan as the annealing temperature increases to 500°C. This result may be interpreted by the model of EL2 electron trap to be presented in this chapter. The experimental evidence which may be used to support the modelling of EL2 will be presented in chapter VII.

Section 6.1 reviews the EL2 electron trap in GaAs. Theoretical model of EL2 electron trap is described in section 6.2. Section 6.3 discusses the method of determining the potential wells for the EL2 trap levels from analyzing the field enhanced emission rates deduced from the nonexponential DLTS data. Summary and conclusions are given in section 6.4.

6.1. Review of the EL2 Electron Trap in GaAs.

Activation energy of EL2 electron trap covers the energy range from $E_C - 0.75\text{eV}$ to $E_C - 0.83\text{eV}$, as reported by many previous investigators^[73-91]. This trap has been observed in GaAs grown by the Bridgmann^[77,78], LEC^[79-85], VPE^[86,87], and MOCVD^[88-91] methods, as well as high temperature heat-treated GaAs samples^[92]. However, this level was not observed in the LPE^[93] and MBE^[94] grown GaAs epitaxial materials. Recent studies of the LEC bulk grown GaAs reported by Taniguchi et al^[74] have found that $E_C - 0.77\text{eV}$ electron trap exists in the front section of LEC GaAs ingot, whereas, $E_C - 0.82\text{eV}$ level is the dominant trap level appeared in tail section of the ingot. The same result was reported in MOCVD grown GaAs epilayers by

Watanabe et al [75]. They found that EL2a ($E_c - 0.83\text{eV}$) was the dominant trap level for GaAs grown at 720 to 740°C, while EL2b ($E_c - 0.76\text{eV}$) was the dominant trap level for GaAs grown at 630 to 660°C. In their annealing studies, Day et al [94] reported that EL2b was observed in as-grown MBE n-GaAs material; the results further revealed that this level can be annealed out at 800°C for 1/2 hour or at 700°C for 1 hour. Whereas, EL2a was not observed in the as-grown MBE n-GaAs. The EL2a level can be created by thermal annealing process and its trap concentration can be enhanced by high temperature annealing. These results indicate that EL2 electron trap may be due to two different trap levels. One of them is the EL2a ($E_c - 0.83\text{eV}$) electron trap and the other is EL2b ($E_c - 0.76\text{eV}$) electron trap. Our model and experimental evidence have shown that these two electron traps have different physical origins.

Studies of the LEC grown GaAs [79,95] have shown that n-type, (S.I.) material can be grown only from melts above a critical As composition, and the EL2a level was native defect observed in this material. Ga-rich melts were found to yield p-type, low resistivity GaAs crystal. Ta et al [79] reported that EL2a level was observed in As-rich GaAs material. GaAs samples prepared by LPE method are grown from a Ga-rich solution, whereas, VPE GaAs samples are commonly prepared in an As-rich gas ambient, in which growth rate and surface morphology are optimized [95]. The EL2a level was not observed in as-grown MBE n-GaAs material [94]. However, it was found that EL2a level can be created and its trap density can be enhanced by high temperature annealing (above 500°C) [94]. There is clear evidence that the EL2a trap can only be observed in GaAs grown under As-rich or high arsenic pressure case. The high arsenic pressure will enhance the formation of V_{Ga} , and As-rich case will increase the number of As_i [89]. Thus, the EL2a level is associated with gallium vacancy, arsenic interstitial or their

complexes [96], and is not related to oxygen impurity complex [97].

In undoped GaAs material, Watanabe et al [75,89] have shown that the concentration of EL2b level is proportional to $([AsH_3]/[TMG])^{1/4}$. However, the concentration of EL2a level is proportional to $([AsH_3]/[TMG])^{1/2}$. They also found that densities of EL2a and EL2b level would increase with increasing growth temperature for the MOCVD grown GaAs. Bhattacharya et al [87] observed a linear dependence of the EL2a trap density on $[As]/[Ga]$ ratio in MOCVD GaAs. Lagowski et al [78] have found that the concentration of EL2a level was increased with increasing As pressure during Bridgmann bulk growth, while, Miller et al [86] found that the density of EL2a level was increased with increasing $[AsH_3]/[GaCl]$ ratio in VPE grown GaAs. Li et al [21] also found that the density of EL2a level was decreased with decreasing $[AsCl_3]/[Ga]$ ratio in the Ga-rich VPE GaAs.

In the S-doped GaAs, Watanabe et al [75,89] found that density of EL2b level decreases with increasing dopant concentration of sulfur impurity. The density of EL2a level was found to decrease with increasing concentration of shallow donor dopants (Si, Se, Te) as was observed by Lagowski et al [78]. Donor concentration above a threshold value ($1 \times 10^{17} \text{ cm}^{-3}$) led to a rapid elimination of EL2 trap [78]. This is consistent with our observation [98] in which no EL2 trap level was detected in MOCVD GaAs with Sn dopant density higher than $3 \times 10^{17} \text{ cm}^{-3}$. If group VI (Se, Te, S) elements occupy the As lattice site and combined with gallium vacancy to form antisite-vacancy ($A_{As}V_{Ga}^-$) complexes, then the concentration of V_{Ga} will be decreased. Thus, the probability of forming an arsenic antisite (As_{Ga}) defect will be greatly reduced [87]. Johnson et al [99] used photoluminescence upconversion method to observe the EL2a level, and concluded that this level is due to arsenic antisite defect. The fact that EL2a level is a donor type defect was also supported by the observed field dependence of emission rates [48,73]. This is consistent with the modelling

of native point defect described in the previous chapter. We conclude that arsenic antisite defect is the only grown-in defect which is observed in As-rich or high arsenic pressure case, but is not observed in Ga-rich and low arsenic pressure case. From the experimental evidence, it can be shown that EL2a trap is due to antisite defect, As_{Ga}^{++} , formed during the post-grown cooling [94,99], as will be discussed further in next section.

6.2. Theoretical Modelling of the EL2 Electron Trap in GaAs.

We shall next present a new model for explaining the EL2 level vs different $[As]/[Ga]$ ratio for the MOCVD and VPE grown GaAs samples. Assuming that the mole fraction ratio of $[As]$ to $[Ga]$ is equal to r , it can be shown that for $r > 1$, the concentration of EL2a level is proportional to $(r-1)^{1/2}$, and the concentration of EL2b level is proportional to $(r-1)^{1/4}$. In this section, the kinetics of EL2 formation in GaAs are described. In the growth process, vacancies, interstitials and antisites are formed in high temperature thermal equilibrium. In the cooling process, vacancies migrate to form EL2a and EL2b electron trap. In the annealing process, EL2b trap level is transferred to EL2a trap level after thermal annealing. These three different processes of defect formation in GaAs are discussed next.

6.2.1. Growth process:

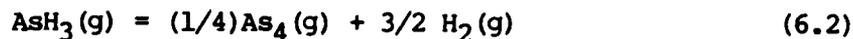
Defect formation under thermal equilibrium for the case of $r > 1$

(a) MOCVD grown GaAs epitaxial material:

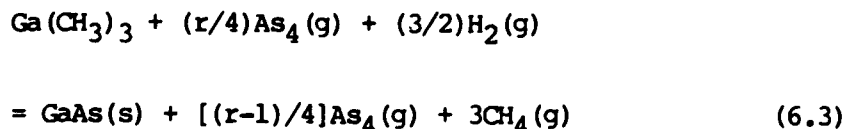
Arsine (AsH_3) and trimethylgallium (TMG) were used as sources for As and Ga in MOCVD grown GaAs. Let the mole fraction ratio of arsine to TMG be r , then:

$$[AsH_3]/[Ga(CH_3)_3] = r \quad (6.1)$$

If we assume $[Ga(CH_3)_3]$ equal to 1, then $[AsH_3]$ will be equal to r , where the square bracket in Eq.(6.1) represents the mole fraction of arsine and TMG gas. In the crystal growth arsine will decompose into $As_4(g)$ or $As_2(g)$, depending on the growth temperature. In general, arsine will decompose into $As_4(g)$ in the epitaxial growth (growth temperature below $1000^\circ C$), while arsine will decompose into $As_2(g)$ in the melt growth in which the growth temperature is above $1400^\circ C$ [64]. The growth temperature for MOCVD process is usually below $1000^\circ C$, and thus the reaction of arsine can be written as:



The chemical reaction of $As_4(g)$ and TMG can be described by:



If $GaAs(g)$ is completely deposited on surface of $GaAs$ substrate, then the extra $As_4(g)$ will be decomposed into $As_{As}(s)$ or As_j , by the following reactions[100]:



Eqs.(6.4) and (6.5) may be obtained from Eqs.(5.1) through Eq.(5.7). These two equations are the dominant reactions during crystal growth. The reaction of Eq.(6.6) can be neglected compared to Eqs.(6.4) and (6.5). The law of mass action for Eqs.(6.4) through (6.6) is given by:

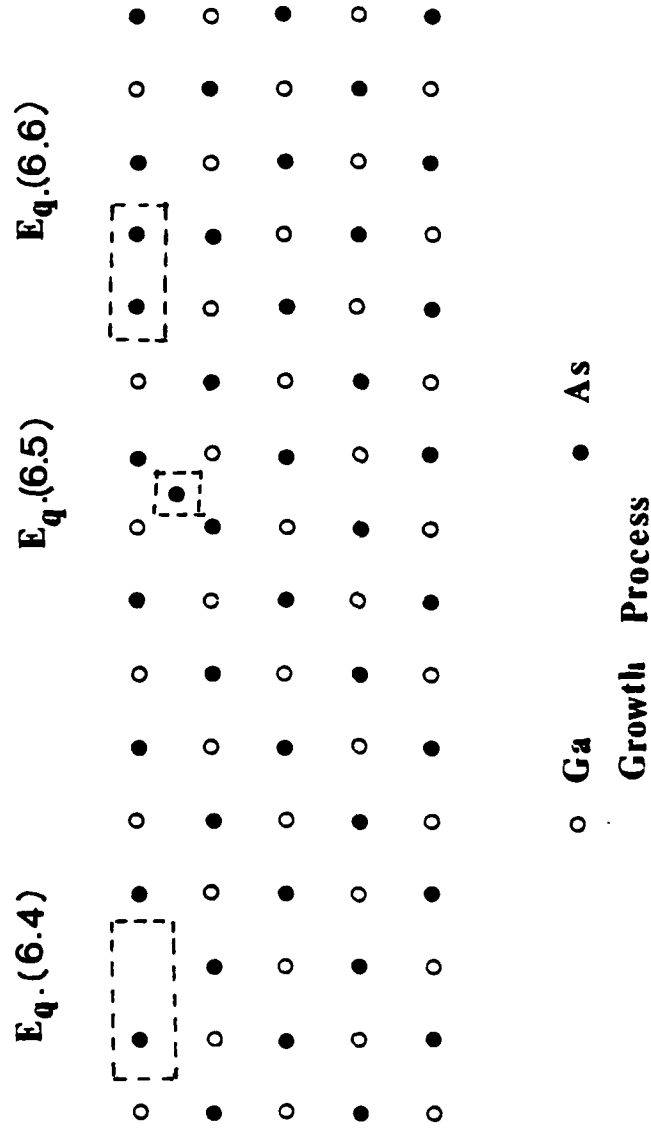
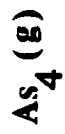


Fig.6.1 As_{As} or As atoms are deposited onto the GaAs substrate during crystal growth.

$$k_1 = [As_{As}(s)] [V_{Ga}] / [As_4(g)]^{1/4} \quad (6.7)$$

$$k_2 = [As_j] / [As_4(g)]^{1/4} \quad (6.8)$$

$$k_3 = [As_{As}(s)] [As_{Ga}] / [As_4(g)]^{1/4} \quad (6.9)$$

From Eqs.(6.7) - (6.9), yields the concentration of V_{Ga} , As_j , and As_{Ga} .

$$\begin{aligned} [V_{Ga}] &= k_1 [As_4(g)]^{1/4} / [As_{As}(s)] \\ &= k_1 [(r-1)/4]^{1/4} = k_1' (r-1)^{1/4} \end{aligned} \quad (6.10)$$

$$[As_j] = k_2' (r-1)^{1/4} \quad (6.11)$$

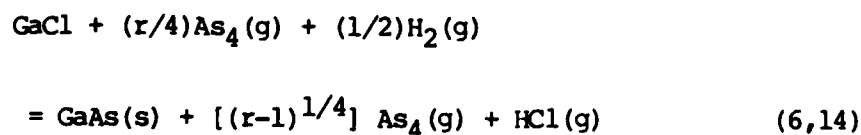
$$[As_{Ga}] = k_3' (r-1)^{1/2} \quad (6.12)$$

(b) VPE grown GaAs epitaxial material:

Arsine (AsH_3) and gallium chloride ($GaCl$) were used as sources for As and Ga in the VPE grown GaAs. Let the mole fraction ratio of arsine and gallium chloride be r , then:

$$[AsH_3] / [GaCl] = r \quad (6.13)$$

If we assume $[GaCl]$ equal to 1, then $[AsH_3]$ will be equal to r . The reaction of $As_4(g)$ and $GaCl$ can be expressed by



From Eq.(6.14), it is noted that there is $(r-1)^{1/4}$ extra $As_4(g)$ in the reaction tube, and thus As atoms will be deposited on As sites or As interstitial according to Eqs.(6.4) to (6.6). Therefore, the concentrations of V_{Ga} , As_j , and As_{Ga} can be expressed by:

$$[V_{Ga}] = k_4 [As_4(g)]^{1/4} / [As_{As}(s)] = k_4' (r-1)^{1/4} \quad (6.15)$$

$$[As_j] = k_5' (r-1)^{1/4} \quad (6.16)$$

$$[As_{Ga}] = k_6' (r-1)^{1/2} \quad (6.17)$$

From Eqs.(6.10) to (6.12) and (6.15) to (6.17), it is noted that for both MOCVD and VPE grown GaAs, the density of V_{Ga} is proportional to $(r-1)^{1/4}$; the density of As_j is proportional to $(r-1)^{1/4}$; and the density of As_{Ga} is proportional to $(r-1)^{1/2}$.

6.2.2. Cooling process:

Formation of arsenic antisite (As_{Ga}) and arsenic antisite-plus-arsenic vacancy ($As_{Ga}V_{As}$) defects occurs when V_{Ga} migrates into As_j or As_{As} sites under thermal nonequilibrium condition. Thus, the EL2a level may be attributed to the As_{Ga} defect, while EL2b level is due to $As_{Ga}V_{As}$. Fig.6.2 shows the cooling process of GaAs layers. This may be further exemplified as follows. The As_{Ga} defect can be formed by V_{Ga} and As_j , which is written as:



The $As_{Ga}V_{As}$ can be formed by V_{Ga} migration to its neighbor (As_{As}) site, and is given by:



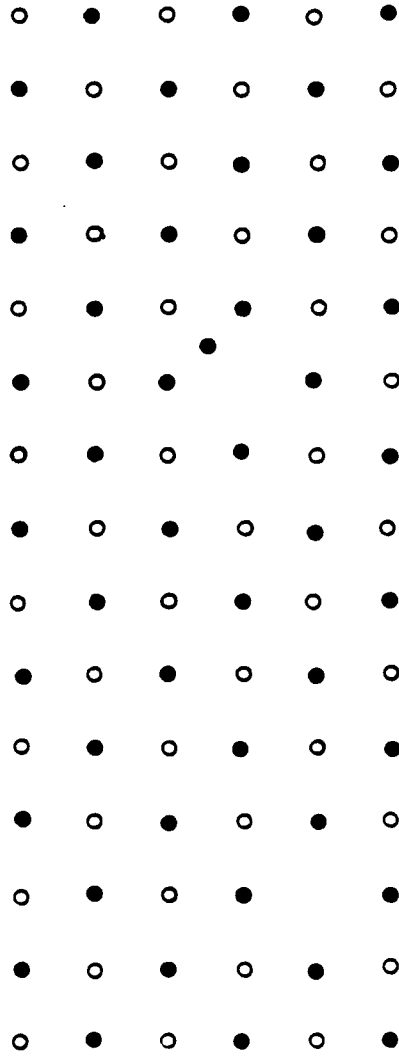
The mass action law for the reaction equations given in Eqs.(6.18) and (6.19) is described by:

$$K_a = [As_{Ga}] / [As_j] [V_{Ga}] \quad (6.20)$$

$$K_b = [As_{Ga}V_{As}] / \{ [V_{Ga}] [As_{As}(s)] \} \quad (6.21)$$

Eq. 6.19

Eq. 6.18



○ Ga ● As

Cooling Process

Fig.6.2 Migration of V_{Ga} to As_i or As_{As} site to form complex defect during the cooling period of crystal growth.

The As_{Ga} and $As_{Ga}V_{As}$ defect concentrations are given respectively by

$$[As_{Ga}] = K_a [As_i] [V_{Ga}] = K_a''(r-1)^{1/2} \quad (6.22)$$

$$[As_{Ga}V_{As}] = K_b [V_{Ga}] = K_b''(r-1)^{1/4} \quad (6.23)$$

Fig.6.3 shows the densities of EL2a and EL2b trap as a function of $[As]/[Ga]$ mole fraction ratio as predicted by Eqs.(6.22), (6.23) and the published experimental data^[75,87,101]. The results show that for $r > 1$, the density of EL2a trap is proportional to $(r-1)^{1/2}$, and the density of EL2b trap varies with $(r-1)^{1/4}$, as predicted by Eqs.(6.22) and (6.23).

6.2.3. Annealing process:

The EL2a level may be formed from EL2b via thermal annealing. Fig.6.4 shows the formation mechanisms of EL2b and EL2a. Note that EL2b level may gain sufficient thermal energy, and decomposes into V_{Ga} according to the inverse reaction of Eq.(6.19) when the annealing temperature is higher than 500 °C. As_{Ga} is formed when the V_{Ga} migrate to the As_i site, according to Eq.(6.18). This is supported by the experimental data of Taniguchi et al^[74] and Day et al^[94].

6.3. Determination of Potential Well for the EL2 Electron Trap from Field Enhanced Emission Rate Analysis.

As discussed above, the most probable physical origin for the EL2a trap is due to arsenic antisite defect, and the possible origin of EL2b trap is attributed to arsenic antisite-plus-arsenic vacancy complex defect. The charge state for these electron traps may be revealed if the type of potential well is known. This can be done by studying the field dependent emission rates deduced from the nonexponential DLTS response for these electron traps, as was described in chapter IV.

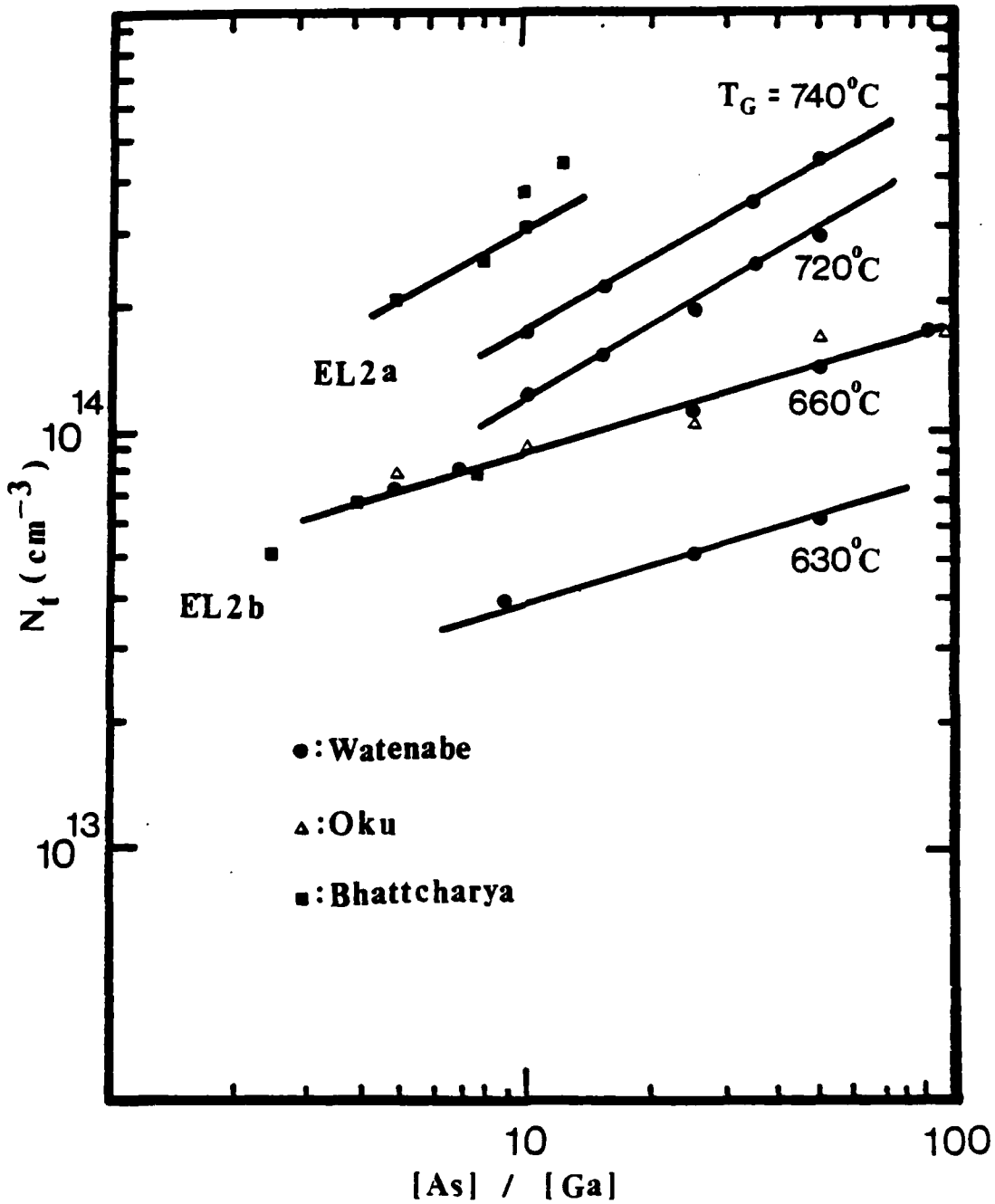
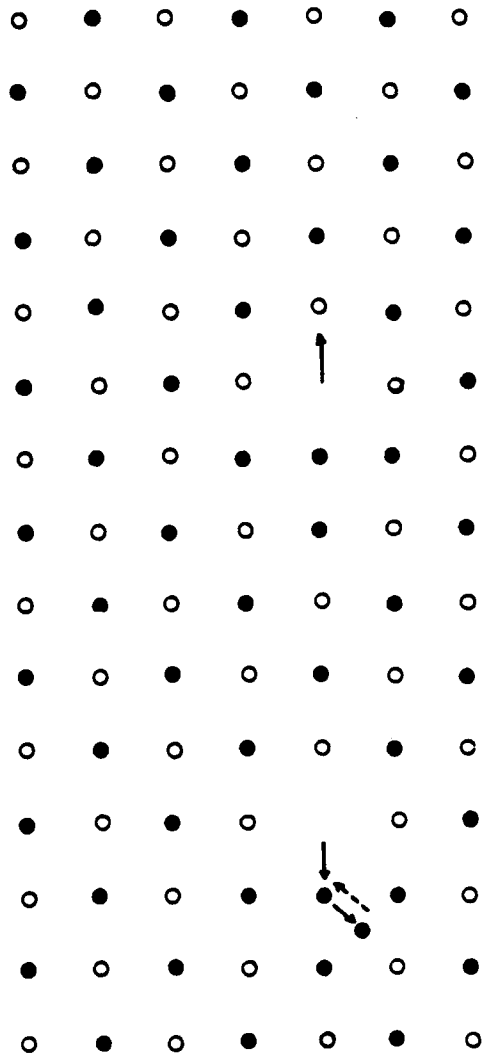


Fig.6.3 The calculated density of EL2-a and EL2-b electron traps in GaAs vs $[As]/[Ga]$ mole fraction ratios, as compared with the published data. For EL2-a, N_t varies with $(r-1)^{1/2}$, and $(r-1)^{1/4}$ for the EL2-b level.



○ Ga ● As
Annealing Process

Fig.6.4 The mechanism of annihilating an EL2-b trap and the creation an EL2-a electron trap in GaAs during thermal annealing process.

The type of potential well for the EL2a electron trap was analyzed from the theoretical calculations of nonexponential DLTS response in GaAs. A comparison of the calculated DLTS response with the measured DLTS data will enable us to determine the potential well for this electron trap. We have calculated the nonexponential DLTS response for four different types of potential wells, namely, the Coulombic well, Dirac well, square well and polarization well for the EL2a trap, and the results are shown in Fig.6.5. Fig.6.6 shows the calculated DLTS signal and the experimental DLTS data for the Coulombic potential well with single and double charge states. The capture cross section (σ_n) of $8 \times 10^{-14} \text{ cm}^2$ was used in the calculations. A comparison of the calculated nonexponential DLTS response with the measured DLTS data shows that the observed EL2a trap is best fitted to a Coulombic potential well with double charge state. Fig.6.7 shows the theoretical nonexponential DLTS response of Coulombic potential well with double charge state for different emission constants [$1/\gamma = 34.4, 86.6, 172, 344, \text{ and } 866 \text{ s}^{-1}$].

The field dependent emission rates for the Coulombic potential well can be derived by taking into account the three-dimensional Poole-Frenkel effect and phonon-assisted tunneling effect, and can be expressed by:

$$e_{nHC}/e_{n0} = \left\{ \int_0^{2\pi} \int_0^{\pi/2} \sin(\theta) \exp(\Delta E_{tj}/kT) d\theta d\phi + \int_0^{2\pi} \int_0^{\pi/2} \sin(\theta) d\theta d\phi / 4\pi \right\} \\ + \int_0^{(E_{ci} - \Delta E_{ci})/kT} \exp\{z - z^{3/2} [4(2m^*)^{1/2} (kT)^{3/2} / 3q\hbar F] \\ [1 - (\Delta E_{tj}/zkT)^{5/3}] \} dz \quad (6.24)$$

where e_{n0} is the emission rate at zero electric field. ΔE_{tj} is the Poole-Frenkel barrier due to the external electric field. $\Delta E_{tj} = q[qF \cos(\theta) / \pi \epsilon_0 \epsilon_s]^{1/2}$, and F is the applied electric field. The first term in Eq.(6.24)

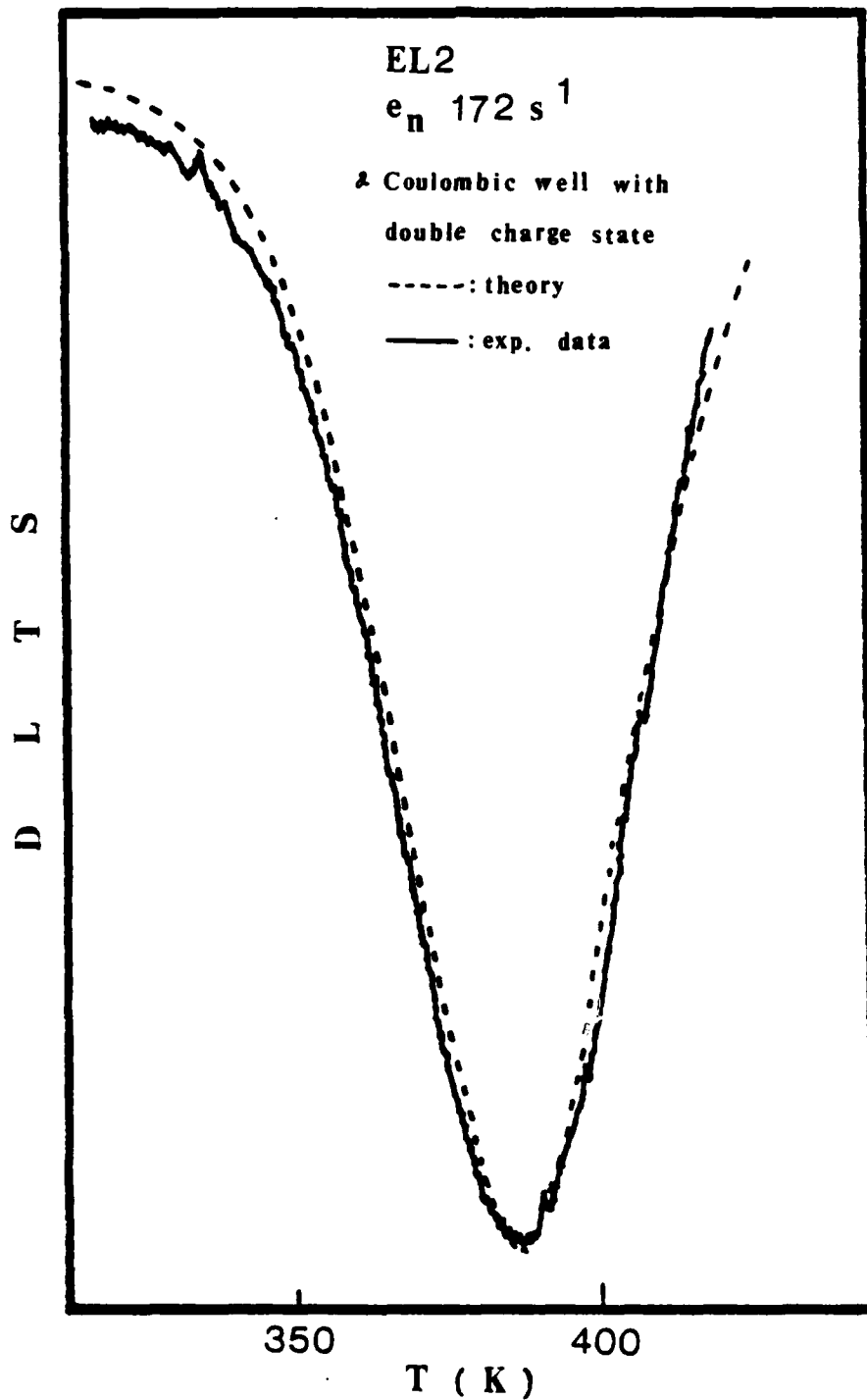


Fig.6.5 DLTS scan of EL2—a electron trap in GaAs. Solid line: experiment; dash line: theoretical calculation, assuming Coulombic well with double charge state.

is due to the three-dimensional Poole-Frenkel effect, and the second term is due to the phonon-assisted tunneling effect. Since the electric field varies with position within the depletion region of a reverse biased p-n junction, the emission rate is not constant within the same region. The DLTS response due to the nonuniformed emission rates can in general be expressed by $S(\nu) = \sum \exp(-e_{ni}t_1) - \sum \exp(-e_{ni}t_2)$.

A comparison of our theoretical calculations of the nonexponential DLTS response due to the field dependent emission rates with the measured DLTS data reveals that the potential well for the EL2a electron trap is due to Coulombic well with double charge state, and hence the most likely physical origin for this electron trap is attributed to As_{Ga}^{++} . This conclusion is consistent with the EL2 modelling based on the kinetic equations and defect structure as discussed in the previous section.

6.4. Summary and Conclusions

In this chapter, we presented a new defect model for the EL2 electron trap in the undoped GaAs. EL2 level is attributed to two types of native point defects. One is designated as the EL2b ($E_C - 0.76\text{eV}$) electron trap, and the other is denoted as the EL2a ($E_C - 0.83\text{eV}$) electron trap. The physical origin of EL2a is attributed to arsenic antisite (As_{Ga}) defect, whereas, the physical origin of EL2b level is attributed to the arsenic antisite-plus-arsenic vacancy ($As_{Ga}V_{As}$). Based on this model, relationship between the density of EL2a and EL2b trap levels vs $[As]/[Ga]$ ratio in the MOCVD and VPE grown GaAs was established. The result shows that density of EL2a trap is directly proportional to the mole fraction ratio of $(r-1)^{1/2}$, but the density of EL2b trap is proportional to the mole fraction ratio of $(r-1)^{1/4}$. This prediction is supported by experimental data for the MOCVD and VPE grown GaAs.

VII. STUDY OF GROWN-IN DEEP LEVEL DEFECTS VS GROWTH PARAMETERS IN VPE, LEC, LPE and MOCVD Grown GaAs.

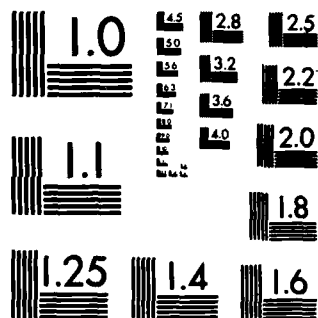
Studies of grown-in deep level defects in GaAs grown by VPE, LEC, LPE, and MOCVD techniques under various growth conditions will be described in this chapter.

7.1. Study of Grown-in Deep Level Defects vs Growth Parameters in VPE GaAs Layers.

Detailed study of the grown-in deep level defects vs substrate orientation and gas phase stoichiometry in the VPE GaAs layers grown by a novel Ga/AsCl₃/H₂ reactor [which is under high arsenic pressure and Ga-rich conditions] has been made, using DLTS and C-V methods. Density of electron traps vs [Ga]/[As] ratios of 2/1, 3/1, 4/1, 5/1, and 6/1 was determined for the VPE GaAs layers grown on <100>, <211A>, and <211B> oriented semi-insulating (S.I.) Cr-doped GaAs substrates. Two electron traps with energies of E_c-0.71 eV (i.e., EB4) and E_c-0.83 eV (i.e., EL2a) were observed in the samples studied. Results showed that density of both electron traps depends strongly on the [Ga]/[As] ratio for the <211A> and <211B> oriented samples, and less strongly for the <100> oriented samples. For example, in the <211A> (i.e., Ga-rich face) oriented samples; the density of EB4 and EL2a electron traps was found to decrease with increasing [Ga]/[As] ratio, while reverse trend was found for the <211B> (i.e., As-rich face) oriented samples. As for the <100> oriented samples, the density of EL2a level may either increase or decrease with increasing [Ga]/[As] ratio. The physical origins of this trap is attributed the arsenic antisite (As_{Ga}⁺⁺), as was discussed in chapter VI. As for the EB4 level, the results are less conclusive, and further study is needed.

7.1.1. Introduction:

Although the AsCl_3 epitaxial growth system is the most widely used method for the growth of microwave device materials, only limited information is available on how variation of the $[\text{Ga}]/[\text{As}]$ ratio in the gas phase composition can affect the materials produced. In most AsCl_3 reactors, this ratio is not easily controlled being a function of source efficiency, wall deposit extensiveness, flow rates, etc. If stoichiometry related defects or defect complexes are important in the VPE GaAs growth, it might be expected that the $[\text{Ga}]/[\text{AsCl}_3]$ ratio in the growth environment is important. Miller et al [86] have studied the effect of gas-phase stoichiometry on deep levels in the VPE GaAs grown by the hydride system with $[\text{AsH}_3]/[\text{GaCl}]$ ratio varying from 1/3 to 3/1. A deep-level electron trap (EL2a) with energy of $E_c - 0.83$ eV was observed in their study; its density was found to depend on the mole fraction ratio of Ga to As atom. Similar studies were also reported by Merenda [102] in the VPE GaAs grown by the chloride system and the MOCVD grown GaAs [5,90,91]. None of these studies have looked into the effects of varying substrate orientation and $[\text{Ga}]/[\text{As}]$ ratio on the deep-level defects in the VPE GaAs epilayers as will be reported in this chapter. To facilitate our study, a novel AsCl_3 vapor phase epitaxial reactor [31,103] was used to grow the GaAs epitaxial layers; the system is capable of operation with a variable controlled $[\text{Ga}]/[\text{As}]$ ratio. The GaAs epilayers were grown on three different orientations (i.e., $\langle 100 \rangle$, $\langle 211A \rangle$, and $\langle 211B \rangle$) substrates. DLTS and C-V methods were employed to determine the density of deep-level defects vs $[\text{Ga}]/[\text{As}]$ ratio in the VPE GaAs layer.



MICROCOPY RESOLUTION TEST CHART
NATIONAL BUREAU OF STANDARDS-1963-A

7.1.2. Experimental Details

The VPE GaAs epitaxial layers used in this study were grown by a novel AsCl_3 reactor system^[31,103]. The basic design of this reactor is like the usual two bubbler AsCl_3 reactor used for the MESFET growth^[104]. The novel feature of our reactor is the addition of a third bubbler which feeds a cracking furnace and then a second source chamber to allow operation in a GaCl rich mode. It uses a six-zone clamshell furnace which rolls off sideways allowing an end to end gas flow system. The third or control bubbler feeds a cracking furnace that is maintained at 900°C when in use.

The GaAs epilayers were grown on $\langle 100 \rangle$, $\langle 211A \rangle$, and $\langle 211B \rangle$ oriented S.I. Cr-doped GaAs substrates with growth temperatures ranging from 710°C to 750°C . To facilitate our study of the effect of orientation on the grown-in defects in the VPE GaAs, seven growth runs were made for this study (e.g., 77A, 77B, and 77BB were grown in the same run, etc.). The gas phase stoichiometry was controlled by varying the $[\text{Ga}]/[\text{As}]$ ratios from 2/1 to 6/1. Al-GaAs Schottky barrier structures were fabricated from these VPE GaAs epilayers for the DLTS and C-V measurements. Density and energy levels of the grown-in defects in these VPE GaAs samples were determined from the C-V and DLTS data. The results are presented next.

7.1.3. Results and Discussions.

In this section, we present the results of our DLTS and C-V measurements on the VPE GaAs samples described in preceding section. The DLTS scans of electron traps as a function of $[\text{Ga}]/[\text{As}]$ ratio for different runs and substrate orientations are shown in Fig.7.1 through Fig.7.9. Fig.7.1 shows the DLTS scans of electron traps as a function of the $[\text{Ga}]/[\text{As}]$ ratio, for samples with $\langle 211A \rangle$ orientation. In general, one to two electron traps (i.e., $\text{EB4} = E_c - 0.71 \text{ eV}$, and $\text{EL2a} = E_c - 0.83 \text{ eV}$) were

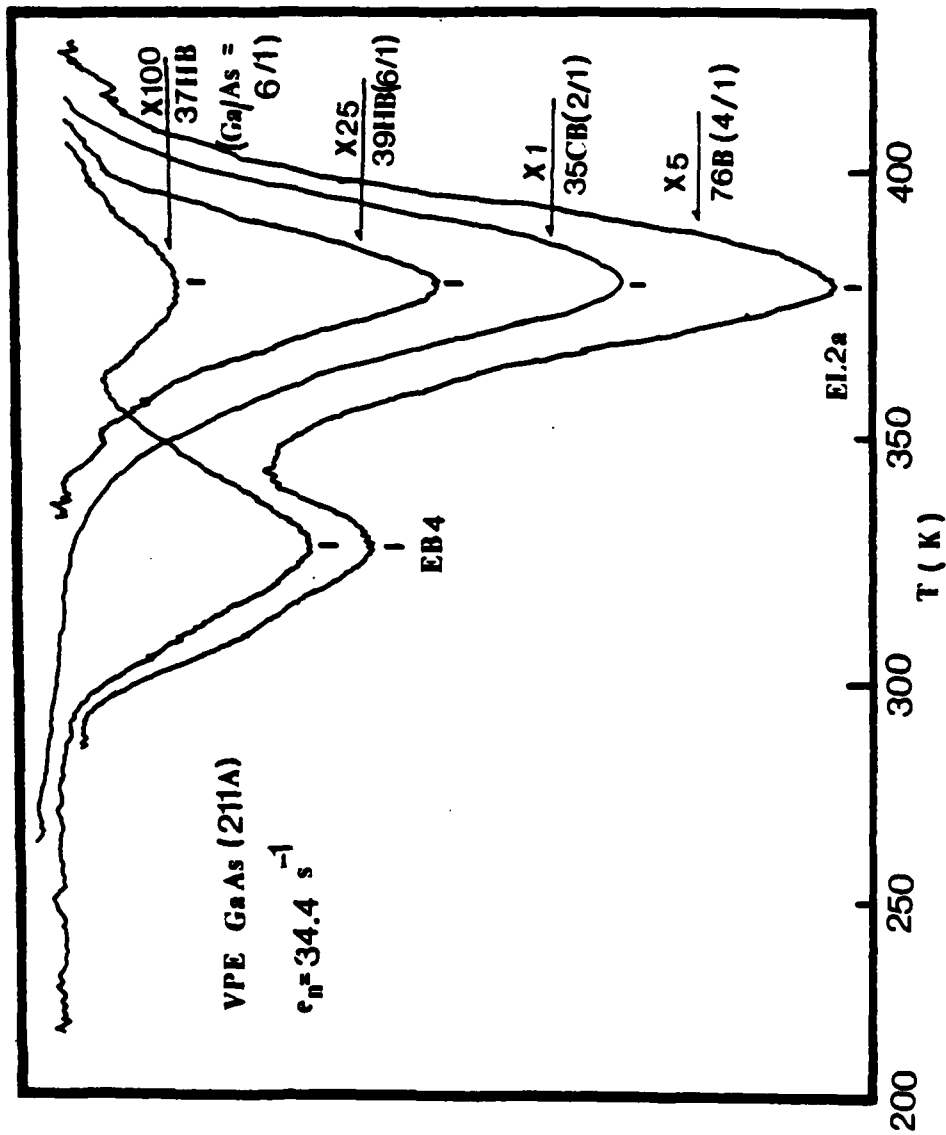


Fig.7.1 DLTS scans of electron traps for VPE GaAs grown on (211 A) oriented substrates with [Ga]/[As] ratio varies from 2/1 to 6/1.

observed in these samples. Note that sample 37HB with the highest [Ga]/[As] ratio (i.e., 6/1) has the lowest density for EL2a electron trap, while sample 35 CB with the lowest [Ga]/[As] ratio (i.e., 2/1) has the highest density of EL2 electron trap. Thus, for the <211A> orientated samples (i.e., Ga-rich face), the density for EL2a level decreases with increasing [Ga]/[As] ratio; this same trend was also observed in EB4 electron trap. Fig.7.2 shows the DLTS scans of electron traps as a function of the [Ga]/[As] ratio for epilayers grown on the <100> oriented substrates. Results showed that the density of EL2a level may either increase or decrease with increasing [Ga]/[As] ratio, depending on the concentrations of V_{Ga} or As_j formed during crystal growth. To explain this, modelling presented in chapter VI appears to be adequate for this high arsenic pressure and Ga-rich condition. We suggested that EL2a level is attributed to the As_{Ga} arsenic-antisite defect which is formed by the migration of V_{Ga} defect to As_j site after crystal cooling, as shown in Eq.(6.18). VPE GaAs layers are grown under high arsenic pressure condition. In the case of <211A> oriented samples, V_{Ga} should be suppressed by the following reaction under the Ga-rich condition.



Thus, the density of EL2a level will decrease with increasing [Ga]/[As] ratio, as is the case of <211A> samples shown in Fig.7.1. On the other hand, in the case of <211B> oriented samples, arsenic face will prevent the reaction of Eq.(7.1) in the Ga-rich case. At this case, the concentrations of As_j and V_{Ga} levels shall be enhanced with increasing [Ga]/[As] ratio. Therefore, the density of EL2a level will increase with increasing [Ga]/[As] ratio; this is the case for <211B> oriented samples. This defect model seems adequate for predicting the orientation dependence of the density of EL2a vs [Ga]/[As] ratio, as is shown in Fig. 7.9. Fig. 7.3

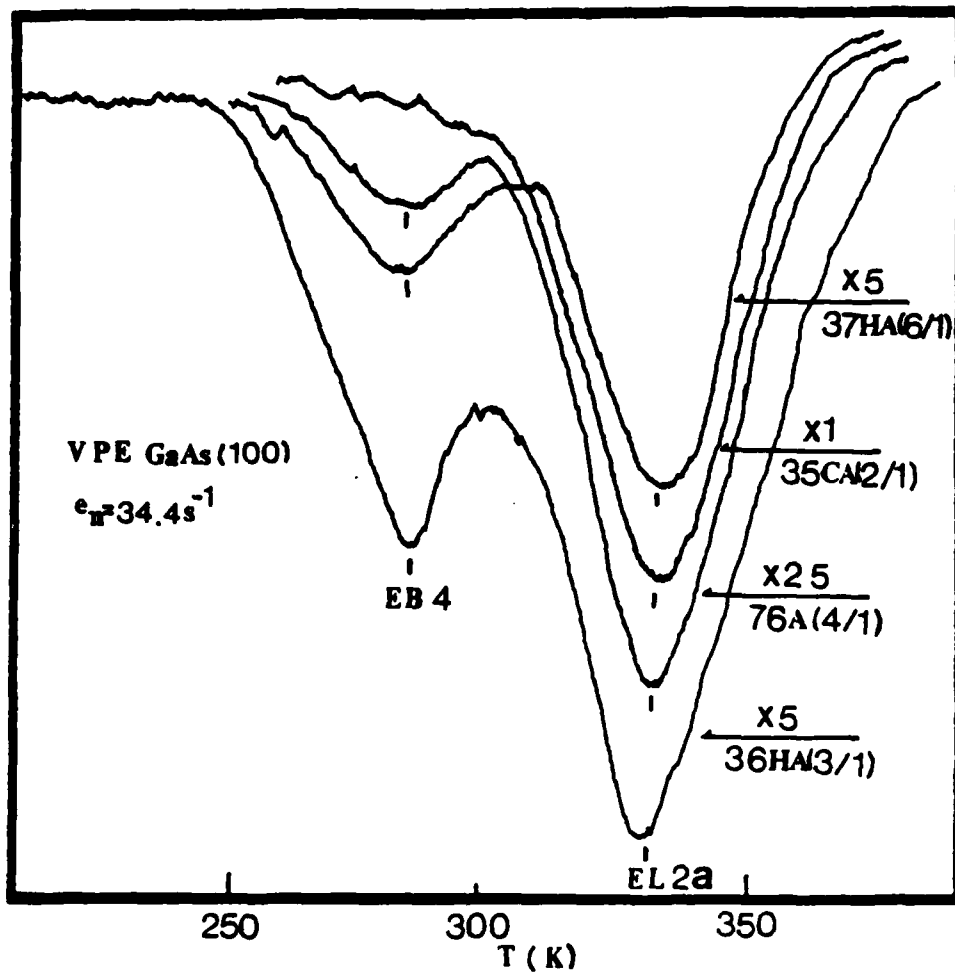


Fig.7.2 DLTS scans of electron traps in VPE GaAs grown on (100) substrates with [Ga]/[As] ratio varying from 2/1 to 6/1.

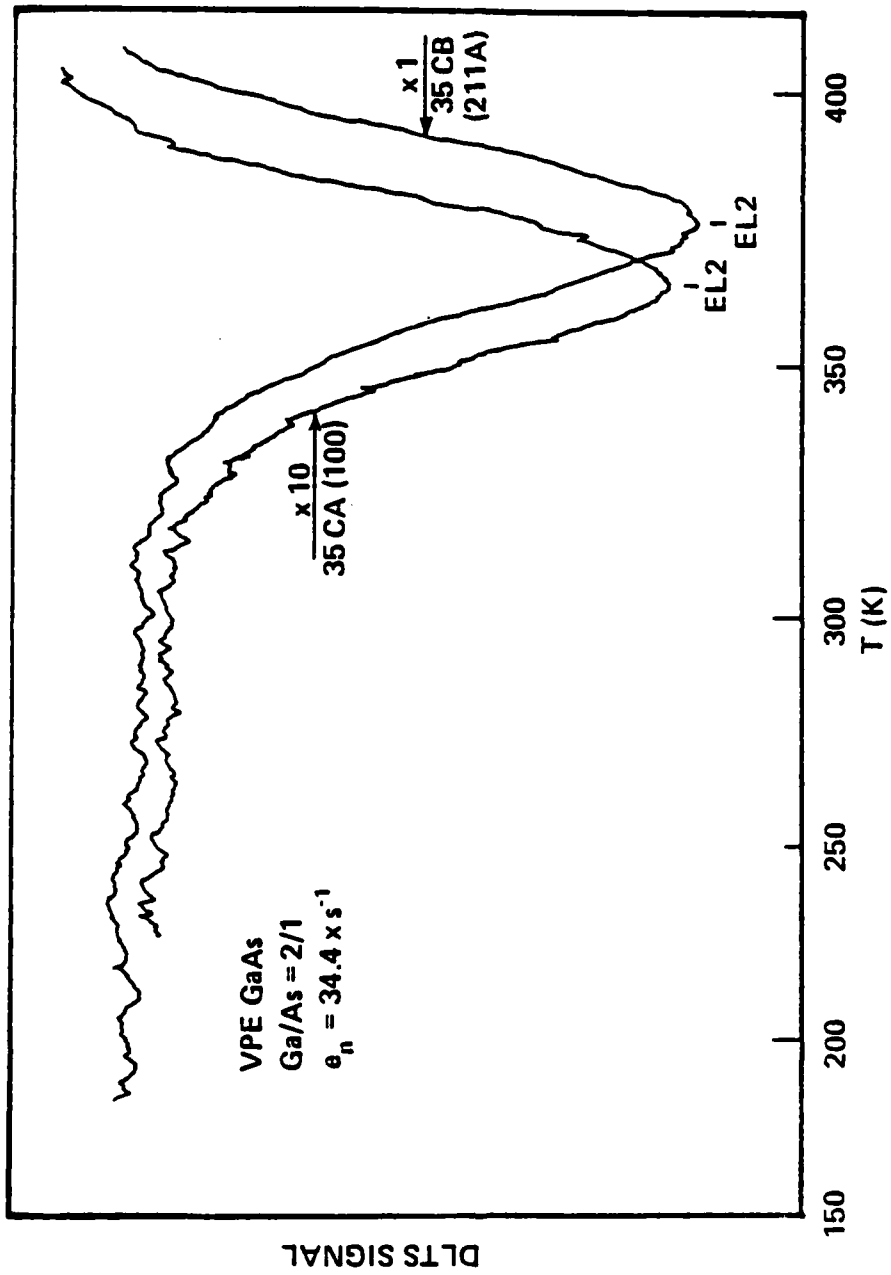


Fig.7.3 DLTS scans of electron trap for VPE GaAs grown on (211 A) and (100) oriented substrates with [Ga]/[As] ratio equal to 2/1.

shows the DLTS scans of electron traps for sample 35CA $\langle 100 \rangle$ and sample 35CB $\langle 211A \rangle$ with $[Ga]/[As]$ ratio equal to 2/1. These two samples were grown in the same run side by side at $715^{\circ}C$. The DLTS results showed that density of EL2a electron trap for the $\langle 211A \rangle$ sample is significantly higher than that of the $\langle 100 \rangle$ sample (i.e., $1.24 \times 10^{14} \text{ cm}^{-3}$ vs. $7.6 \times 10^{12} \text{ cm}^{-3}$). The reason for this may be attributed to the fact that during crystal growth in high arsenic pressure condition, the density of V_{Ga} is higher in the $\langle 211A \rangle$ face than that in the $\langle 100 \rangle$ face for $[Ga]/[As]$ ratio equal to 2/1. The EB4 electron trap was not observed in both samples shown in Fig.7.3. Fig.7.4 shows the DLTS scans of electron trap for sample 75A $\langle 100 \rangle$ and sample 75B $\langle 211A \rangle$ with $[Ga]/[As]$ ratio equal to 3/1. Note that the EL2a level was observed only in sample 75A while EB4 level was observed only in 75B sample. The growth temperature for both samples was held at $725^{\circ}C$. Fig.7.5 shows the DLTS scans of electron traps for samples 76A $\langle 100 \rangle$ and 76B $\langle 211A \rangle$. The results showed that both EL2a and EB4 electron traps were observed in these two samples. Density of EL2a and EB4 levels was higher for sample 76B $\langle 211A \rangle$ than sample 76A $\langle 100 \rangle$. Fig.7.6 shows the DLTS scans of electron traps for samples 77B $\langle 211A \rangle$, 77A $\langle 100 \rangle$, and 77BB $\langle 211B \rangle$. These three samples were grown side by side at $750^{\circ}C$ and with $[Ga]/[As]$ ratio equal to 4/1. Both EL2a and EB4 electron traps were observed in these three samples; the density of EL2a and EB4 levels was highest for sample 77BB, followed by samples 77B, and 77A. Fig.7.7 show the DLTS scans of electron traps for samples 78B $\langle 211A \rangle$ and 78BB $\langle 211B \rangle$ grown at $725^{\circ}C$ and with $[Ga]/[As]$ ratio equal to 5/1. The results showed that EL2a level was the dominant electron trap for sample 77BB while only EB4 level was observed in sample 78B. Fig.7.8 shows the DLTS scans of electron traps for samples 37HA $\langle 100 \rangle$ and 37HB $\langle 211A \rangle$ grown at $725^{\circ}C$ and

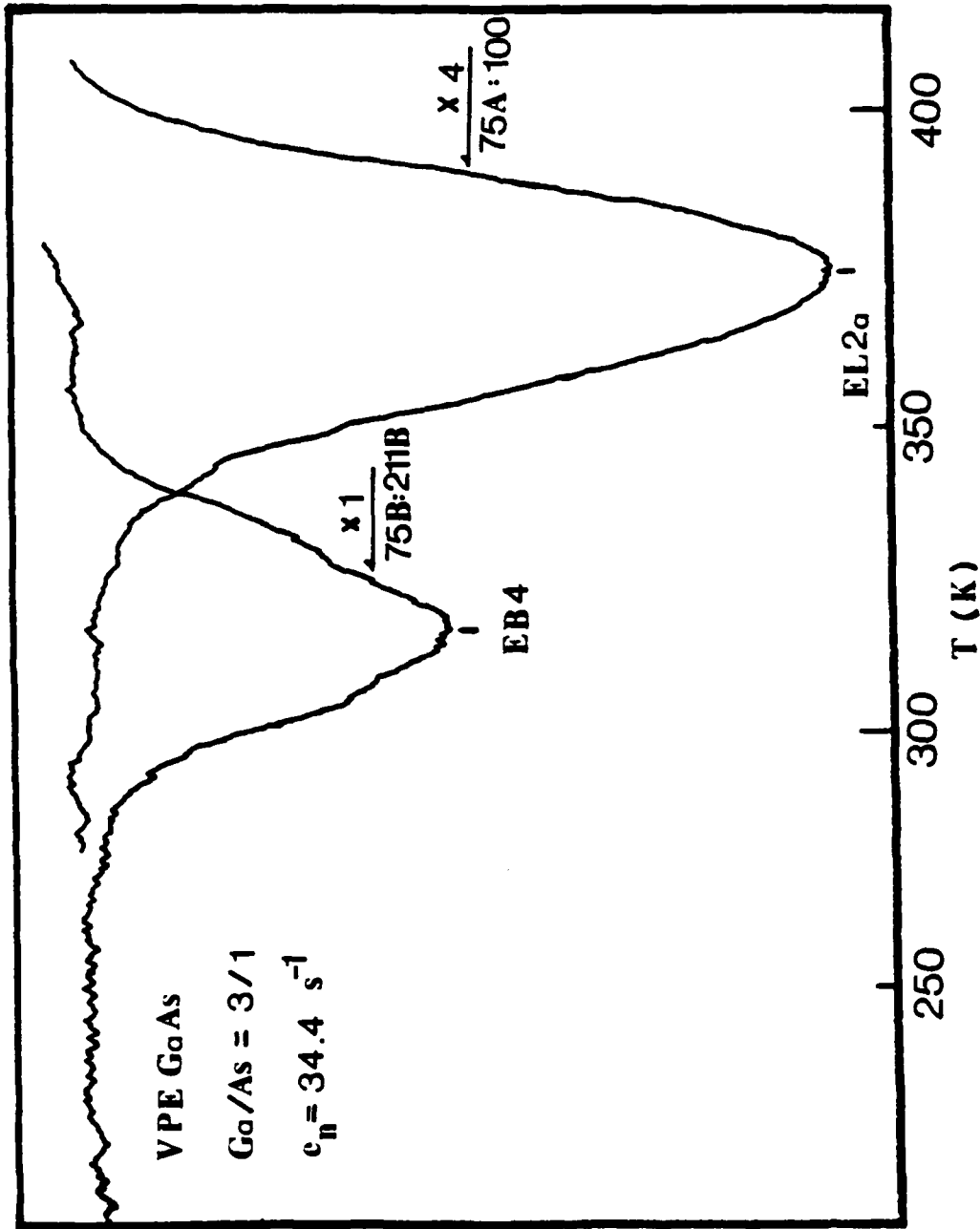


Fig.7.4 DLTS scans of electron trap for VPE GaAs grown on (211 A) and (100) oriented substrates with $[Ga]/[As]$ ratio equal to 3/1.

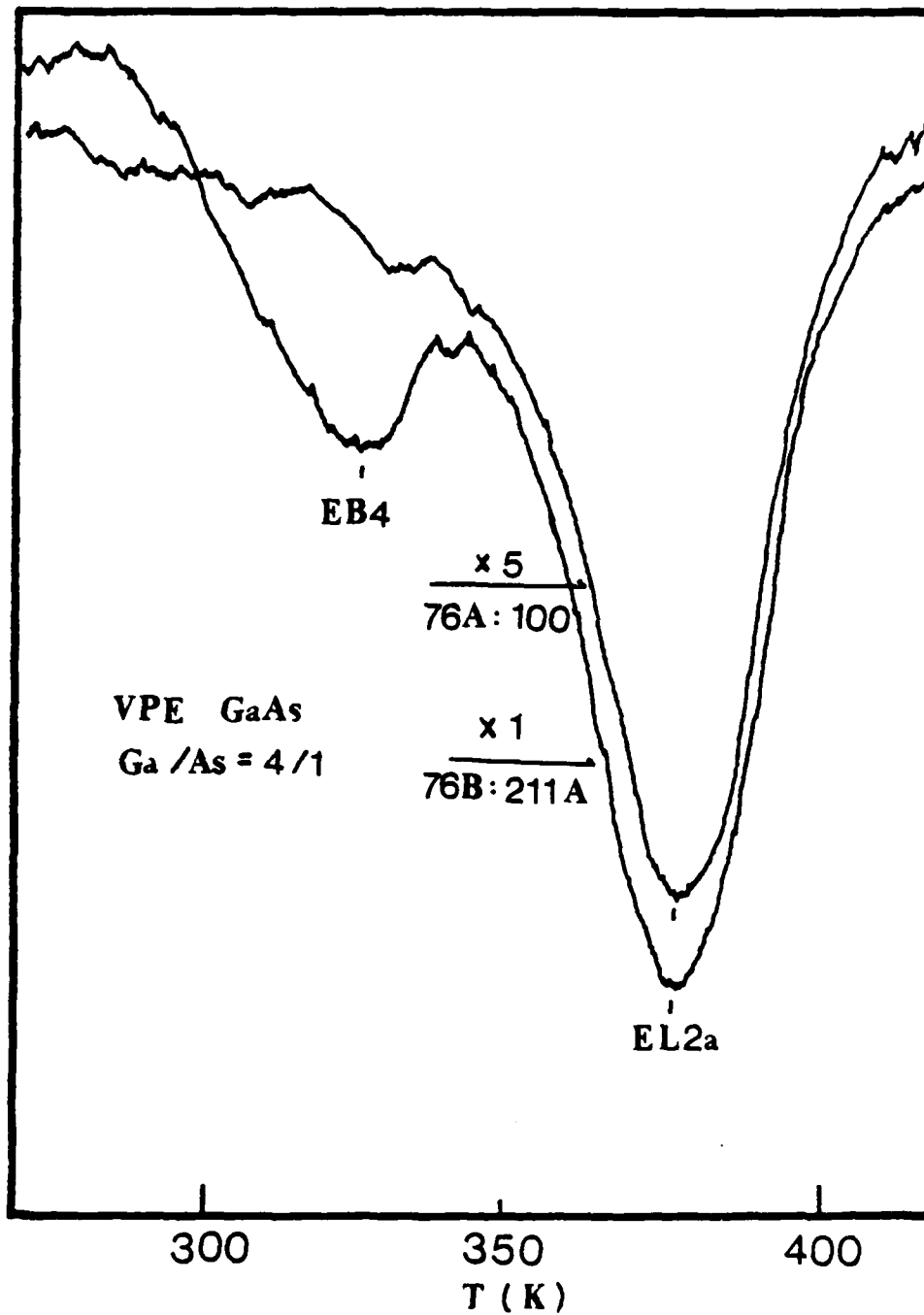


Fig.7.5 DLTS scans of electron traps in VPE GaAs grown on (100) (211 A) substrates with [Ga]/[As] ratio equal to 4/1.

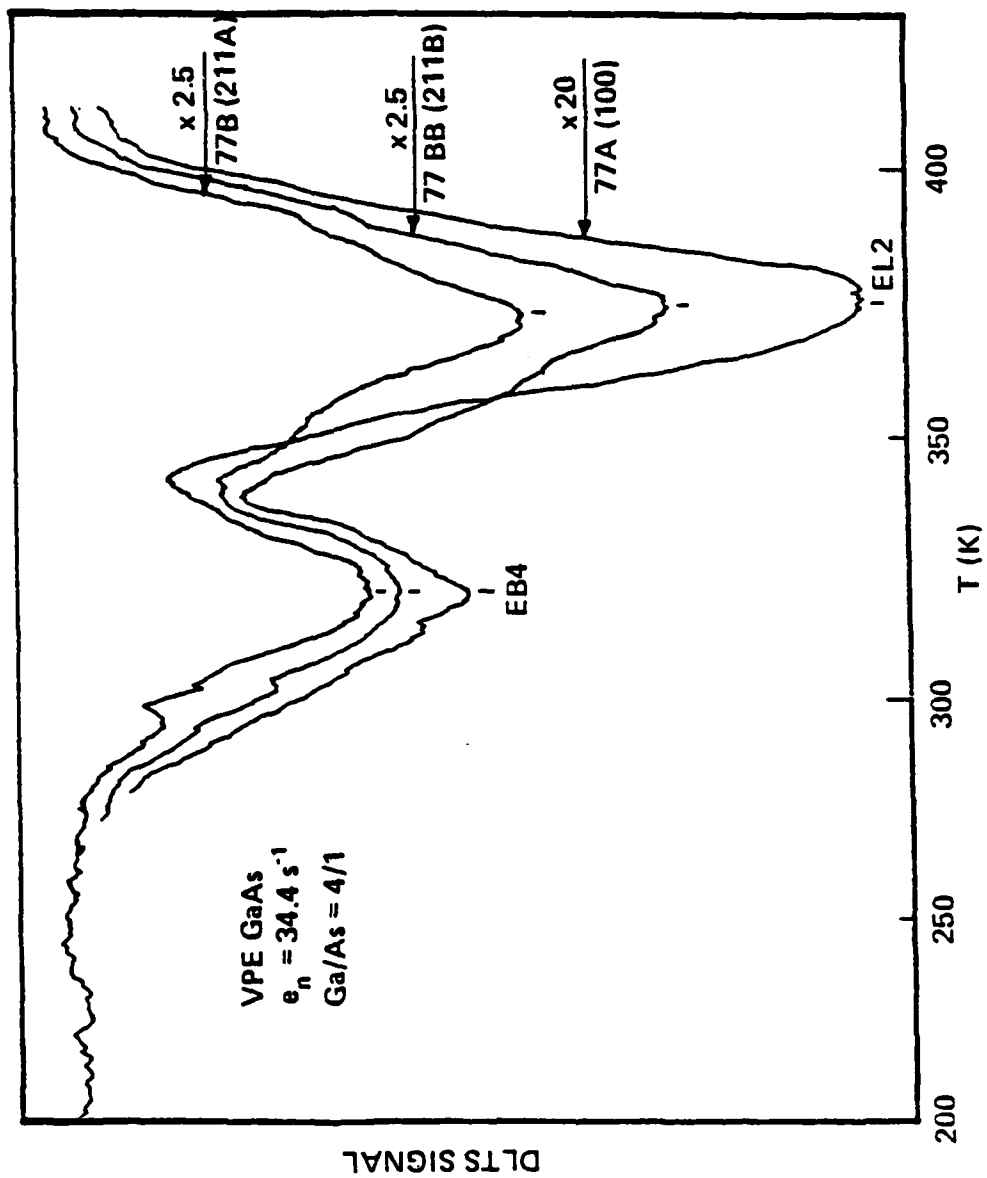


Fig.7.6 DLTS scans of electron traps for VPE GaAs grown on (211 A), (211B) and (100) oriented substrates with [Ga]/[As] ratio equal to 4/1.

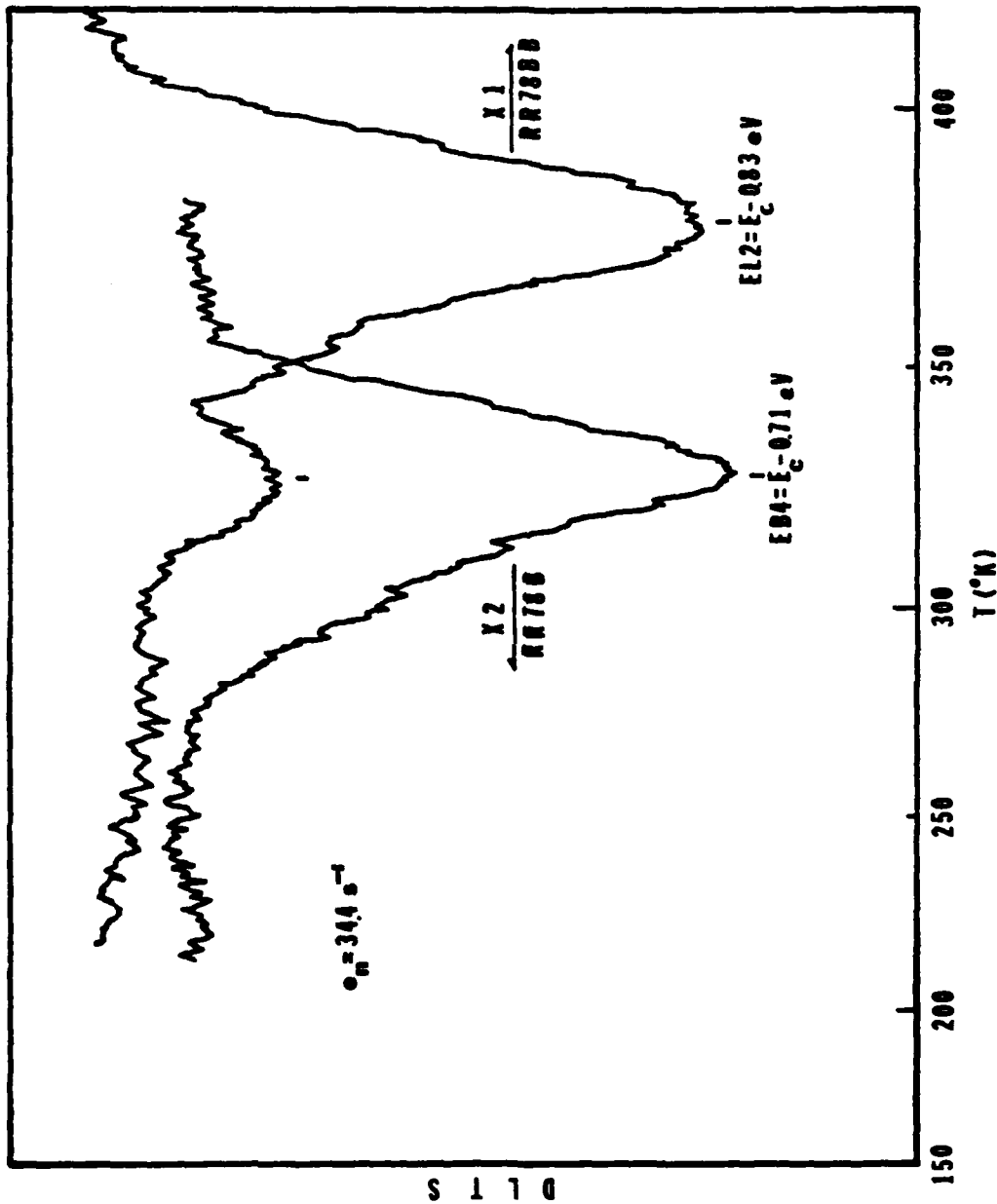


Fig.7.7 DLTS scans of electron traps for VPE GaAs grown on (211 A) and (211B) substrates with [Ga]/[As] ratio equal to 5/1.

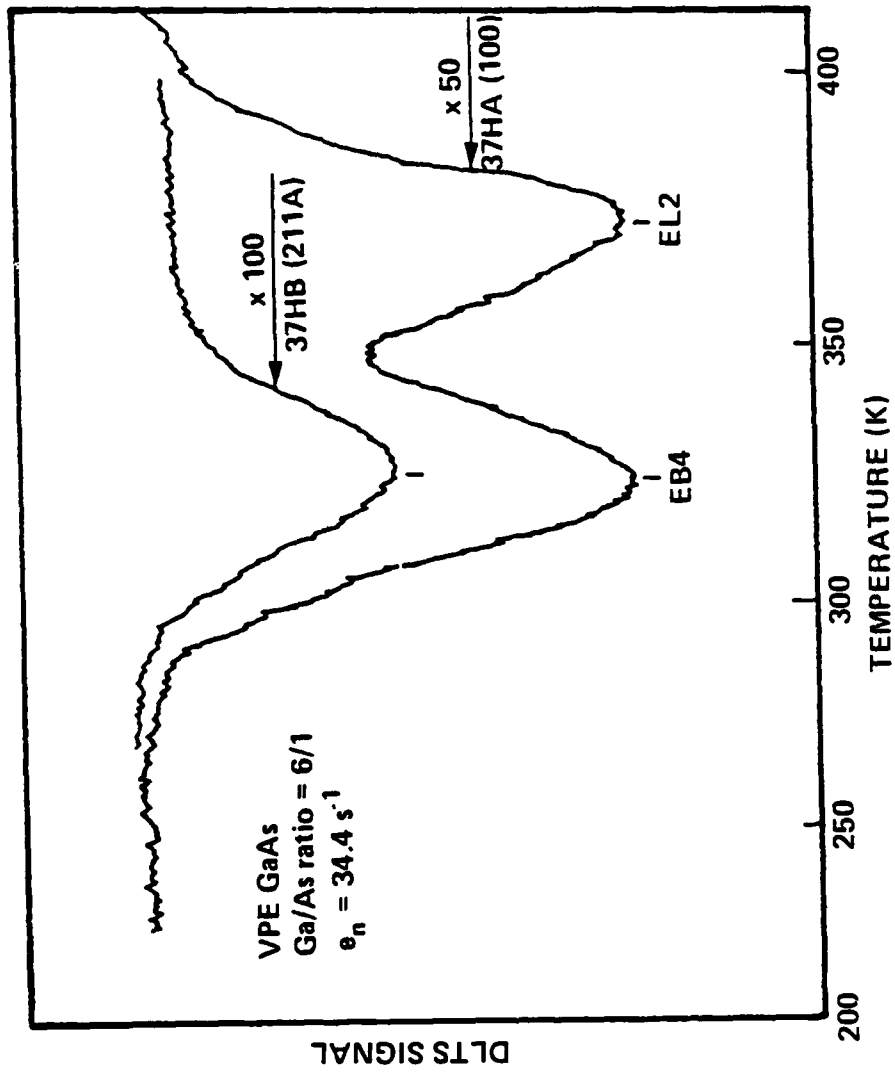


Fig.7.8 DLTS scans of electron traps in GaAs grown on (211 A) and (100) substrates with [C] = [As], e_n equal to 6/1.

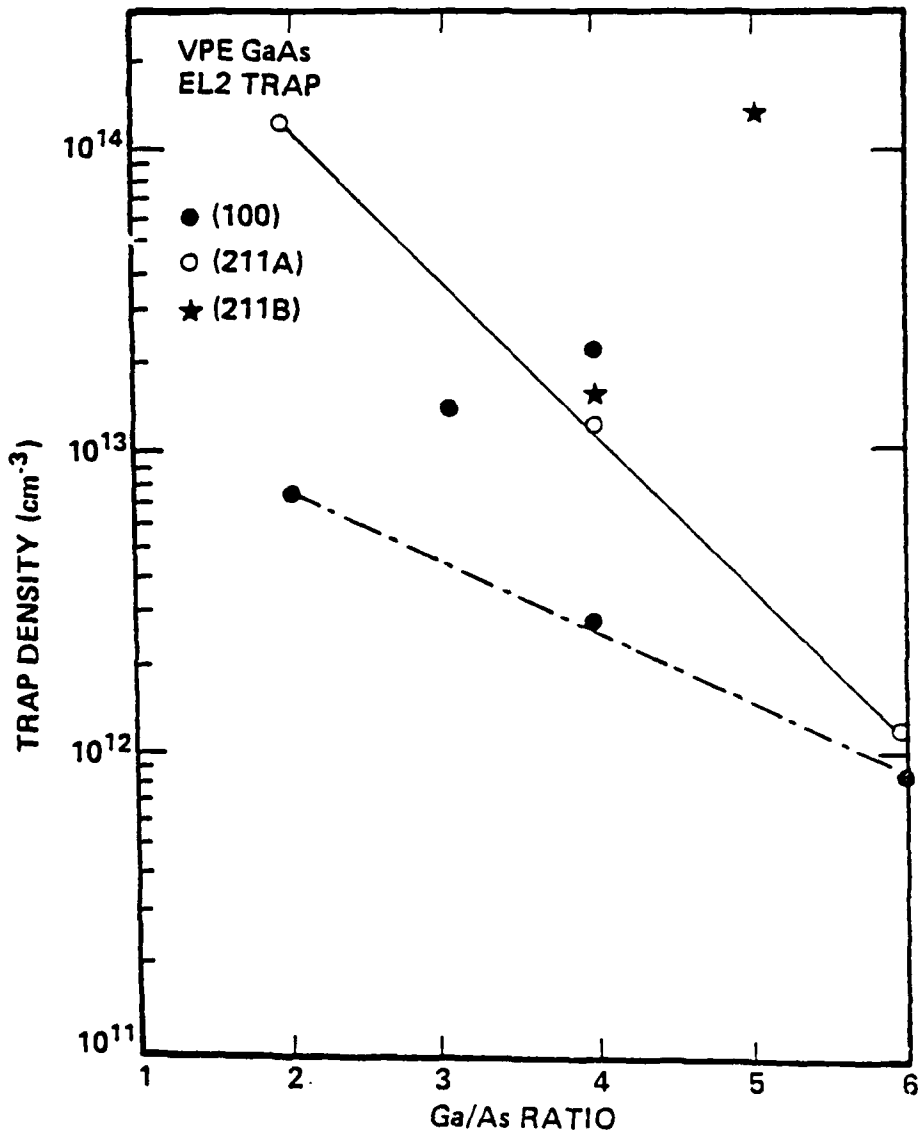


Fig.7.9 Density of EL2 electron traps in VPE GaAs grown on (100), (211 A), and (211B) substrates as a function [Ga]/[As] ratio.

with [Ga]/[As] ratio equal to 6/1. The results showed that both EL2a and EB4 level was observed in sample 37HB. To sum up the results shown in Fig. 7.1 through Fig.7.8 concerning the effects of orientation, [Ga]/[As] ratio, and the growth temperature on the density of EL2a and EB4 levels, we plot in Fig.7.9 the density of EL2a level vs [Ga]/[As] ratio for three substrate orientations. In Fig. 7.9, it is clearly shown that density of EL2a level was found to decrease with increasing [Ga]/[As] ratio for the $\langle 211A \rangle$ oriented samples and to increase with increasing [Ga]/[As] ratio for the $\langle 211B \rangle$ oriented samples; for the $\langle 100 \rangle$ oriented samples the density of EL2a level may increase or decrease with increasing [Ga]/[As] ratio, depending on the V_{Ga} or As_i defects formed during crystal growth. Table 7.1 summarizes the defect parameters deduced from our DLTS and C-V measurements on twelve VPE GaAs samples prepared under different growth conditions and substrate orientations.

7.1.4 Summary and Conclusions.

A study of the grown-in deep level defects in VPE GaAs vs. substrate orientations, [Ga]/[As] ratios, and growth temperature has been carried out in this chapter. One to two electron traps (i.e., $EB4 = E_C - 0.71$ eV, and $EL2 = E_C - 0.83$ eV) have been observed in these VPE GaAs samples. From the results of our DLTS and C-V analysis, it is found that:

- (1) background carrier concentrations are two to five times higher for the $\langle 211A \rangle$ samples than the $\langle 100 \rangle$ samples;
- (2) defect density was in general higher for the $\langle 211 \rangle$ samples than the $\langle 100 \rangle$ oriented-samples;
- (3) density of EL2a level was found to decrease with increasing [Ga]/[As] ratio for the $\langle 211A \rangle$ samples, and increases with [Ga]/[As] ratio for the $\langle 211B \rangle$ samples;

- (4) for the $\langle 100 \rangle$ samples, the density of EL2a level may increase or decrease with $[Ga]/[As]$ ratio depending on the As_i or V_{Ga} defect density formed during crystal growth;
- (5) the EL2a level is attributed to the arsenic antisite defect (As_{Ga}^{++}), formed after crystal cooling;
- (6) for the EB4 electron trap, which is not commonly observed in the VPE GaAs, and its origin is not known.

Table 7.1 Electron trap parameters in VPE GaAs grown with different substrate orientations and growth temperatures.

Sample No.	Orientation	N_D (cm^{-3})	E_T (eV)	Electron Traps			Ga/As ratio	Growth temp. ($^{\circ}\text{C}$)
				N_T (cm^{-3})	E_T (eV)	N_T (cm^{-3})		
35 CA	100	6.7×10^{14}	$E_{B4} = E_C - 0.71$	-	$E_{T1} = E_C - 0.83$	7.6×10^{12}	2/1	715
35 CB	211A	1.7×10^{15}	"	-	"	1.2×10^{14}	2/1	715
75 A	100	7.2×10^{14}	"	-	"	1.5×10^{13}	3/1	725
75 B	211B	3×10^{15}	"	3.9×10^{13}	"	-	3/1	725
76 A	100	3×10^{15}	"	2×10^{12}	"	2.2×10^{13}	4/1	725
76 B	211A	5.5×10^{15}	"	3×10^{13}	"	9×10^{13}	4/1	725
77 A	100	1×10^{15}	"	8×10^{11}	"	2.6×10^{12}	4/1	750
77 B	211A	7.2×10^{15}	"	1×10^{13}	"	1.2×10^{13}	4/1	750
77 BB	211B	5.6×10^{15}	"	1×10^{13}	"	1.6×10^{13}	4/1	750
78 B	211A	3.7×10^{15}	"	4.3×10^{13}	"	-	5/1	725
78 BB	211B	1×10^{16}	"	2.9×10^{13}	"	1.4×10^{14}	5/1	725
37 HA	100	1.3×10^{15}	"	1×10^{12}	"	8.6×10^{11}	6/1	725
37 HB	211A	3.1×10^{15}	"	2.4×10^{11}	"	-	6/1	725
39 HB	211A	7.2×10^{14}	"	-	"	1.2×10^{12}	6/1	720

7.2. Study of Grown-in Deep Level Defects vs Growth Parameters in LEC Grown GaAs

In this section, we present the results of our study of the native defects observed in the LEC grown bulk GaAs. Both p-type GaAs and n-type GaAs have been studied. An acceptor level located at 80 meV from the valence band edge has been observed in the LEC grown p-GaAs. For n-GaAs, a study of the effect of heat treatment on the native defects on samples annealed at 200, 300, and 500°C for one hour in hydrogen (H₂) ambient has also been carried out in this work.

7.2.1 Intrinsic Double Acceptor Level in LEC Grown p-GaAs

Two p-type GaAs specimens grown by the LEC method were chosen for this study. Ohmic contacts were made by evaporation of Ag-Mn alloy, and an Al-Schottky barrier structure was used for C-V and DLTS measurements.

Fig.7.10 shows the DLTS scan of hole trap observed in both sample A and B. The apparent activation energy was obtained from the Arrhenius plot of the hole emission rate e_p/T^2 vs $1/kT$. The measured activation energy for this hole trap is 130 meV from the valence band. The true activation energy of this hole trap is 80 meV if correction due to the temperature dependent capture cross section is taken into account (i.e., $\sigma_p = 7.1 \times 10^{-15} \exp(-\Delta E_p/kT) \text{ cm}^2$, where $\Delta E_p = 50 \text{ meV}$). Thus, it is evident that this hole trap observed by the DLTS experiment is the same center observed in the 1.441 eV emission under photoluminescence experimental excitation and Hall measurements.^[17] This hole trap is a double charged acceptor center, and is due to the gallium antisite defect, $\text{Ga}_{\text{As}}^{--}$. The density of this hole trap was found to vary from 10^{15} to 10^{16} cm^{-3} .

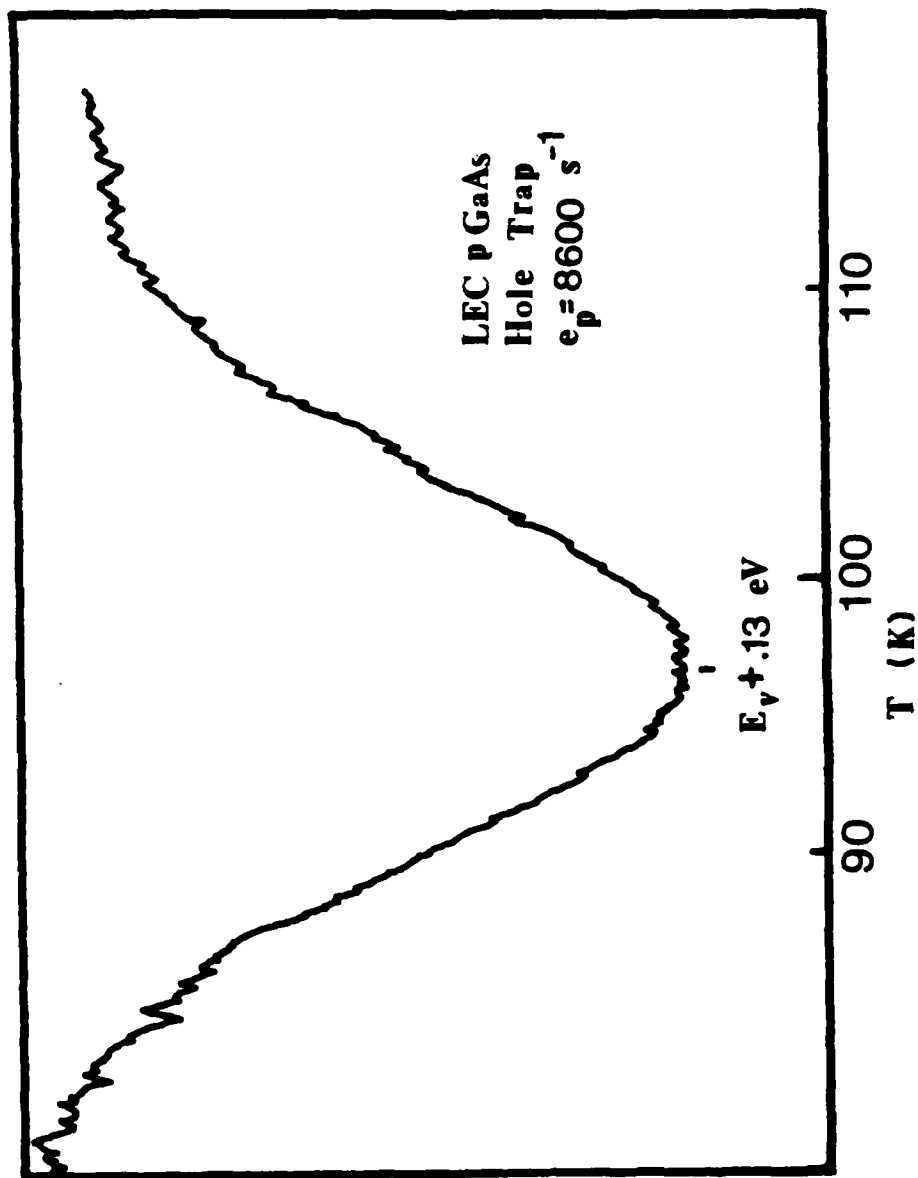


Fig. 7.10 DLTS scan of hole trap for LEC grown p-GaAs. This hole trap is attributed to the Ga_{As} antisite defect.

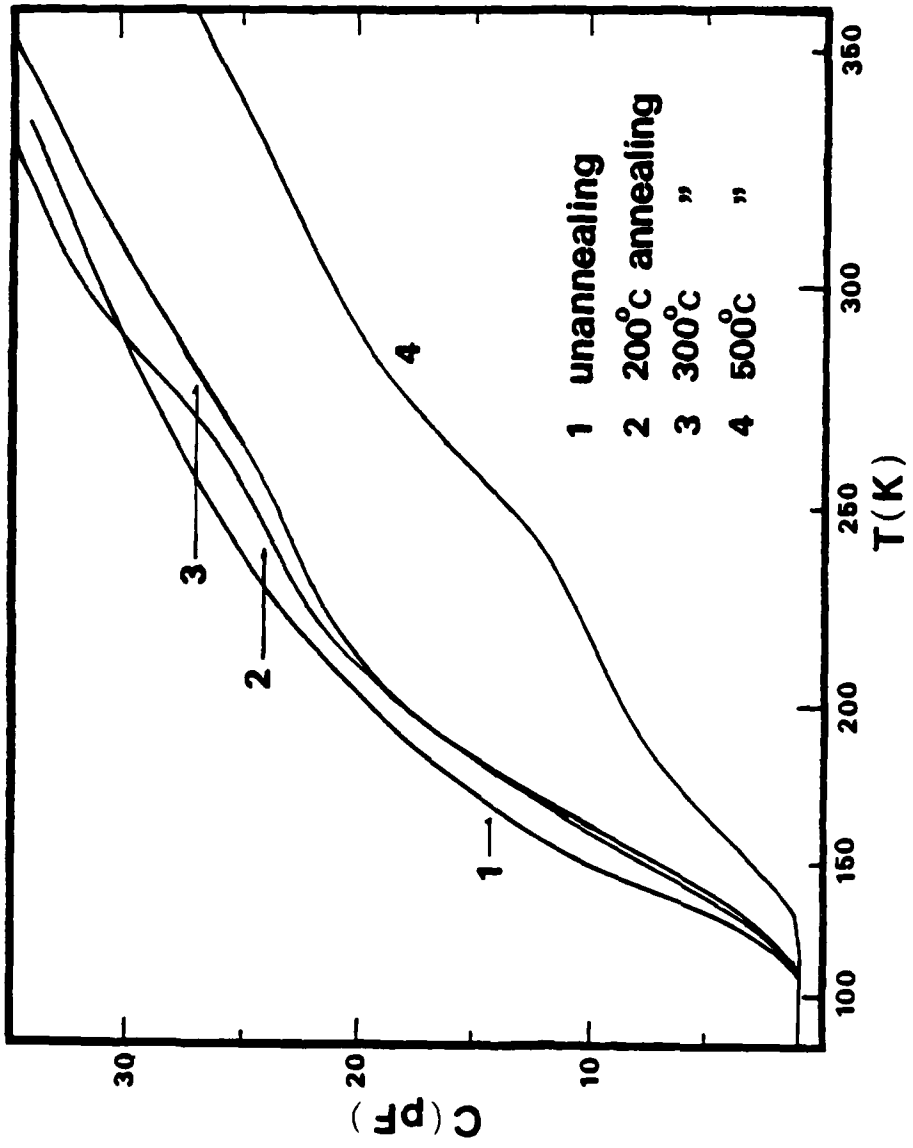


Fig.7.11 Thermally stimulated capacitance (TSCAP) scans for the as-grown and thermally annealed LEC grown p-GaAs specimen.

7.2.2 Study of Deep Level Defects vs Annealing Temperature in LEC Grown n-GaAs

In the following, the results of the TSCAP and DLTS measurements on the LEC n-GaAs materials annealed in hydrogen ambient are discussed. Fig. 7.11 shows the TSCAP scans for the Schottky diodes fabricated from LEC grown n-type GaAs materials at a reverse bias of -2 volts. From this figure, it is noted that the capacitance values for samples annealed at 200 and 300°C for one hour in H₂ ambient show little change from the unannealed sample. However, as the annealing temperature raises to 500°C, the capacitance value decreases by more than 50% from the unannealed sample, indicating a large reduction in free carrier density in the 500°C annealed sample. This may be due to the introduction of the EL2a electron trap by the 500°C annealing process, as is evidenced by our DLTS data. The capacitance steps observed in the TSCAP scans such as those occurred at 130 and 240°K for sample annealed at 500°C are due to the electron emission from the corresponding electron traps, the exact energy level for these electron traps can be determined from the DLTS technique.

The DLTS scans of electron traps for the LEC grown GaAs annealed at 500°C in H₂ ambient for one hour are shown in Fig. 7.12 and 7.13. The defect density deduced from the DLTS measurements are summarized in table 7.2. For samples unannealed or annealed at 200 and 300°C for one hour, there are three electron traps with energies of $E_c - 0.35\text{eV}$, $E_c - 0.61\text{eV}$, and $EL2b = E_c - 0.76\text{eV}$ observed in these samples. As the annealing temperature increases to 500°C, a new electron trap with energy of $E_c - 0.83\text{eV}$ (EL2a level) is emerged into the DLTS scans along with two other electron traps (ie., $E_c - 0.35$ and 0.61eV), while EL2b level disappeared; this is shown in Fig. 7.13. The $E_c - 0.35\text{eV}$ level is the main electron trap observed in these

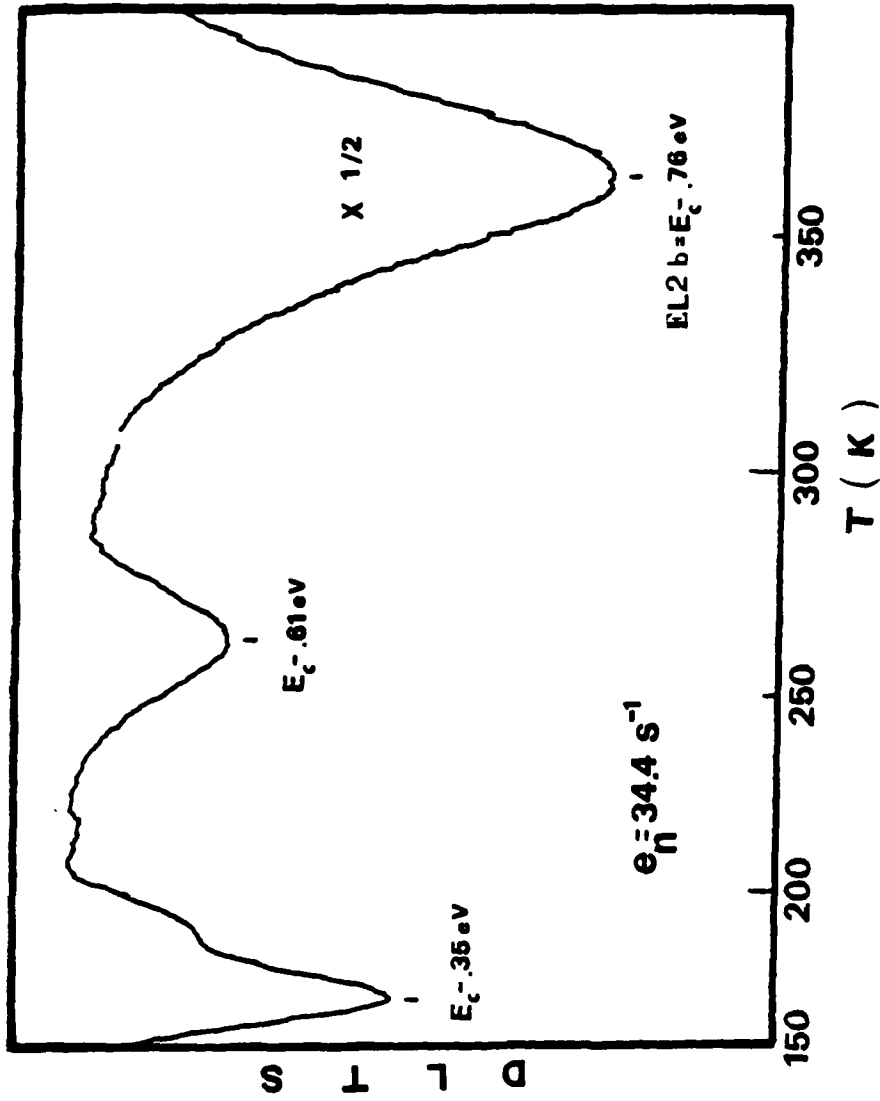


Fig.7.12 DLTS scans of electron traps in the LEC grown n-GaAs specimen.

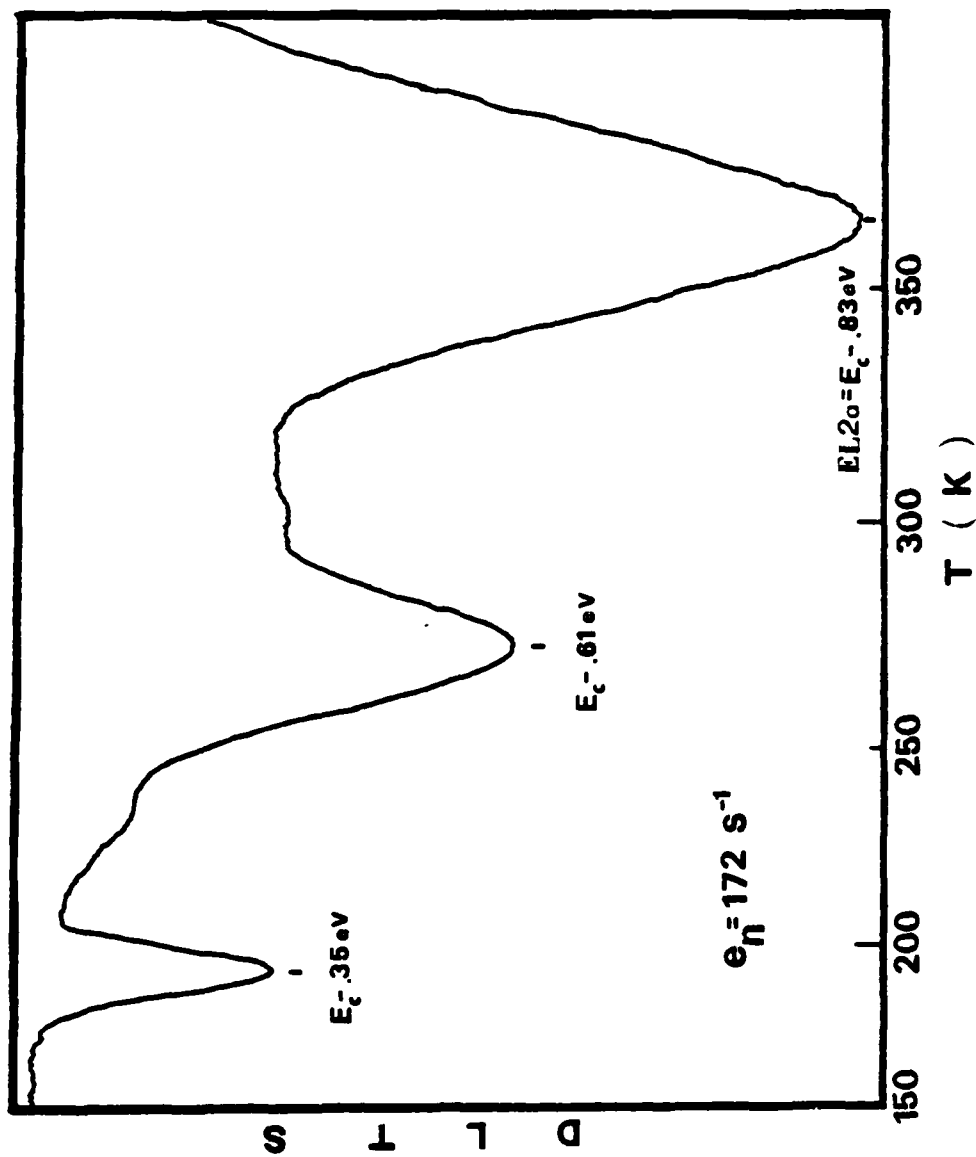


Fig.7.13 DLTS scans of electron traps in the LEC grown n-GaAs specimen annealed at 500 C in H₂ ambient.

Table 7.2 Electron trap parameters in LEC grown n-GaAs for different annealing temperatures.

Samples	N_D (cm ⁻³)	E_T (eV)	N_T (cm ⁻³)	σ_n (cm ²)
Unanneal (As grown)	7.1×10^{15}	$E_1 = E_c - 0.35$	3.3×10^{15}	6.0×10^{-14}
		$E_3 = E_c - 0.61$	1.3×10^{14}	1.2×10^{-13}
		$E_4 = E_c - 0.76$	1.6×10^{15}	7.1×10^{-14}
200°C, H ₂ 1 hour	5×10^{15}	E_1	5×10^{14}	6.0×10^{-14}
		E_3	4×10^{14}	1.2×10^{-13}
		E_4	2.5×10^{14}	7.1×10^{-14}
300°C, H ₂ 1 hour	4.3×10^{15}	E_1	1.1×10^{15}	6.0×10^{-14}
		E_3	1×10^{14}	1.2×10^{-13}
		E_4	1.3×10^{14}	7.1×10^{-14}
500°C, H ₂ 1 hour	3.3×10^{15}	E_1	6×10^{14}	6.0×10^{-14}
		E_3	2.6×10^{13}	1.2×10^{-13}
		$E_5 = E_c - 0.83$	7.2×10^{14}	5×10^{-13}

* Annealing performed in H₂ ambient for one hour.

LEC: Liquid Encapsulated Czochralski technique.

N_T measured at the 2 μ m depletion width.

LEC grown GaAs samples. This trap has also been reported by Martin et al [77] in the bulk GaAs and by Fairman et al [106] in the VPE grown GaAs. The reduction in free carrier density with increasing annealing temperature along with large capture cross section for these electron traps indicating that they are acceptor type electron traps. Another interesting study on these traps is concerned with the spatial dependence of the defect density for each electron trap. This is obtained by performing the bias dependence of the DLTS scans, and the results are illustrated in Fig.7.14. From the DLTS scans as a function of the reverse bias voltage, the spatial dependence of trap density is determined for each trap. Fig. 7.15 show the spatial dependence of the electron traps observed in the 200°C annealed samples. It is shown that for all the samples studied here, the defect density is highest at the surface, and decreases as it moves away from the interface of the metal GaAs Schottky contact; the trap density becomes constant deep into the bulk region (ie., 2um) of the GaAs substrate, indicating that all these electron traps are bulk related defects. Mircea et al [30] have also observed a similar defect density profile for the $E_C - 0.61\text{eV}$ level in which the density of $E_C - 0.61\text{eV}$ was increased by the mechanical damage near the surface of GaAs specimen.

Fig. 7.16 shows the spatial dependence of the $E_C - 0.35\text{eV}$ electron trap in the unannealed and annealed samples. The results showed that density of the $E_C - 0.35\text{eV}$ trap was decreased with increasing annealing temperature. EL2b trap was annealed out followed by a 500°C annealing in H_2 ambient for one hour. Recently, Day et al [94] has observed the $E_C - 0.35\text{eV}$ and EL2b = $E_C - 0.76\text{eV}$ traps in the MBE grown n-GaAs, and found that both $E_C - 0.35\text{eV}$ and EL2b traps can be annealed out at 800°C for 1/2 hour. To explain their results, the EL2 model proposed in previous chapter appears to be adequate

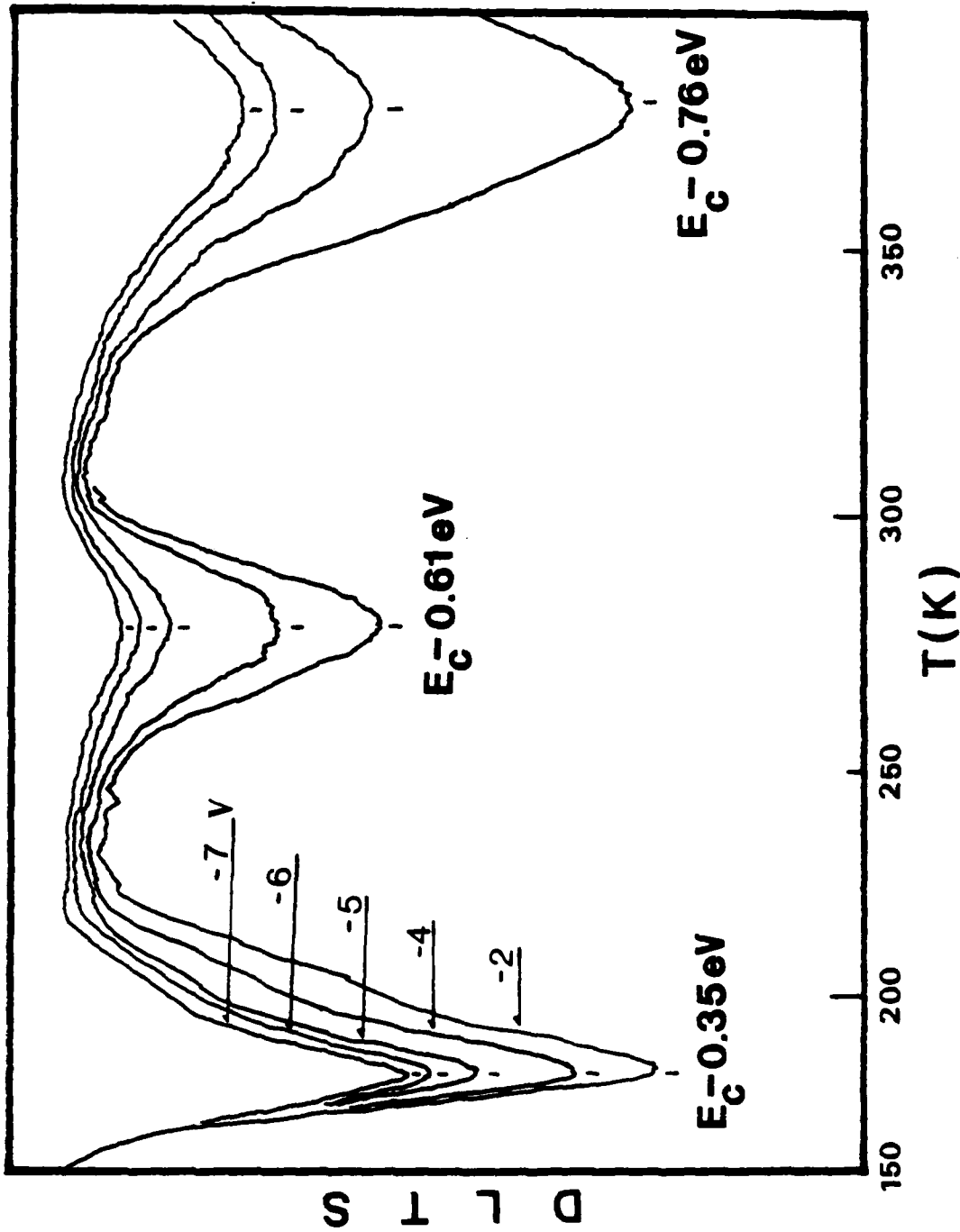


Fig.7.14 DLTS scans of electron traps in the LBC grown n-GaAs specimen under different reverse bias conditions.

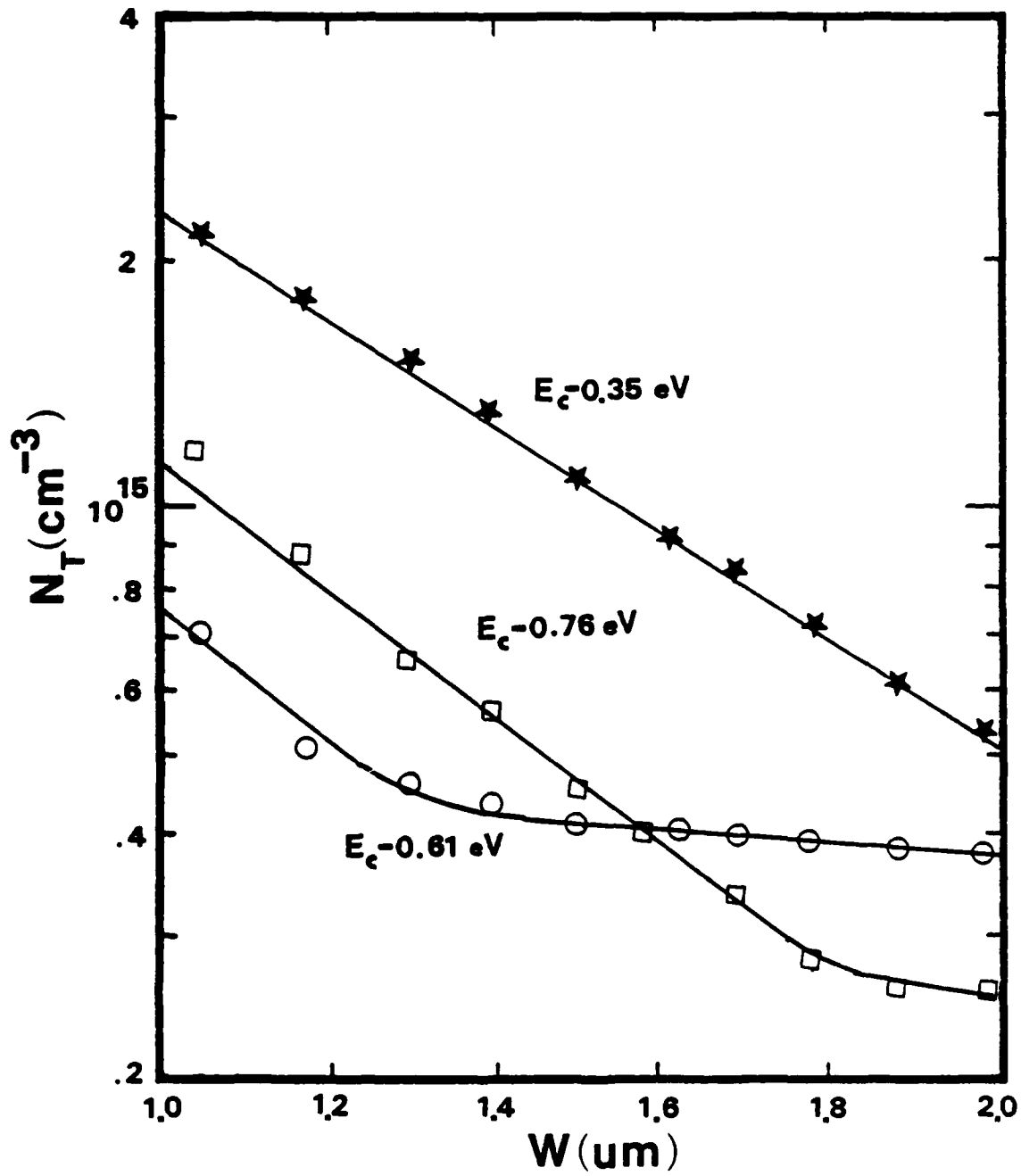


Fig.7.15 Density of electron traps in the 200 C annealed GaAs specimen as a function of the depletion layer width.

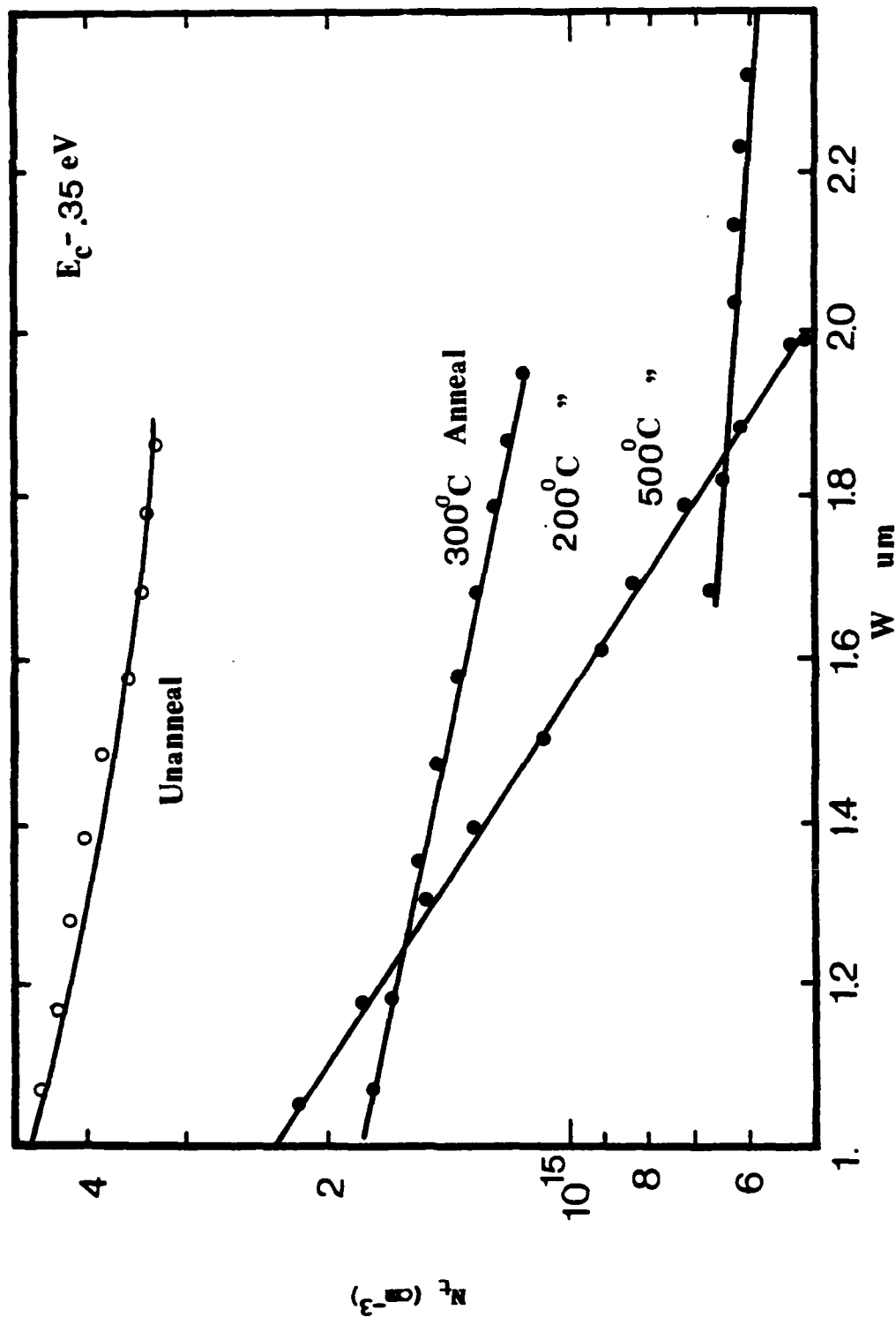


Fig.7.16 Density of $E_c=0.35$ eV electron trap vs depletion layer width in LEC grown n-GaAs for different annealing temperatures.

for this case. The physical origin of EL2b trap is attributed to $As_{Ga}V_{As}$ complex. At $500^{\circ}C$ annealing temperature, the EL2b level (i.e., the $As_{Ga}V_{As}$) will decompose into V_{Ga} , and its reaction equation is given by:



Note that at high annealing temperatures (eg., $T_a > 500^{\circ}C$), the trap may be formed by the migration of V_{Ga} defect to the As_j site to form an arsenic-antisite defect as was predicted by Eq.(6.18). This defect model seems adequate for explaining change of the EL2b trap to EL2a level at high annealing temperatures as shown above.

7.3. Grown-in Deep Level Defects vs Growth Parameters in the LPE n-GaAs Layers.

Samples of LPE GaAs were prepared for studying grown-in defects vs growth temperature and growth rate in the high purity n-GaAs epilayers. These samples were prepared by infinite solution melt LPE technique grown at 700 and $800^{\circ}C$ with cooling rate of 0.4 and $1^{\circ}C/min.$, respectively. Fig.7.17 shows the DLTS scans of electron trap ($EB4=E_c-0.71eV$) for samples grown at 700 and $800^{\circ}C$ with cooling rate of $1^{\circ}C/min.$. Note that for the same cooling rate, sample grown at $800^{\circ}C$ has defect density six times lower than that of the $700^{\circ}C$ grown sample. On the other hand, for sample grown at 700 and $800^{\circ}C$ with a cooling rate of $0.4^{\circ}C/min.$, no electron traps were detected in these samples. The results of our DLTS and C-V measurements on the LPE GaAs were summarized in table 7.3. The background concentration in these samples is around $10^{16} cm^{-3}$.

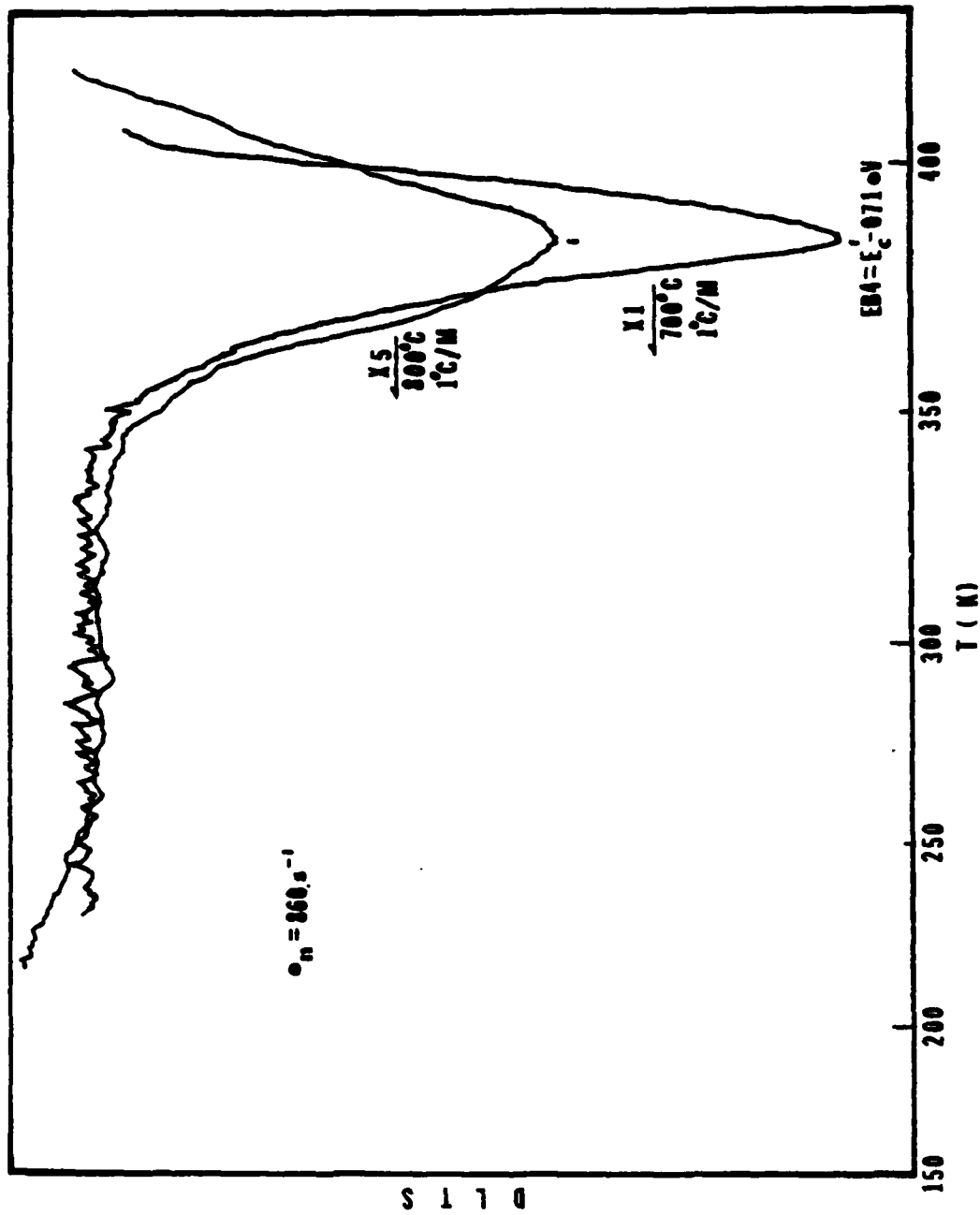


Fig.7.17 DLTS scans of electron trap for two LPE GaAs grown at 700 and 800 C with 1 C/min. cooling rate.

7.4. Grown-in Deep Level Defects vs Growth Parameters in MOCVD Grown n-GaAs Epi-layers.

Characterization of native defects in n-GaAs epilayers grown on S.I. GaAs and S.I. Ge substrates by the MOCVD technique has been studied. The Sn-doped GaAs epilayer on S.I. GaAs substrate was grown at 700°C for 30 min. with [Ga]/[As] ratio of 11/1, and the dopant density was $4.1 \times 10^{17} \text{ cm}^{-3}$. As for the Sn-doped GaAs epilayer on the S.I. Ge substrate, the sample was prepared at 706°C for 30 min. with [Ga]/[As] ratio of 7/1; the background concentration was found to vary between 10^{16} to $1.9 \times 10^{17} \text{ cm}^{-3}$. Fig.7.18 shows the DLTS scan for n-GaAs layers on S.I. GaAs substrate. The result shows that there is one electron trap with energy of $E_c - 0.6 \text{ eV}$. This trap level is corresponding to the $E_c - 0.61 \text{ eV}$ for the LEC grown GaAs samples. As for the GaAs layer on S.I. Ge-substrate, one hole trap with energy of $E_v + 0.75 \text{ eV}$ and the density of $1.7 \times 10^{13} \text{ cm}^{-3}$ was observed in this sample.

7.5. Summary and Conclusions.

From the results of our study of the grown-in defects in the LEC, VPE, LPE, and MOCVD GaAs samples, it is clear that grown-in defects and the background concentration are sensitive to the growth conditions, stoichiometry, and substrate orientations. Table 7.4 shows the trap level observed in this study. The main conclusions are listed as follows:

- (1) EL2a = $E_c - 0.83 \text{ eV}$ electron trap is attributed to the $(\text{As}_{\text{Ga}}^{++})$ arsenic-antisite defect which was observed in VPE GaAs, and in 500°C annealed (H₂) LEC grown GaAs.
- (2) EL2b = $E_c - 0.76 \text{ eV}$ electron trap is attributed to the $\text{As}_{\text{Ga}}\text{V}_{\text{As}}$ complex which was observed in the LEC grown GaAs. This level was annealed out by a 500°C hydrogen gas heat treatment.

- (3) $E_v + 0.08\text{eV}$ hole trap was observed in the LEC grown p-GaAs samples. The physical origin of this hole trap is believed to be due to Ga_{As} gallium-antisite defect as confirmed by the Hall effect and photoluminescence measurements.
- (4) Reducing the temperature cooling rate during crystal growth is beneficial for reducing the density of grown-in defects in LPE GaAs epilayers.

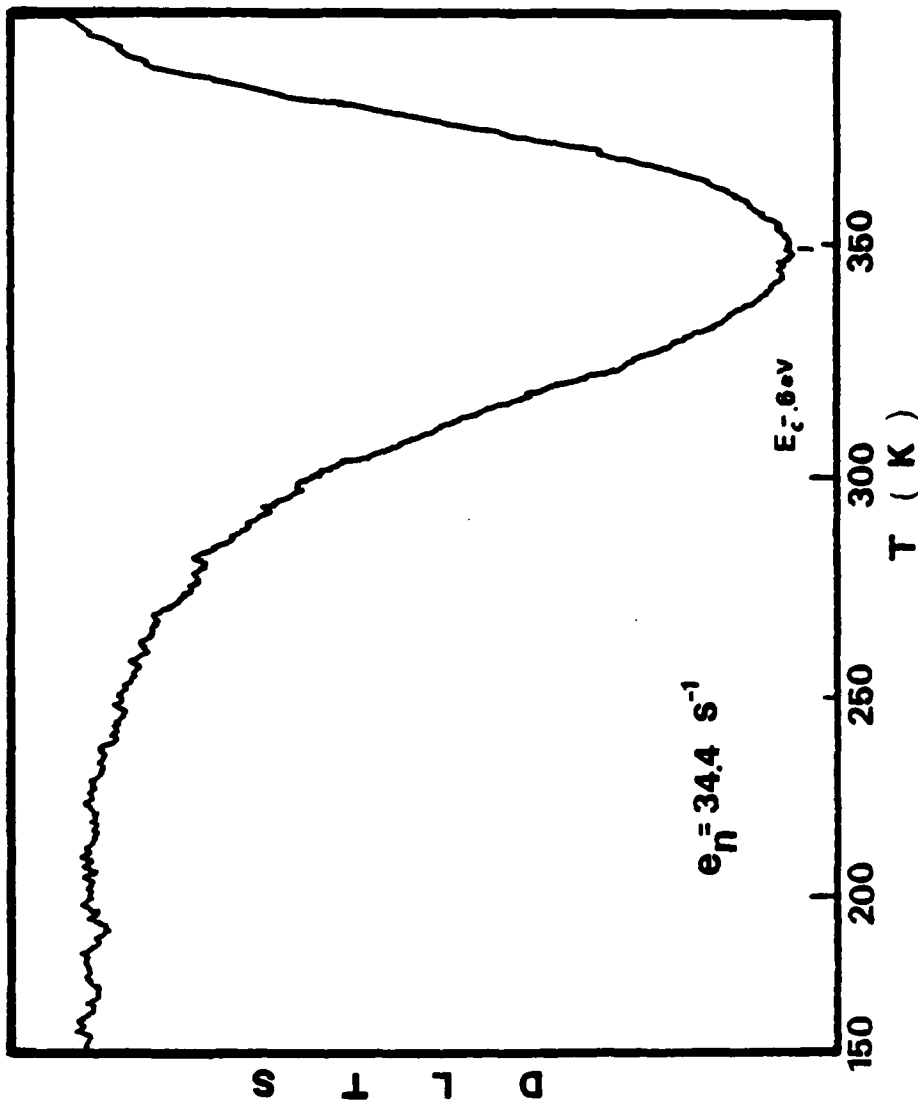


Fig.7.18 DLTS scan of electron trap in MOCVD GaAs grown on S.I.GaAs substrate.

Table 7.3 Grown-in deep-level defects in LPE GaAs*

Samples	Growth temperature and cooling rate	Electron trap Level (eV)	N_t (cm^{-3})	N_D (cm^{-3})	Epilayer thickness (μm)
LEPI-45	700°C, 0.4°C/min.	-	-	9×10^{15}	2
LEPI-46	" 1°C/min.	$E_C - 0.71$	10^{14}	1.6×10^{16}	3
LEPI-43	800°C, 0.4°C/min.	-	-	10^{16}	5
LEPI-44	" 1°C/min.	$E_C - 0.71$	1.6×10^{13}	2×10^{16}	7.5

* Grown by infinite solution melt liquid phase epitaxial technique at Hughes Research Lab.

Table 7.4 Grown-in defects observed in LEC, LPE, and MOCVD grown GaAs.

Samples	Trap level
	$E_C - 0.35\text{eV}$ $E_C - 0.6\text{ eV}$ $E_C - 0.71\text{eV}$ $E_C - 0.76\text{eV}$ $E_C - 0.83\text{eV}$ $E_V + 0.08\text{eV}$
n-GaAs	*
n-LPE	*
n-LEC	* *
p-LEC	*
n-MOCVD	*
Possible Origins	As _{Ga} V _{As} As _{Ga} ⁺⁺ Ga _{As}

VIII. SUMMARY AND CONCLUSIONS

A detailed theoretical and experimental study of the grown-in deep-level defects and radiation-induced defects in GaAs has been carried out in this research. The main contributions from this research include: (i) Development of a new defect model for predicting native defects and defect density vs growth parameters in GaAs, (ii) modelling and new interpretation of the EL2 electron trap in GaAs, (iii) determination of the energy level and trap density for a large number of deep-level traps observed in GaAs grown by LEC, VPE, LPE, and MOCVD techniques under different growth and annealing conditions, (iv) determination of the potential well for several electron traps in GaAs from the field enhanced emission rates deduced from the DLTS data, which enable us to determine the charge state of each trap in GaAs. The research findings described in this report has led to the following conclusions:

(1) A theoretical model for interpreting the nonexponential capacitance transients due to electric field dependent emission rate of trapped charge has been developed. Based on the nonexponential capacitance transient, theoretical calculations of DLTS response for the deep level traps in GaAs were made using five different potential wells; namely, the Coulombic well, Dirac well, square well, polarization well, and dipole well. A comparison of the theoretical calculation of the nonexponential DLTS response with the DLTS data for each trap level enable us to determine the potential well for each trap in GaAs. This method has been applied to determine the charge state and the physical origins of the EL2 electron trap in GaAs.

(2) A theoretical model for predicting native point defects in GaAs has been developed. The chemical thermodynamic principles are employed to derive the density of vacancy and interstitial defects during crystal growth and under thermal equilibrium condition. After crystal growth, the thermal kinetic equations are employed to predict the antisite defect. The results show that : (i) high purity GaAs material can be grown for the low arsenic pressure case under optimum cooling condition. (ii) GaAs grown under higher arsenic pressure condition (e.g., LEC, VPE and MOCVD grown GaAs) will produce more native point defects than under lower arsenic pressure condition (e.g., LPE grown GaAs), (iii) arsenic antisite defect can only be observed in GaAs grown under As-rich or high arsenic pressure condition; this defect can not be produced under low arsenic pressure and Ga-rich conditions.

(3) A new defect model for the EL2 electron trap in GaAs was developed in this study. The EL2 electron trap is attributed to two different native point defects. One is designated as the EL2a ($E_C - 0.83\text{eV}$) electron trap, and the other is denoted as the EL2b ($E_C - 0.76\text{eV}$) electron trap. The physical origin for the EL2a level is attributed to the arsenic antisite ($\text{As}_{\text{Ga}}^{++}$) defect, whereas, the physical origin for the EL2b level is attributed to the arsenic- antisite and arsenic- vacancy complex ($\text{As}_{\text{Ga}}\text{V}_{\text{As}}$). Based on this model, relationship between the density of EL2a and EL2b trap levels vs $[\text{As}]/[\text{Ga}]$ mole fraction ratio in the MOCVD and VPE grown GaAs is established. The result shows that density of EL2a trap is proportional to the mole fraction ratio of $(r-1)^{1/2}$; while the density of EL2b trap is proportional to the mole fraction ratio of $(r-1)^{1/4}$, where $r = [\text{As}]/[\text{Ga}]$. This prediction is in good agreement with experimental data reported for the MOCVD and VPE grown GaAs.

(4) From the results of our DLTS study of the grown-in defects in the LEC, VPE, LPE, and MOCVD GaAs samples, it is shown that grown-in defects and the background concentration are sensitive to the growth conditions, stoichiometry, and substrate orientations. The main technical findings from this study include: (i) EL2a electron trap was observed in VPE grown GaAs and in LEC grown GaAs annealed at 500°C in H₂ ambient; (ii) EL2b electron trap was observed in the unannealed LEC grown GaAs, and its density can be reduced by low temperature thermal annealing; (iii) a shallow hole trap with energy of $E_v + 0.08$ eV was observed in the LEC grown p-GaAs. The physical origin of this hole trap is attributed to the gallium antisite (Ga_{As}) defect; (iv) using slow temperature cooling rate after crystal growth is beneficial for reducing the density of grown-in defects in the LPE grown GaAs. The theoretical modelling of native point defects and EL2 electron trap in GaAs described in this work was found in good agreement with the experimental results for the deep-level defects in GaAs grown by different growth techniques and growth conditions presented in this report.

Studies of radiation induced deep-level defects in the LPE grown GaAs irradiated by one-MeV electron irradiation and low energy proton irradiation under different irradiation and annealing conditions have also been carried out in this research program, and the results have been presented in the 1983 AFOSR Annual Technical Report.

IX. PUBLICATIONS AND CONFERENCE PRESENTATIONS

1. S. S. Li, W. L. Wang, P. W. Lai, R. Y. Loo, G. S. Kamath, and R. C. Knechtli, "Deep level defects and recombination parameters in proton irradiated AlGaAs-GaAs solar cells," 14th IEEE Photovoltaic Special Conference, San Diego, Cal., p.1080 (1980).
2. S.S. Li, W. L. Wang, P. W. Lai, R. Y. Loo, G. S. Kamath, and R. C. Knechtli, "Deep level defects, recombination mechanisms and their correlation to the performance of low-energy proton- irradiated AlGaAs-GaAs solar cells." IEEE Trans.on Electron Devices, Vol. ED-27, N-4, p.857 (1980).
3. S. S. Li, W. L. Wang, P. W. Lai, and R. T. Owen, "Deep Level Defects and Diffusion Length Measurements in Low Energy Proton Irradiated GaAs," J. Electronic Materials, V9, N2, p.335 (1980).
4. P. C. Colter, C. W. Litton, D. C. Renolds, D. C. Look, P. W. Yu, S. S. Li, and W. L. Wang, "A Novel Ga/AsCl₃/H₂ Reactors for Controlling Stoichiometry in the Growth of Vapor Phase Epitaxial GaAs." Proc. of the International Symposium on Semiconductor Growth Technology, V.323, p.328 (1982).
5. S. S. Li, W. L. Wang, R. Y. Loo, and W. P. Rahilly, "Defects and Annealing Studies in One-MeV Electron Irradiated (AlGa)As- GaAs Solar Cells." Presented at the Space Photovoltaic and Radiation Effects Conference, at NASA Lewis Research Center, April (1982).

6. S. S. Li, W. L. Wang, R. Y. Loo, and W. P. Rahilly, "Deep level Defects and Annealing Studies in One-MeV Electron Irradiated GaAs Solar Cells." Proceeding of the 16th IEEE Photovoltaic Specialists Conference, Sept. p.211 (1982).
7. P. W. Yu, W. C. Mitchel, M. C. Mier, S. S. Li, and W. L. Wang, "Evidence of intrinsic double acceptor in GaAs." Appl. Phy. Lett. 41(6), p.532 (1982).
8. S. S. Li, W. L. Wang, P. C. Colter, and C. W. Litton, "Study of grown-in Deep-level Defects vs. Growth Parameters in GaAs Grown by the VPE Technique," J. Electronic Materials, V.12, p.223 (1983).
9. S. S. Li, W. L. Wang, R. Y. Loo, and W. P. Rahilly, "Study of Deep - level Defects and Annealing Effects in Undoped and Sn-doped GaAs Irradiated by One-MeV Electrons." Solid State Electron., V.26, N9, p.835 (1983).
10. S. S. Li, W. L. Wang, R. Y. Loo, and W. P. Rahilly, "Defect Studies in One-MeV Electron Irradiated GaAs and in $Al_xGa_{1-x}As$ P-N Junction Solar Cells," presented at the Space Photovoltaic Workshop, NASA Lewis Research Center. Oct., (1983)
12. W. L. Wang and S. S. Li, "Defect Studies in One-MeV Electron Irradiated and Low Energy Proton Irradiated GaAs Solar Cells." presented at the 17th IEEE Photovoltaic Specialists Conference, Orlando, FL. May 1-3, (1984).

13. W. L. Wang, S. S. Li, and T. J. Anderson, "Modeling of the EL2 electron trap in GaAs." Accepted for publication in Solid State Electronics, (1984).
14. S. S. Li, W. L. Wang and E. H. Shaban, "Characterization of Grown-in Defects in Zn-doped InP," Solid State Comm., vol.51, no.1, p.15 (1984).
15. W. L. Wang and S. S. Li, "Determination of Potential Well of the Deep-level traps using field enhancement emission rate analysis of nonexponential DLTS in GaAs." paper to be presented at the 1984 International Electronic Devices and Materials Symposium, Hsinchu, Taiwan, Sept.4 - 6, (1984).
16. W. L. Wang and S. S. Li, "On the Physical Origins and New Interpretation of the EL2 Electron Trap in GaAs," to be presented at the International Conference on Solid State Devices and Materials, Kobe, Japan, Aug.31 - Sept.2 (1984).

X. REFERENCES

1. A.G.Miles, "Impurity and Defect levels in Gallium Arsenide." May (1981).
2. A.J.R.Dekock, S.D.Ferris, L.C.Kimerling, and H.J.Leamy, *Appl. Phys. Lett.*, 27, p.313 (1975).
3. T.Kamejima, *J. Appl. Phys.*, 50, p.3312 (1979).
4. S.Fujita, S.M.Bedair, M.A.Littlejohn, and J.R.Hauser, *J. Appl. Phys.* 51, p.5438 (1980).
5. P.K.Bhattacharya, J.W.Ku, and J.T.Owen, *Appl. Phys. Lett.*, 36, 304 (1980).
6. C.T.Sah and V.G.V.Redd, *IEEE ED-11*, p.3014 (1974).
7. D.V.Lang, *J. Appl. Phys.*, 45, N7, p.3014 (1974).
8. H.Kressel, *J. Elect. Mater.*, 3, p.747 (1974).
9. K.K.Johnson, S.R.Steele, and P.E.Whittier, *Inst. Phys. Conf. Ser.* N45, p.38 (1979).
10. A.G.Miles, "Deep impurity in Semiconductors.", John Wiley & Sons, New York (1973).
11. S.S.Li, W.L.Wang, and E.H.Shaban, "Characterization of the grown-in defects in Zn-doped InP." *Solid State Communication*, in press.
12. W.L.Wang and S.S.Li, "Determination of potential well of deep-level traps using field enhancement emission rate analysis of nonexponential DLTS in GaAs." to be presented at the International Electronic Devices and Materials Symposium, Hsin Chu, Taiwan, R.O.C. Sept. (1984)
13. W.L.Wang, S.S.Li, and T.J.Anderson, "Modelling of the EL2 electron trap in GaAs." accepted in *Solid State Electronics*, (1984).
14. D.V.Lang, *J. Appl. Phys.*, 45, N7, p.3023 (1974).
15. P.Omling, L.Samulson, and H.G.Grimmeiss, *J. Appl. Phys.*, 54, p.5117 (1983).

16. Alex C.Wang and C.T.Sah, J. Appl. Phys., 55, N2, p.565 (1984).
17. P.W.Yu, W.C.Mitchel, M.C.Mier, S.S.Li, and W.L.Wang, Appl. Phys. Lett., 41, N6, p.532 (1982).
18. S.S.Li, W.L.Wang, P.W.Lai, R.Y.Loo, G.S.Kamath, and R.C.Knechtli, IEEE Trans. Electron Devices, ED-27, N4, p.857 (1980).
19. S.S.Li, W.L.Wang, P.W.Lai, and R.T.Owen, J. Electron Mater. 9, N2, p.335 (1980).
20. S.S.Li, W.L.Wang, R.Y.Loo, and W.P.Rahilly, Proc. of the 16th IEEE photovoltaic Specialists Conf., p.211 (1982).
21. S.S.Li, W.L.Wang, R.Y.Loo, and W.P.Rahilly, Solid State Electronics, 26, N9, p.835 (1983).
22. W.L.Wang and S.S.Li, Proc. of the 17th IEEE photovoltaic Special. Conf., May, Orlando, FL. (1984).
23. K.Sakai and T.Ikoma, Appl. Phys., 5, p.165 (1974).
24. F.Hasegawa and A.Majerfeld, Electron Letter, 11, p.286 (1975).
25. H.Lefevre and M.Schulz, Appl. Phys., 12, p.45 (1977).
26. D.V.Lang and R.A.Logan, J. Electron Mater., 4, p.1053 (1975).
27. D.V.Lang and L.C.Kimerling, "Lattice defects in semiconductor.", p.581 (Inst. of Phys.), London (1974).
28. D.V.Lang, A.Y.Cho, A.C.Gossard, M.Ilegens, and W.Wiegmann, J.Appl. Phys., 47, p.2558 (1976).
29. A.Ashby, G.G.Ashen, G.G.Roberts, D.J.Ashen, and J.B.Mullin, Solid State Comm., 20, p.61 (1976).
30. A.Mircea and A.Mitonneau, Appl. Phys., 8, p.15 (1975).
31. S.S.Li, W.L.Wang, P.C.Colter, and C.W.Litton, J. Electronic Materials., 12, p.223 (1983).
32. A.Mitonneau, G.M.Martin, and A.Mircea, "Inst. of Phys.", London, 33 (1977).

33. A.Mitonneau, G.M.Martin, and A.Mircea, *Electronic Letter*, 13, N22, p.666 (1977).
34. R.S.Muller and T.I.Kamins, "Device electronics for integrated circuits.", John Wiley & Sons Inc., (1977).
35. P.W.Lai, Master Thesis (1979).
36. C.T.Sah, *IRE Trans.ED-19*, p.94 (1972).
37. R.R.Senechal and J.Basinski, *J. Appl. Phys.*, 39, p.3723 (1968).
38. C.T.Sah, *Solid State Electronics*, 13, p.759 (1970).
39. H.Okuski and Y.Tokumaru, *Jap. J. Appl. Phys.*, 20, p.145 (1982).
40. H.Tomokage, H.Nakashima, and K.Hasimoto, *Jap. J. Appl. Phys.*, (1981).
41. S.M.Sze, "Physics of Semiconductor Devices.", second edition (1983).
42. W.Schottky and W.T.Read, Jr., *Phys. Rev.*, 87, N5, p.835 (1952).
43. C.H.Henry and D.V.Lang, *Phy. Rev. B*, V15, p.989 (1977).
44. A.F.Tasch, Jr., and C.T.Sah, *Phys. Rev. B1*, p.800 (1970).
45. T.T.Nguyen, K.L.Wang, and G.P.Li, *Appl. Phys. Lett.* 44 (2), p.211 (1984).
46. H.Tomokage, H.Nakashima, and K.Hashimoto, *Jap. J. Appl. Phys.* 21, p.67 (1982).
47. W.E.Phillips, and J.R.Lowney, *J. Appl. Phys.*, 54, p.2786, (1983).
48. S.Makram-Ebeid, Narayan, and Tan, eds. "Defects in semiconductors", p.495, (1981).
49. S.Makram-Ebeid, *Appl. Phys. Lett.* 37, p.464, (1980).
50. K.L.Wang, and G.P.Li, *S. S. Communication*, 47 (4), p.233, (1983).
51. G.P.Li, and K.L.Wang, *S. S. Electronics*, 26 (9), p.825, (1983).
52. R.M.Logan, and D.T.J.Hurle, *J. Phys. Chemistry Solids*, p.1739, (1971).
53. G.Vincent, A.Chantre, and D.Bois, *J. Appl. Phys.* 50 (8), p.5484, (1979).
54. P.A.Martin, B.G.Streetman, and K.Hess, *J. Appl. Phys.* 52 (12), p.7409, (1981).

55. M. Lax, Phys. Rev. 119 (5) p.1502, (1960).
56. E. N. Korol, Sov. Phys. Solid States, 19, p.1327, (1977).
57. J. Frenkel, Phys. Rev. 54, p.647, (1938).
58. J. L. Harke, J. Appl. Phys. 39, p.4871, (1968).
59. A. K. Jonscher, Thin Solid Films, 1, p.213 (1967).
60. K. Huang, "Statistical Mechanics", John Wiley (1960).
61. L. I. Schiff, "Quantum mechanics", McGraw-Hill, (1962).
62. V.T. Bublik, A.N.Morozov, V.B.Osvenski, L.I.Gaidai, S.P.Grishina,
and O.G.Portnov, Sov.Phys.Crystallography, Vol. 24,N.6, p.704 (1979).
63. D.T.Hurle, J. Phys. Chem. Solid, Vol. 40, p.613 (1979).
64. J.A.Van Vechten, J.Electronchem.Soc. Vol. 122, N. 3, p. 423 (1975).
65. J. A. Van Vechten, Phys. Rev., V.182, p.891 (1969).
66. P. F. Fewster, J. Phys.Chem.Solids.,Vol. 42, N. 10, p.883 (1981).
67. A. Munoz-Yague, and S. Baceiredo, J. Electrochem. Soc., Solid State
Science and Technology, Vol. 129, N. 9, p. 2108 (1982).
68. D. T. J. Hurle, J. Phys. Chem. Solids, Vol. 40, p. 627 (1979).
69. D. T. J. Hurle, J. Phys. Chem. Solids, Vol. 40, p.639 (1979).
70. G. Brouwer, Philips Res. Rep., Vol. 9, p.366 (1954).
71. J. A. Van Vechten, J. Electronchem. Soc., Vol.122, N.3, p.417 (1975).
72. D. V. Lang and L. C. Kimerling, Phys.Rev.Lett., Vol. 33, p.489 (1974).
73. L. C. Kimerling and J. L. Benton, Appl.Phys.Lett., Vol. 39, N.5,
p.410 (1981).
74. M. Taniguchi and T. Ikoma, J. Appl. Phy. 54, p.6448 (1983).
75. M. O. Watanabe, A. Tanebe, T. Udagawa, T. Nakanisi, and Y.Zohta, Jap.
J. Appl. Phys. 22, p.923 (1982).
76. M. R. Brozel, I. Grant, R. M. Ware, and D. J. Stirland, Appl. Phys.
Lett, 42, p.610 (1983).
77. G. M. Martin, Appl. Phys. Lett., Vol. 39, N.9, p.747 (1981).

78. J. Lagowski, H. C. Gatos, J. M. Parsey, K. Wada, M. Kaminska, and W. Walukiewicz, Appl. Phys. Lett., Vol. 40, N.4, p.342 (1982).
79. L. B. Ta, H. M. Lokgood, A. Rohatgi, and R. N. Thomas, J. Appl. Phys., Vol. 53, N.8, p.5771 (1982).
80. R. T. Chen, D. E. Holmes, P. M. Asbeck, and C. G. Kirkpatrick, Electron Materials. Conf. in Burlington, Vermont, June (1983).
81. A. T. Hunter, J. P. Baukus, H. Kimura, H. V. Winston, and O. J. Marsh, Electronics Materials. Conf., (1983).
82. T. Kikuta, K. Terashima, and K. Ishida, Electron Materials. Conf. (1983).
83. S. Sriram, M. El-Muradi, and M. B. Das, Electron Materials. Conf. (1983).
84. M. S. Skolnick, Electron Materials. Conf. (1983).
85. M. R. Brozel, I. Grant, R. M. Ware, and D. J. Stirland, Appl. Phys. Lett. Vol. 42, N.7, p.610 (1983).
86. M. D. Miller, G. H. Olsen, and M. Ettenberg, Appl. Phys. Lett., Vol. 31, N.8 p.538 (1977).
87. P. K. Bhattacharya, A. Majerfeld, and A. K. Saxena, Inst. Phys. Conf. Serv., Vol. 45, Ch.3, p.199 (1979).
88. P. K. Bhattacharya, J. W. Ku, and J. T. Owen, Appl. Phys. Lett., Vol. 36, p.304 (1980).
89. M. D. Watanabe, A. Tanaka, T. Nakanisi, and Y. Zohta, Jap. J. Appl. Phys., Vol. 20, N.6, p.L429 (1981).
90. H. Z. Zhu, Y. Apathi, and T. Ikoma, J. Crystal Growth, Vol. 55, p.154 (1981).
91. E. E. Wagner, D. E. Mars, G. Hom, and G. B. Stringfellow, J. Appl. Phys., Vol. 51, N.10, p.5434 (1980).
92. K. Konda, J. Lagowski, and H. C. Gatos, Electron Materials Conf. (1983).
93. D. V. Lang, Inst. Phys. Conf. Serv., N. 31, Ch. 1, p.70 (1977).
94. D. S. Day, J. D. Oberstar, T. J. Drummond, H. Morkoc, A. Y. Cho, and B. G. Streetman, J. Electron Materials., vol. 10, N.3, p.445 (1981).

95. D. E. Holmes, R. T. Chen, K. R. Elliot, and C. G. Kirkpatrick, Appl. Phys. Lett., Vol. 40, p.46 (1982).
96. R. E. Eustom, C. J. Nuesa, J. R. Apport, and J. J. Gannon, J. Electrochem. Soc., Vol. 121, p.1516 (1974).
97. A. M. Huker, N. T. Link, M. Valladom, J. L. Debrum, G. M. Martin, A. Mitanneau, and A. Mircea, J. Appl. Phys., Vol. 50, p.4022 (1979).
98. S. S. Li, "Annual Technical Report", Air Force Office of Scientific Research (1983).
99. E. H. Johnson, J. Kafales, R. W. Davis, and W. A. Dyes, Appl. Phys. Lett., Vol. 40, N.11, p.993 (1982).
100. M. O. Watanabe, T. Udagawa, T. Nakanisi, and Y. Zohta, Proc. 2nd Conf. Semi-insulating III-V Materials, Evian, p.283 (1982).
101. M. Oku, Y. Zohta, A. Tanaka, and T. Nakanisi, 28th Joint Meeting of Societies in Applied Physics, Japan, p.483 (1981).
102. P. Merenda, J. Crystal Growth, 13/14, p.331 (1972).
103. P. C. Colter, C. W. Litton, D. C. Reynolds, D. C. Look, P. W. Yu, S. S. Li, and W.L.Wang, Proc. SPIESymposium on SemiconductorCrystal Technology, Jan. (1982).
104. T. Nozaki, M.Ogawa, and H.Watanabe, Gallium Arsenide and Related Compounds 1974, p.46 (1975).
105. Y. Zou, GaAs and Related Compounds, Inst. of Phys. Conf. Series, Vienna (1980).
106. R. D. Fairman, F.J.Morin and J.R.Oliver, Inst. Phys. Conf. Serv., N 45, Ch.2, p.134 (1979).

END

FILMED

10-84

DTIC